

Broadband and conformal metamaterial based Perforated absorber using 3-D printing Technology

*Project report submitted to
Indian Institute of Information Technology, Nagpur,
in partial fulfillment of the requirements for the award of
the degree*

Bachelor of Technology In Electronics and Communication Engineering

by

Om Manoj Gupta (BT20ECE016)

Amit Yadav (BT20ECE027)

Guna Sai Kiran Nekkanti (BT20ECE075)

Under the guidance of

Dr. Paritosh Peshwe



***Indian Institute of Information Technology,
Nagpur 441108 (India)***

2024

Broadband and conformal metamaterial based Perforated absorber using 3-D printing Technology

*Project report submitted to
Indian Institute of Information Technology, Nagpur,
in partial fulfillment of the requirements for the award of
the degree*

Bachelor of Technology In Electronics and Communication Engineering

by

Om Manoj Gupta (BT20ECE016)

Amit Yadav (BT20ECE027)

Guna Sai Kiran Nekkanti (BT20ECE075)

Under the guidance of

Dr. Paritosh D. Peshwe



***Indian Institute of Information Technology,
Nagpur 441108 (India)***

2024

Department of Electronics and Communication Engineering

Indian Institute of Information Technology, Nagpur



Declaration

We, **Om Manoj Gupta, Amit Yadav, Guna Sai Kiran Nekkanti**, hereby declare that this project work titled "**Broadband and conformal metamaterial based Perforated absorber using 3-D printing Technology**" is carried out by us in the **Department of Electronics and Communication Engineering** of Indian Institute of Information Technology, Nagpur. The work is original and has not been submitted earlier whole or in part for the award of any degree/diploma at this or any other Institution /University.

Sr. No.	Enrollment No.	Name	Signature
1.	BT20ECE016	Om Manoj Gupta	
2.	BT20ECE027	Amit Yadav	
3.	BT20ECE075	Guna Sai Kiran Nekkanti	

Date: 17th May, 2024

Department of Electronics and Communication Engineering

Indian Institute of Information Technology, Nagpur



Declaration

We, **Om Manoj Gupta, Amit Yadav, Guna Sai Kiran Nekkanti**, Enrollment No **BT20ECE016, BT20ECE027, BT20ECE075**, understand that plagiarism is defined as any one or the combination of the following:

1. Uncredited verbatim copying of individual sentences, paragraphs or illustrations (such as graphs, diagrams, etc.) from any source, published or unpublished, including the internet.
2. Uncredited improper paraphrasing of pages or paragraphs (changing a few words or phrases, or rearranging the original sentence order).

3. Credited verbatim copying of a major portion of a paper (or thesis chapter) without clear delineation of who did or wrote what. (Source: IEEE, the institute, Dec.2004)

I have made sure that all the ideas, expressions, graphs, diagrams, etc. that are not a result of my own work, are properly credited. Long phrases or sentences that had to be used verbatim from published literature have been clearly identified using quotation marks.

I affirm that no portion of our work can be considered as plagiarism and I take full responsibility if such a complaint occurs. I understand fully well the guide of the thesis may not be in a position to check for the possibility of such incidences of plagiarism in this body of work.

Sr. No.	Name	Signature
1.	Om Manoj Gupta	
2.	Amit Yadav	
3.	Guna Sai Kiran Nekkanti	

Date: 17th May, 2024

Certificate

This is to certify that the project titled "**Broadband and conformal metamaterial based Perforated absorber using 3-D printing Technology**", submitted by **Om Manoj Gupta, Amit Yadav, Guna Sai Kiran Nekkanti** in partial fulfillment of the requirements for the award of the degree of **Bachelor of Technology in Department of Electronics and Communication Engineering**, IIIT Nagpur. The work is comprehensive, complete and fit for final evaluation.



Dr. Paritosh Peshwe
Assistant Professor, Department of
Electronics and Communication
Engineering, IIIT Nagpur

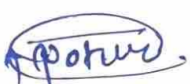
Date - 17/05/2023



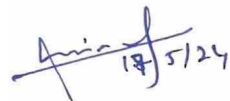
(Industry Expert's Name)



(Academic Expert's Name)



(Industry Expert's Signature)



(Academic Expert's Signature)


(Name and Sign of HoD)
IIIT Nagpur

ACKNOWLEDGEMENT

We extend our heartfelt thanks to **Dr. Paritosh D. Peshwe**, Assistant Professor in the Department of ECE and our institute-level supervisor, for his unwavering support, guidance, and encouragement throughout the project. His insights, experience, vision, and enthusiastic participation were invaluable and served as a source of inspiration for us. We are deeply grateful for his excellent mentorship, which has helped us achieve success in our project.

We would like to express our profound gratitude to **Megh Sainadh Patinavalasa**, a PhD student in the Department of Electrical Engineering at the Indian Institute of Technology Indore, and **Dr. Saptarshi Ghosh**, an assistant professor in the same department, for their invaluable support and assistance in seeing our project through to completion, as well as in the fabrication and testing of our project at **IIT Indore**.

We are grateful to our departmental peers for their unwavering support and encouragement during our research endeavor. We want to express our profound appreciation to our friends, as well as to those whose names are not listed, for providing us with direct or indirect support during every circumstance, be it favorable or unfavorable.

We would like to express our sincere appreciation to **Chaitra Guruvelli, Ojasvi Thakre, and Rachit Gupta**, our junior fellows in the Department of ECE, for their excellent coordination that greatly facilitated the completion of our project.

Lastly, we would like to express our appreciation to all individuals who have supported us in any way throughout this endeavor.

Om Manoj Gupta

Amit Yadav

Guna Sai Kiran Nekkanti

ABSTRACT

This study presents a comprehensive investigation into the design and optimization of conformal absorbers employing metamaterials and leveraging the versatility of 3D printing technology. Two distinct designs are proposed, each offering unique advantages and catering to different application scenarios. The primary focus lies in achieving high-performance electromagnetic absorption over a broad frequency range while ensuring flexibility and adaptability for various practical uses.

The first design introduces a groundbreaking structural innovation, integrating an air gap within a perforated substrate. This design not only facilitates lightweight construction but also enables exceptional broadband performance, spanning the X, Ku, and K bands. Through rigorous parametric analysis and meticulous simulation studies, the absorber's performance parameters were finely tuned, resulting in absorption levels consistently surpassing 90% across a remarkable bandwidth exceeding 20 GHz. Furthermore, the absorber demonstrates remarkable polarization insensitivity and maintains stability even under oblique incidences of up to 45 degrees, showcasing its suitability for a wide array of applications requiring conformal and flexible electromagnetic absorption.

In addition to the design optimization, an equivalent circuit model is developed to provide deeper insights into the absorption mechanism. Analysis of surface current distribution and electric field distribution at absorption frequencies offers a detailed understanding of the absorber's functionality. The absorber's fabrication process is facilitated through cost-effective 3D printing technology, with resistive ink uniformly coated onto the substrate using the screen-printing process. Furthermore, a second design variant is introduced, offering slightly reduced bandwidth while maintaining effectiveness in the X and Ku bands, providing a versatile solution tailored to specific application requirements. Overall, this study underscores the potential of combining metamaterials with 3D printing for the development of high-performance conformal absorbers with diverse frequency coverage and adaptable fabrication capabilities, opening doors to a wide range of practical electromagnetic applications.

Keywords: ***3-D printing, metamaterial absorber, perforated geometry, Broadband Absorber, conformal, Resistive Ink, Polarization Insensitive***

TABLE OF CONTENTS

LIST OF FIGURES	vi
LIST OF TABLES	viii
LIST OF ABBREVIATIONS	ix
1 INTRODUCTION	1
1.1 Motivation and Overview	1
1.2 Objectives of the Project	3
1.3 Organization of the Thesis	4
2 BACKGROUND KNOWLEDGE	5
2.1 BroadBand Metamaterial Absorber	5
2.2 Flexible and Conformal Absorbers	6
2.3 Role of Flexible Absorber in Real Life Applications	7
2.4 Overview of Frequency Selective Surfaces(FSS)	7
2.4.1 Absorber	8
2.4.2 Polarizer	8
2.4.3 Radome	8
2.5 Overview of Substrate Materials for Absorber	9
2.5.1 Dielectric constant and Loss tangent	9
2.5.2 Thickness	10
2.5.3 Flexibility	10
2.5.4 Effect of Temperature and Moisture	10
2.6 Overview of Air Spacer between Substrate and Ground Plate	11
2.7 Absorber Parameters	12
2.7.1 Dielectric constant and Loss tangent	12

2.7.2	Reflection Coffeicient	12
2.7.3	Absorptivity	13
2.7.4	Types of incidence:	14
2.7.4.1	Normal Incidence	14
2.7.4.2	Oblique Incidence	14
2.7.5	Polarization Conversion Ratio(PCR)	15
2.7.6	Input impedance	15
2.7.7	Equivalent Circuit	15
2.7.8	Electric Field Distribution	17
2.7.9	Surface Current Distribution	17
2.8	Testing and measurments	18
3	LITERATURE REVIEW	19
3.1	Previous Research Paper	19
3.1.1	Research Paper [35] (Absorber)	19
3.1.2	Research Paper [36] (Absorber)	20
3.1.3	Research Paper [37] (Multiband)	20
3.1.4	Research Paper [38] (Multiband)	21
3.1.5	Research Paper [39] (Broadband)	21
3.1.6	Research Paper [40] (Broadband)	22
3.1.7	Research Paper [41] (Broadband)	22
3.1.8	Research Paper [42] (Broadband)	23
3.1.9	Research Paper [43] (Broadband)	23
3.1.10	Research Paper [44] (Broadband)	24
3.1.11	Research Paper [45] (Polarization insensitive)	24
3.1.12	Research Paper [46] (Polarization insensitive)	25
3.1.13	Research Paper [47] (Polarization insensitive)	25
3.1.14	Research Paper [48] (Polarization insensitive)	26
3.1.15	Research Paper [49] (Textile Substrate)	26
3.1.16	Research Paper [50] (Textile Substrate)	27
3.1.17	Research Paper [51] (Textile Substrate)	27
3.1.18	Research Paper [52] (Flexible)	28
3.1.19	Research Paper [53] (Flexible)	28

3.1.20 Research Paper [32] (Air Gap)	29
3.1.21 Research Paper [54] (Air Gap)	29
3.1.22 Research Paper [55] (Air Gap)	30
3.1.23 Research Paper [56] (Air Gap)	30
3.1.24 Research Paper [57] (Air Gap)	31
3.1.25 Research Paper [31] (Conformal)	31
3.1.26 Research Paper [58] (Conformal)	32
3.1.27 Research Paper [59] (Conformal)	32
3.1.28 Research Paper [60] (Conformal)	32
3.1.29 Research Paper [61] (Resistive ink)	33
3.1.30 Research Paper [62] (Resistive ink)	33
3.1.31 Research Paper [19] (Resistive ink)	34
3.1.32 Research Paper [63] (Resistive ink)	34
4 PROPOSED WORK	35
4.1 Absorber Design Flow	36
4.1.1 Absorber Design 1	36
4.1.2 Absorber Design 2	39
5 FABRICATION AND TESTING	43
5.1 Fabrication	43
5.1.1 3-D Printing Technology	43
5.1.2 Resistive Ink Painting	44
5.1.3 Air Gap Control	45
5.1.4 Integration of Copper tape	46
5.1.5 Fabricated Pictures	46
5.2 Testing	47
5.2.1 Measurment setup	47
5.2.1.1 Anechonic Chamber	47
5.2.1.2 Antenna Configuration	47
5.2.1.3 Measurment Equipment	48
5.2.1.4 Data Acquisition and analysis	49

6 RESULTS AND DISCUSSION	50
6.1 Performance Analysis of Proposed Absorber Designs	50
6.1.1 Absorber Design 1	50
6.1.1.1 S_{11} Parameter	51
6.1.1.2 Absorptivity	52
6.1.1.3 Impedance (Z_{in})	52
6.1.1.4 Polarization (Normal Incidence)	53
6.1.1.5 Oblique Incidence	54
6.1.1.6 Polarization Conversion Ratio (PCR)	55
6.1.1.7 Parametric Analysis	56
6.1.1.8 Field Distribution	57
6.1.1.9 Surface Current Density	59
6.1.2 Absorber Design 2	61
6.1.2.1 S_{11} Parameter	61
6.1.2.2 Absorptivity	62
6.1.2.3 Impedance (Z_{in})	63
6.1.2.4 Polarization (Normal Incidence)	64
6.1.2.5 Oblique Incidence	65
6.1.2.6 Polarization Conversion Ratio (PCR)	66
6.1.2.7 Equivalent Circuit Analysis	66
6.1.2.8 Parametric Analysis	68
6.1.2.9 Field Distribution	72
6.1.2.10 Surface Current Density	74
6.1.2.11 Bending Analysis Simulation	76
6.1.3 Comparison with previous work	77
7 CONCLUSION	78
7.1 Conclusion	78
7.2 Future Scope	78
REFERENCES	79

LIST OF FIGURES

4.1	The Floquet technique: a) boundary conditions of a unit cell and b) CST MWS model of an infinite periodic array.	36
4.2	Evolution of Absorber-1 shape from iteration 0 to iteration 4	36
4.3	Evolution of Geometry of Absorber-1 from iteration 0 to iteration 3	37
4.4	Variation of Absorptivity of Proposed Absorber-1 from iteration 0 to iteration 4	37
4.5	Evolution of Absorber-2 shape from iteration 0 to iteration 4	39
4.6	Evolution of Geometry of Absorber-2 from iteration 0 to iteration 2	39
4.7	Modification in Substrate Shape for absorber-2	40
4.8	Variation of reflection coefficient (S11) of Absorber Design 2 with iterations	40
4.9	Variation of Absorptivity of Proposed Absorber-2 from iteration 0 to iteration 4	41
4.10	Topology of final proposed absorber-2: (a) top view, (b) side view	42
5.1	Fabrication Flow for Proposed absorbers	43
5.2	3D Printing (a) Printer, (b) Process	43
5.3	Resistive Ink Material Used	44
5.4	Ink painting on proposed absorber (a) Absorber-1 and (b) Absorber-2	45
5.5	Air Gap Stand	45
5.6	Ground Plane	46
5.7	Fabricated Designs	46
5.8	Schematic diagram of experimental setup along with ABmm Vector Network Analyzer (VNA) and two horn antenna (transmitter and receiver), and fabricated prototype.	47
5.9	Measurment Setup (a) Horn antenna Setup-1 (4-18GHz), (b) Horn antenna Setup-2 (18-25GHz)	48
5.10	Vector Network Analyzer (VNA)	49
6.1	Final Simulated proposed absorber 1	50

6.2	Simulated proposed absorber 1 (a) Reflection Coefficient (S11) and (b) Absorptivity	51
6.3	Simulated reflection coefficient (S11) of proposed absorber 1	51
6.4	Simulated Absorptivity of Proposed Broadband Absorber 1	52
6.5	Normalized Input Impedance of Proposed Absorber 1.	53
6.6	various polarization angles under normal incidence.	54
6.7	Simulated absorptivity at different incident angles.	55
6.8	For Proposed Broadband Absorber 1.	56
6.9	Variation of the different design parameters of the proposed broadband absorber 1. .	57
6.10	Variation of Electric Field of Proposed Absorber 1	58
6.11	Variation of Magnetic Field of Proposed Absorber	58
6.12	Variation of Surface Current Distribution of Proposed Absorber 1 on resistive ink .	59
6.13	Variation of Surface Current Distribution of Proposed Absorber 1 on Resistive Ink .	60
6.14	Final Simulated proposed absorber 2	61
6.15	Simulated proposed absorber-2 (a) Reflection Coefficient (S11) and (b) Absorptivity	61
6.16	Simulated and measured reflection coefficient (S11) of proposed absorber-2	62
6.17	Simulated and Measured Absorptivity of Proposed Broadband Absorber-2	62
6.18	Normalized Input Impedance of Proposed Absorber-2.	63
6.19	Simulated reflection coefficient of the proposed broadband absorber-2 for various polarization angles under normal incidence.	64
6.20	Simulated absorptivity at different incident angles.	65
6.21	For Proposed Broadband Absorber-2.	66
6.22	Equivalent Circuit Model.	68
6.23	Variation of the different design parameters of the proposed broadband absorber-2. .	69
6.24	Variation of the different design parameters of the proposed broadband absorber-2. .	70
6.25	Relation of Electric and Magnetic Field	72
6.26	Variation of Electric Field of Proposed Absorber-2	72
6.27	Variation of Magnetic Field of Proposed Absorber-2	73
6.28	Relation of Electric and Magnetic Field	74
6.29	Variation of Surface Current distribution of Proposed Absorber-2 on resistive ink .	74
6.30	Variation of Surface Current Distribution of Proposed Absorber-2 on Ground plane .	75
6.31	Bending analysis of a Unit cell of Proposed absorber	76
6.32	Simulated Reflectivity curve for different cylindrical radii.	76

List of Tables

4.1	Optimized design parameters of proposed absorber-1 in Figure 4.6a and 4.6b	38
4.2	Optimized design parameters of proposed absorber-2 in Figure 4.6a and 4.6b	42
6.1	Optimized design parameters of Equivalent circuit in Figure 6.22a	67
6.2	Comparison Table	77

LIST OF ABBREVIATIONS

MM - Metamaterial

MA - Metamaterial Absorber

EM - Electromagnetic

SRR - Split Ring Resonator

CSRR - Complementary Split Ring Resonator

FSS - Frequency Selective Surface

MTM - Metamaterial

THz - Terahertz

GHz - Gigahertz

MHz - Megahertz

PEC - Perfect Electric Conductor

PMC - Perfect Magnetic Conductor

RCS - Radar Cross Section

S-parameter - Scattering Parameter

FEM - Finite Element Method

CST - Computer Simulation Technology (software)

HFSS - High-Frequency Structure Simulator (software)

MEMS - Micro-Electromechanical Systems

PCB - Printed Circuit Board

TL - Transmission Line

BW - Bandwidth

Q-factor - Quality Factor

RF - Radio Frequency

UV - Ultraviolet

IR - Infrared

LOD - Loss of Dielectric

WBAN - Wireless Body Area Networks

SAR - Specific Absorption Rate

IEEE - Institute of Electrical and Electronics Engineers

FCC - Federal Communications Commission

Chapter 1

INTRODUCTION

This chapter provides a brief overview, motivation, and importance of research on wideband conformal metamaterial absorber using 3D printing and resistive ink.

1.1 Motivation and Overview

The motivation for our thesis comes from the increasing demand for Broadband Conformal Absorbers, Electromagnetic (EM) metamaterials consist of a periodic configuration of subwavelength resonators that, because of their unique characteristics, such as negative permittivity, negative permeability, and refractive index, can be characterized as effective materials.[1] Metamaterials, also known as meta-absorbers, have found several uses, including the shrinking of microwave antennas, super Lenses, polarization converters, waveguide structures, frequency-selective surfaces, and sensors.[4] EM wave absorbers are widely used in many different disciplines, including anechoic chambers, stealth technology, reducing radar cross section (RCS), EM wave compatibility, and EM wave interference. [2-3] The microwave absorption of earlier conventional absorbers, such ferrite tile, carbon nanotube, Salisbury screen [5], and Jaumann absorber [6], came at the cost of being thick and heavy. These absorbers are essentially basic radar absorbers, consisting of a resistive sheet spaced $\lambda/4$ away from the metal surface. Since they only match at one frequency, they have a relatively narrow absorption bandwidth while having a simple structure [7-8]. However, due to their resonance mechanisms, the majority of the previously published metamaterial absorbers are narrow bands.

New technologies have made it possible to create circuit analog (CA) absorbers with broad absorption bands by printing periodic resistive-conductive patterns on dielectric surfaces. [9-11] Because of its substantial ohmic loss, the resistive elements absorb incident electromagnetic waves over a wide frequency range, while the grounded dielectric substrates aid in impedance matching. These high-impedance surfaces are widely used to create wideband absorbers due to their greater efficiency.

[12-14] The capacitive circuit (CC) method is another alternative wideband design that has just been introduced using multi-layer technology. [15] These CA and CC absorbers can be implemented in several ways, such as by painting resistive inks [18] or attaching lumped resistors [16] with resistive coatings [17]. Nevertheless, the initial pair of methods are comparatively costly, delicate when it comes to fabricating massive arrays and challenging to utilize in outdoor settings.

Conversely, resistive ink can achieve broadband absorption by being uniformly printed (on any of the dielectric substrates) using a number of affordable technologies. [19] The majority of CA-based broadband absorbers have been built using printed circuit board (PCB) etching techniques on dielectric substrates that are readily available in the market. Not only may the total weight of the dielectric be reduced by careful management during the printing process, [20] but by selecting appropriate substrate patterns, the structure can also be made mechanically stable. Additionally, the 3-D printing process is more economical in terms of production time, chemical waste, and fabrication costs when compared to PCB etching. [21-22] A few 3-D printed microwave absorber structures have recently been created using stand-up resistive film arrays, in which the substrate sidewalls are coated with resistive patches. [23-24] The geometries suffer from enormous thickness despite having a wide absorption band because several standing wave modes cause the absorptions. Furthermore, the majority of these constructions lack strong mechanical components that make them unsuitable for use in real-world situations. [25]

Designers have recently begun to focus on using perforated dielectrics formed of honeycomb structures and other materials to provide mechanical stability to their designs. As a result, we are seeing the development of broadband lightweight structures. [19] Additionally, in order to increase bandwidth, various resonators of varying sizes are layered; nonetheless, the primary limitation in stacking is thickness.[26] Nevertheless, the substrates used to create these kinds of broadband absorbers were stiff and did not conform to curved surfaces. This constraint limits the practical applicability of metamaterial absorbers to some degree. Consequently, researchers created conformal and flexible metamaterial absorbers that are single, multiband, and broadband nonetheless, the primary limitation with these absorbers is still bandwidth.[27-30] However, the majority of conformal absorbers employ rubber[31] as their substrate and resistors[32] to achieve a wide bandwidth; No study has been done on conformal-based absorbers that achieve a wide bandwidth without utilizing resistors. As a result, research on a wideband conformal metamaterial absorber using 3D printing and resistive ink has re-

cently increased.

This work presents the development of a lightweight metamaterial absorber using 3-D printing technology. We present a conformal, broadband, ultra-thin, polarization-insensitive microwave absorber in this work. To achieve broadband absorption concurrently, a lossy resistive ink has been uniformly painted in resonant loop patterns.

1.2 Objectives of the Project

- **Design and Optimization:** Develop innovative designs for conformal absorbers using metamaterials and 3D printing technology. Conduct comprehensive parametric analysis and simulation studies to optimize the absorber's performance parameters, such as absorptivity, bandwidth, and frequency coverage.
- **Broadband Performance:** Achieve high-performance electromagnetic absorption over a broad frequency range, spanning the X, Ku, and K bands. Ensure that the absorber demonstrates absorption levels consistently exceeding 90% across the desired frequency spectrum.
- **Flexibility and Adaptability:** Ensure that the absorber design offers flexibility and adaptability for various practical applications requiring conformal and flexible electromagnetic absorption. This includes maintaining effectiveness under different incident wave polarizations and oblique incidences up to 45 degrees.
- **Mechanism Understanding:** Develop an equivalent circuit model to gain insights into the absorption mechanism of the proposed absorber designs. Analyze surface current distribution and electric field distribution at absorption frequencies to understand the underlying physics and optimize the design further.
- **Fabrication:** Fabricate the absorbers using cost-effective 3D printing technology. Utilize resistive ink and the screen-printing process to uniformly coat the absorber onto the substrate. Ensure that the fabrication process is scalable and compatible with mass production requirements.

1.3 Organization of the Thesis

The report presents the project work in the form of 6 chapters, each of which is briefly described below and structured accordingly:

- **Chapter 1** provides a brief overview, motivation, and importance of research on wideband conformal metamaterial absorber
- **Chapter 2** deals with providing an explanation of important background topics that are necessary for understanding the thesis, such as Broadband, Conformal, and Flexible Absorbers, and general Absorber parameters.
- **Chapter 3** gives a better understanding and highlights remarkable milestones achieved by previous researchers in this domain, thus paving the way for further improvements.
- **Chapter 4** provides a comprehensive insight into the proposed absorbers, outlining the detailed design process that has been undertaken to ensure superior performance.
- **Chapter 5** focuses on presenting the Fabrication and testing techniques of the proposed absorber designs.
- **Chapter 6** focuses on presenting the results and evaluating the performance of the proposed absorber designs. It also conducts a comparative analysis of the proposed absorbers with existing broadband metamaterial absorbers.
- **Chapter 7** provides a concluding summary of the entire project.

Chapter 2

BACKGROUND KNOWLEDGE

This Chapter deals with providing an explanation of important background topics that are necessary for understanding the thesis, such as BroadBand Metamaterial Absorbers, flexible and Conformal Absorbers, general ABsorber parameters, and Testing.

2.1 BroadBand Metamaterial Absorber

Broadband metamaterial absorbers represent a cutting-edge solution in electromagnetic wave management, offering efficient absorption across a wide frequency range. These absorbers leverage metamaterials, engineered structures with properties not typically found in natural materials, to achieve their broadband capabilities. By carefully designing the geometric arrangement, composition, and dimensions of the metamaterial elements, engineers can tailor the absorbers to efficiently absorb electromagnetic radiation spanning diverse frequencies. This versatility makes broadband metamaterial absorbers highly desirable for a range of applications where traditional absorbers fall short in providing broadband performance.

The operating principle of broadband metamaterial absorbers is rooted in impedance matching, where incident electromagnetic waves encounter the absorber and are effectively matched to its impedance, leading to absorption rather than reflection or transmission. This principle allows for efficient absorption of electromagnetic radiation over a wide frequency range. Typically, broadband absorbers consist of layered structures, with each layer optimized to absorb specific portions of the electromagnetic spectrum. This layered approach contributes to the overall broadband absorption capability of the metamaterial absorber.

Broadband metamaterial absorbers find applications across various industries, including military,

telecommunications, and sensing. In the military sector, they play a crucial role in stealth technology by reducing the radar cross-section of aircraft and other vehicles. In telecommunications, they enhance antenna performance and reduce interference, leading to improved signal quality. Additionally, broadband metamaterial absorbers are utilized in sensors for detecting and measuring electromagnetic radiation across a broad spectrum of frequencies. Despite challenges in fabrication precision and extending performance to higher frequency ranges, broadband metamaterial absorbers continue to hold promise for revolutionizing electromagnetic wave management in diverse applications.

2.2 Flexible and Conformal Absorbers

Flexible and conformal absorbers are advanced materials and structures designed to absorb electromagnetic radiation while being adaptable to irregular surfaces and flexible in their form. Unlike traditional rigid absorbers, which are limited in their application to flat or uniform surfaces, these absorbers offer versatility and adaptability, making them suitable for various practical applications.

Flexible absorbers are engineered using materials that can bend, stretch, or conform to non-planar surfaces without compromising their absorption capabilities. These materials may include polymers, elastomers, or composites with tailored electromagnetic properties. Their flexibility allows them to be integrated into curved or irregular surfaces, such as aircraft wings or vehicle bodies, where traditional absorbers would be impractical.

Conformal absorbers, on the other hand, are designed to conform precisely to the shape of a given surface, ensuring maximum coverage and absorption efficiency. These absorbers often employ advanced manufacturing techniques, such as additive manufacturing or molding, to produce custom shapes that precisely match the contours of the surface they are applied to. By closely conforming to the surface, these absorbers minimize gaps and reflections, enhancing their overall performance.

Applications of flexible and conformal absorbers span a wide range of industries. In aerospace, they are used for stealth technology to reduce the radar cross-section of aircraft and unmanned aerial vehicles (UAVs), allowing for enhanced survivability and mission effectiveness. In automotive applications, they can be integrated into vehicle bodies to minimize electromagnetic interference and improve communication and navigation systems. Additionally, they find use in consumer electronics, medical

devices, and wearable technology, where flexibility and conformability are essential for integration into complex and dynamic environments.

Despite their advantages, challenges remain in the development of flexible and conformal absorbers, including ensuring durability, maintaining performance over time, and optimizing manufacturing processes for cost-effectiveness. However, ongoing research and advancements in materials science and engineering continue to push the boundaries of what is possible, opening up new opportunities for the application of these innovative absorbers in diverse fields.

2.3 Role of Flexible Absorber in Real Life Applications

Flexible, conformal, and metamaterial broadband absorbers are crucial across various sectors:

- **Stealth Technology:** They reduce radar cross-section in aerospace and defense, conforming to surfaces for effective signal absorption.
- **Telecommunications:** They enhance antenna performance, minimizing signal distortion and electromagnetic interference in wireless communication.
- **Solar Energy Harvesting:** These absorbers optimize sunlight absorption in renewable energy applications, improving solar panel efficiency.
- **Sensing and Imaging Systems:** They reduce background noise and enhance signal quality in medical imaging and security applications, enabling accurate detection.

In summary, these absorbers are vital for managing electromagnetic waves, offering innovative solutions across diverse industries.

2.4 Overview of Frequency Selective Surfaces(FSS)

These three have varied purposes, but we mostly use them for FSS-based electromagnetic systems applications:

- Absorber
- Polarizer
- Radome

2.4.1 Absorber

An absorber is a material or structure designed to absorb electromagnetic radiation. Its primary function is to reduce or eliminate reflections, scattering, or transmission of electromagnetic waves. Absorbers are commonly used in applications such as radar cross-section reduction (stealth technology), electromagnetic interference (EMI) shielding, and improving signal-to-noise ratio in sensing and imaging systems. They can be engineered to operate over specific frequency ranges and may come in various forms, including surface coatings, layered structures, or metamaterial designs.

2.4.2 Polarizer

A polarizer is a device that selectively transmits or blocks electromagnetic waves based on their polarization state. It can be used to control the orientation of electromagnetic fields, allowing only waves with a specific polarization orientation to pass through while blocking others. Polarizers are commonly used in optical systems, such as cameras, LCD displays, and 3D glasses, to control glare, improve contrast, or enable 3D visualization. They can be made from materials like polarizing filters, birefringent crystals, or metal grids, depending on the desired application and frequency range.

2.4.3 Radome

A radome is a protective covering or enclosure designed to shield radar equipment or antennas from environmental elements while allowing electromagnetic waves to pass through with minimal distortion. Radomes are typically constructed from materials that are transparent to radar frequencies, such as fiberglass, plastics, or composite materials. They serve to protect sensitive electronic components from weather, wind, debris, and other external factors without significantly affecting the performance of the radar system. Radomes are commonly used in aviation, maritime, and ground-based radar systems to protect antennas mounted on aircraft, ships, or buildings.

In summary, absorbers are used to absorb electromagnetic radiation, polarizers selectively transmit or block waves based on polarization, and radomes protect radar equipment while maintaining electromagnetic transparency. Each component plays a distinct role in electromagnetic systems, contributing to their overall functionality and performance.

2.5 Overview of Substrate Materials for Absorber

A dielectric material is utilized between the Absorber Patch and the ground plane. When evaluating absorber performance, the dielectric constant is crucial. The term "substrate" also applies to the dielectric substance. A variety of dielectric materials are used in the construction of Conformal Absorbers. These materials were selected with care to offer a suitable level of mechanical deformations with little impact from various weather conditions and appropriate EM radiation protection. Below is a discussion of the substrate's characteristics that have an impact on the performance of the flexible absorber and were taken into consideration while selecting PLA as a substrate for designing a Broadband Absorber. Substrate materials for metamaterial absorbers play a crucial role in determining the performance, flexibility, and durability of the absorber structure.

2.5.1 Dielectric constant and Loss tangent

The dielectric constant (ϵ_r) of the substrate affects the resonance frequency and bandwidth of the metamaterial absorber. Higher dielectric constants shift the resonance frequency towards lower frequencies, while lower dielectric constants shift it towards higher frequencies. A higher dielectric constant can increase the electric field confinement within the metamaterial structure, leading to stronger absorption at the resonance frequency. Conversely, a lower dielectric constant may result in weaker absorption. A dielectric mismatch between the substrate and the metamaterial layers can cause impedance mismatch, leading to reflection and reduced absorption efficiency. Matching the dielectric constants of the substrate and the metamaterial layers can improve absorption performance.

The loss tangent($\tan \delta$) of the substrate determines the amount of energy dissipated as heat within the material. Higher loss tangents result in higher absorption losses and lower reflectance. A higher loss tangent can increase absorption efficiency by dissipating more energy within the absorber structure. However, excessively high-loss tangents may lead to excessive heating and degradation of the substrate material. Lossy substrates with high-loss tangents are often preferred for metamaterial absorbers, as they can enhance absorption performance and reduce reflection. However, the choice of substrate material should balance absorption performance with other factors such as mechanical strength, thermal stability, and cost.

2.5.2 Thickness

The thickness of the substrate in flexible and conformal absorbers is a critical factor influencing their performance and application suitability. For flexible absorbers, thinner substrates offer greater flexibility, enabling them to conform to irregular surfaces without compromising integrity. However, there's a balance to strike with mechanical strength and durability. Thinner substrates may lack robustness, while thicker ones can add weight and rigidity. In conformal absorbers, substrate thickness affects how well the absorber conforms to the surface it's applied to. Thinner substrates minimize gaps, enhancing absorption, but thicker ones may offer better mechanical support and protection. Ultimately, selecting the optimal substrate thickness involves considering factors like flexibility, durability, weight, and application requirements.

2.5.3 Flexibility

Thinner substrates offer greater flexibility and conformability to curved or irregular surfaces. They can bend and flex more easily, allowing the absorber to conform to complex shapes without compromising its integrity. However, excessively thin substrates may lack mechanical strength and durability, making them prone to tearing or damage during handling or use. Therefore, there's a trade-off between flexibility and mechanical robustness when selecting the substrate thickness for flexible absorbers. The choice of substrate thickness also influences the overall weight and thickness profile of the flexible absorber. Thinner substrates result in lighter and more streamlined absorber structures, which may be advantageous for weight-sensitive applications such as aerospace and wearable technology.

2.5.4 Effect of Temperature and Moisture

Temperature and moisture can greatly impact the performance of substrates in absorbers. High temperatures can alter material properties and cause dimensional changes, affecting the absorber's efficiency and structural integrity. Moisture absorption can degrade substrates over time, leading to changes in electrical properties and promoting the growth of microorganisms. These environmental factors must be carefully considered during material selection and design to ensure optimal performance and durability of absorbers in real-world conditions.

Selecting PLA (Polylactic Acid) as the substrate offers advantages such as temperature stability,

moisture resistance, mechanical properties suitable for flexible and conformal absorbers, desirable dielectric characteristics, and environmental sustainability due to its biodegradability. So we selected PLA($\epsilon_r = 2.1$, $\tan \delta = 0.07$) as a substrate

2.6 Overview of Air Spacer between Substrate and Ground Plate

In absorber designs, incorporating an air spacer between the substrate and a metal ground plate offers significant advantages. Firstly, this configuration provides a notable dielectric contrast between the substrate and the ground plate. This contrast is beneficial for enhancing absorption performance by minimizing reflections and improving impedance matching. By reducing reflections, the absorber can more effectively attenuate incident electromagnetic waves across the desired frequency spectrum.

Moreover, the thickness of the air spacer can be adjusted to tune the absorption characteristics of the absorber. This tunability allows for customization of the absorber's resonance frequency and bandwidth to target specific frequency ranges relevant to the application. By varying the spacer thickness, engineers can optimize the absorber's performance for different operational requirements and environmental conditions.

Additionally, the air spacer serves as a decoupling layer between the substrate and the ground plate, minimizing electromagnetic coupling effects. This decoupling helps to reduce unwanted interactions such as mutual capacitance or inductance, which can affect the absorber's performance and efficiency. By isolating the substrate from the ground plate, the air spacer ensures more predictable and consistent electromagnetic behavior of the absorber.

Furthermore, air spacers offer mechanical flexibility, enabling the absorber to conform to curved or irregular surfaces. This flexibility is particularly advantageous in applications where rigid structures are impractical or incompatible. By allowing the absorber to adapt to varying surface geometries, air spacers expand the range of potential applications for absorber designs, including conformal and wearable technologies.

Lastly, air spacers provide thermal insulation between the substrate and the ground plate due to the poor thermal conductivity of air. This insulation helps to prevent heat transfer between the absorber

and surrounding components, maintaining stable operating temperatures. By minimizing thermal fluctuations, air spacers contribute to the overall reliability and longevity of the absorber in demanding environments. Overall, the incorporation of an air spacer between the substrate and the metal ground plate enhances absorption performance, provides tunability, reduces coupling effects, offers mechanical flexibility, and ensures thermal insulation in absorber designs.

2.7 Absorber Parameters

2.7.1 Dielectric constant and Loss tangent

The quantity of electric potential energy, in the form of induced polarisation, that is stored in a certain volume of material under the influence of an electric field is quantified by the dielectric constant. It is quantified as the ratio of the material's dielectric permittivity to that of dry air or a vacuum.

$$k = \frac{C}{C_0}$$

where C is the permittivity of the substance, C_0 is the permittivity of a vacuum.

Loss tangent, also known as dielectric loss tangent, is a measure of how much energy is lost as heat when an alternating current (AC) electric field is applied to a dielectric material. It is the ratio of the imaginary part of the dielectric constant (representing energy loss) to its real part (representing energy storage) for a material under an AC electric field.

$$k = \frac{\epsilon''}{\epsilon'}$$

where, ϵ' is the real part of the dielectric constant (i.e., the permittivity) of the material, and ϵ'' is the imaginary part of the dielectric constant (i.e., the loss factor) of the material.

2.7.2 Reflection Coffeicient

It quantifies how much of an electromagnetic wave is reflected by an impedance discontinuity in the transmission medium i.e. between transmission line and absorber. The reflection coefficient is equal

to the ratio of the amplitude of the reflected wave to the incident wave.

$$\Gamma = \frac{Z_L - Z_0}{Z_L + Z_0}$$

where, Z_L is Load impedance of patch, Z_0 is Characteristic impedance of the transmission line.

2.7.3 Absorptivity

In metamaterial absorbers, absorptivity refers to the ability of the material to absorb electromagnetic radiation within a certain frequency range. Metamaterial absorbers are engineered materials designed to absorb specific wavelengths of electromagnetic radiation, such as microwaves or infrared light, with high efficiency.

The absorptivity (A) of a metamaterial absorber can be defined as the ratio of the absorbed power ($P_{absorbed}$) to the incident power ($P_{incident}$):

$$A = \frac{P_{incident}}{P_{absorbed}}$$

The absorbed power ($P_{absorbed}$) can be calculated using the following formula:

$$P_{absorbed} = P_{incident} - P_{transmitted} - P_{reflected}$$

Where, $P_{incident}$ is the incident power.

$P_{transmitted}$ is the power transmitted through the material.

$P_{reflected}$ is the power reflected off the material.

For a two-port network, such as a metamaterial absorber, the S-parameters are typically represented as follows:

S_{11} : The reflection coefficient at Port 1, which represents the ratio of the reflected wave to the incident wave at Port 1.

S_{21} : The transmission coefficient from Port 1 to Port 2, which represents the ratio of the transmitted wave to the incident wave at Port 1.

The absorptivity (A) of the metamaterial absorber can be related to its S-parameters as follows:

$$A = 1 - |S_{11}|^2 - |S_{21}|^2$$

This formula indicates that the absorptivity is related to both the reflection and transmission coefficients. A perfect absorber would have $|S_{11}|^2 = |S_{21}|^2=0$, resulting in $A=1$, meaning all incident power is absorbed.

2.7.4 Types of incidence:

In the context of electromagnetic wave propagation and interaction with materials, there are several types of incidence that describe how waves encounter a boundary or interface.

There are mainly two types

- Normal Incidence
- Oblique incidence

2.7.4.1 Normal Incidence

In this case, the incident wave strikes the interface perpendicular (normal) to the surface. The angle of incidence (θ_i) is 0 degrees. This type of incidence is common in many introductory examples and is often used as a reference point for comparing other types of incidence.

2.7.4.2 Oblique Incidence

In oblique incidence, the incident wave strikes the interface at an angle (θ_i) other than 0 degrees. This angle is measured with respect to the normal to the interface. Oblique incidence is encountered in most practical situations and is essential for understanding phenomena like reflection, refraction, and absorption.

In oblique incidence, we again refer to two transverse Incidence depending upon fields.

Transverse Incidence: Also known as TE (Transverse Electric) polarization, transverse incidence refers to a wave where the electric field vector is perpendicular to the direction of propagation. In optics, this corresponds to light with its electric field oscillating perpendicular to the direction of propagation.

Longitudinal Incidence: Also known as TM (Transverse Magnetic) polarization, longitudinal incidence refers to a wave where the magnetic field vector is perpendicular to the direction of propagation. In optics, this corresponds to light with its magnetic field oscillating perpendicular to the direction of propagation.

2.7.5 Polarization Conversion Ratio(PCR)

The Polarization Conversion Ratio (PCR) is a measure used to quantify the efficiency of converting one polarization state of electromagnetic waves into another. It's particularly relevant in devices such as polarization converters, polarization controllers, and polarization-sensitive components in optical and microwave systems.

Let us say the Wave is Travelling in y direction then the Cross-Polarized reflection coefficient is denoted by r_{xy} and the Co-polarized coefficient is denoted by $r - yy$, and PCR is given by the

$$PCR_y = \frac{|r_{xy}|^2}{|r_{xy}|^2 + |r_{yy}|^2}$$

2.7.6 Input impedance

The effective impedance, permittivity, and permeability are related to the reflection and transmission coefficients.

The below equations describe the relationship

$$Z = \sqrt{\frac{(1 + S_{11})^2 - S_{21}^2}{(1 - S_{11})^2 - S_{21}^2}}$$

$$\epsilon_{effective} = \frac{n}{Z}$$

$$\mu_{effective} = n \times Z$$

Z represents impedance, and n, k, and h represent the unit cell's refractive index, wave number, and thickness, respectively.

2.7.7 Equivalent Circuit

Creating an equivalent circuit for a metamaterial absorber involves representing its electromagnetic behavior using lumped circuit elements. This approach simplifies the complex electromagnetic interactions within the absorber into a more manageable circuit model. Here's a general procedure to create an equivalent circuit from an absorber.

Characterization: Begin by thoroughly characterizing the absorber's performance through experimental measurements or electromagnetic simulations. This characterization should include its absorption properties over the desired frequency range.

Identification of Key Components: Identify the key mechanisms responsible for absorption in the metamaterial absorber. This could include resonant elements, lossy components, and any other structures crucial for absorbing electromagnetic energy.

Lumped Element Representation: Assign lumped circuit elements to represent the identified mechanisms. For example:

- **Resistors:** Use resistors to model dissipative losses within the absorber material.
- **Inductors and Capacitors:** Represent any resonant behavior or reactive elements in the absorber with inductors and capacitors.
- **Transmission Lines:** Use transmission lines to represent wave propagation within the absorber structure.

Circuit Topology: Determine the interconnections between the lumped elements based on the absorber's geometry and electromagnetic behavior. This may involve series and parallel connections to accurately capture the absorber's impedance and resonance behavior.

Parameter Extraction: Extract the values of the lumped circuit elements from the absorber's performance data. This typically involves curve fitting or optimization techniques to match the equivalent circuit model to the absorber's measured or simulated behavior.

Validation: Validate the equivalent circuit model by comparing its simulated performance with the absorber's experimental or simulated data. Adjust the circuit parameters as necessary to improve the model's accuracy.

Creating an equivalent circuit for a metamaterial absorber can be challenging due to the complex and often nonlinear nature of its electromagnetic response. However, with careful characterization and modeling, an accurate equivalent circuit can provide valuable insights for absorber design and integration into larger electromagnetic systems.

2.7.8 Electric Field Distribution

The electric field distribution refers to the spatial variation of the electric field intensity within and around the absorber structure. In metamaterial absorbers, the electric field interacts with the structured material, leading to the absorption, reflection, and transmission of electromagnetic energy.

The electric field distribution can be described using Maxwell's equations, which govern electromagnetic wave propagation. The electric field (E) is related to the incident wave, the material properties, and the geometry of the absorber.

In some cases, analytical or numerical methods such as finite-difference time-domain (FDTD) simulations or method of moments (MoM) can be used to calculate the electric field distribution within the absorber structure.

2.7.9 Surface Current Distribution

Surface currents are currents that flow along the surface of a conductor or material interface in response to an incident electromagnetic wave. In metamaterial absorbers, surface currents play a crucial role in absorbing and dissipating electromagnetic energy.

Surface current distribution refers to the spatial distribution of these currents on the surface of the metamaterial structure. These currents arise due to the interaction between the incident electromagnetic wave and the structured material of the absorber.

The surface current distribution can be calculated using techniques such as impedance boundary conditions, where the surface currents are related to the tangential component of the electric field at the interface.

Formally, the surface current density (J_s) can be related to the tangential electric field (E_t) at the surface of the absorber using the surface impedance (Z_s):

$$J_s = Z_s \times E_t$$

Where Z_s depends on the material properties and the geometry of the absorber structure.

Understanding the electric field and surface current distributions is essential for optimizing the design of metamaterial absorbers to achieve efficient absorption of electromagnetic energy within specific frequency ranges. These distributions provide valuable insights into how the absorber interacts with incident waves and dissipates energy through absorption mechanisms.

2.8 Testing and measurements

Testing metamaterial absorbers involves verifying their electromagnetic performance, including absorption efficiency, frequency response, polarization sensitivity, and angle of incidence dependence. Here are several common testing methods:

- **Reflectivity Measurement:** Measure the reflectivity of the absorber over a range of frequencies using techniques such as a vector network analyzer (VNA) or a reflectometer. A low reflectivity indicates high absorption.
- **Absorptivity Measurement:** Calculate the absorptivity of the absorber by subtracting the reflectivity and transmissivity from unity ([Equation]A=1-R-T). Absorptivity can be measured using techniques like integrating sphere measurements or calorimetric methods.
- **Transmission Measurement:** Measure the transmission through the absorber to ensure minimal transmission, especially in applications where the transmitted signal should be minimized.
- **Polarization Sensitivity Testing:** Analyze the absorber's response to different polarization states of incident waves. This can be done by varying the polarization of the incident wave and measuring the absorber's absorption efficiency for each polarization state.
- **Angle of Incidence Dependence:** Test the absorber's performance under various angles of incidence to assess its angular sensitivity. This is particularly important for applications where the incident angle may vary.
- **Near-Field Scanning:** Use near-field scanning techniques to map the electric and magnetic fields near the absorber's surface. This provides detailed information about the distribution of electromagnetic energy and can help optimize the absorber's design.
- **Far-Field Measurements:** Perform far-field measurements to characterize the absorber's radiation pattern and efficiency in redirecting or absorbing incident radiation.
- **Thermal Imaging:** In calorimetric methods, measure the temperature rise of the absorber when exposed to electromagnetic radiation. This can provide indirect evidence of absorbed power.

By employing a combination of these testing methods, engineers can thoroughly evaluate the performance of metamaterial absorbers and ensure they meet the requirements of specific applications, such as radar cross-section reduction, antenna design, electromagnetic interference shielding, and energy harvesting.

Chapter 3

LITERATURE REVIEW

This Chapter gives a better understanding and highlights remarkable milestones achieved by previous researchers in this domain, thus paving the way for further improvements.

3.1 Previous Research Paper

3.1.1 Research Paper [35] (Absorber)

Essence

Metamaterials (MM) represent artificially designed materials with unique properties arising from their geometrical structure, featuring distinctive traits like negative refractive index, Snell's law reversal, Doppler effect reversal, and left-handed behavior. These materials find applications in various fields, including invisibility cloaking, perfect lensing, perfect absorption, and sensing. This review article focuses on the electromagnetic absorption property of structures known as metamaterial absorbers (MMAs). MMAs are composites consisting of multiple layers of metallic patterns separated by dielectric material. These innovative devices facilitate near-unity absorption through various mechanisms, explored in detail within this review. The MMAs are categorized based on their absorption characteristics, such as polarization tunability, broadband operation, and multiband absorption, across different frequency regimes.

3.1.2 Research Paper [36] (Absorber)

Essence

This paper introduces a highly efficient Broadband Metamaterial Absorber (BMA) based on a Manganese–Silica–Manganese three-layer structure with a shaped pattern on the top layer. To maximize absorption efficiency, the geometrical parameters of the absorber are optimized using Particle Swarm Optimization (PSO). The optimized structure, with a thickness of 190 nm, achieves over 94% absorption across the visible band (400–800 nm), boasting an average absorption of 98.72%. Remarkably, it maintains more than 90% absorption over the extended range from 365 to 888 nm, and in the range from 447 to 717 nm, it surpasses 99% absorptivity, providing an ultra-wide bandwidth of 270 nm. The physical mechanism of absorption is elucidated through the exploration of electric and magnetic field distributions. Additionally, the proposed structure exhibits 85% absorption stability for wide incident angles up to 70° for both TE and TM polarizations under oblique incidence. The optimized absorber structure, with its exceptional absorption capabilities, is deemed suitable for various applications, including optical sensors, thermal emitters, and color imaging.

3.1.3 Research Paper [37] (Multiband)

Essence

This paper details the design, fabrication, and measurement of a triple-band metamaterial absorber operating at 8 GHz, 10 GHz, and 12 GHz within the X-band frequency range. The metamaterial unit cell features three concentric copper rings at different radii, printed on a 0.8 mm thick FR4 substrate to achieve triple resonant frequencies. The inherent symmetry of the ring structure ensures the absorber's insensitivity to the polarization state of incident electromagnetic waves for normal incidence, and it exhibits operational effectiveness over a wide range of incident angles. Simulated results indicate high absorbance for normal incident electromagnetic waves, with values of 97.33%, 91.84%, and 90.08% at 8 GHz, 10 GHz, and 12 GHz, respectively. The corresponding full width half maximum (FWHM) values are 5.61%, 2.90%, and 2.33%, maintaining 50% absorbance. The metamaterial absorber sustains 50% absorbance at operating angles of 67° and 64° for TE mode and TM mode, respectively. Experimental results validate the absorber's performance at the three resonant frequencies, achieving absorbance greater than 80%.

3.1.4 Research Paper [38] (Multiband)

Essence

This paper introduces a triple-band polarization-independent metamaterial absorber featuring square-shaped closed ring resonators, designed to operate over a wide angle of incidence. The unit cell, comprising various square loops, is meticulously designed through parametric analysis to achieve a triple-band absorption response. Two bands lie in the C-band, and one resides in the X-band, catering to applications in airborne and surveillance radar signal absorption. Notably, in the X-band, the absorber demonstrates a broadband response with a full width at half maximum bandwidth of 940 MHz (9.43%). The structure exhibits bandwidth-enhanced properties for any angle of polarization under normal incidence and maintains high absorption for angles of incidence up to 60°. The proposed structure is fabricated, and experimental results align well with the simulated responses, affirming the absorber's performance and its potential utility in radar signal absorption applications.

3.1.5 Research Paper [39] (Broadband)

Essence

This study introduces a broadband terahertz (THz) metamaterial absorber, detailing its simulation, implementation, and measurement. The absorber is crafted by stacking 12 metallic bars of varying lengths on three polyimide layers with uniform spacing. This configuration results in a broadband absorption spectrum, achieved by merging multiple successive resonance peaks. The measured total absorption surpasses 95% within the frequency range of 0.81 to 1.32 THz at normal incidence, boasting a 64% full width at half maximum (FWHM) from 0.76 to 1.48 THz. Although absorption decreases with increasing incident angles, it remains above 62% even at a 40° angle. The absorption mechanism is explained, with verification provided by a 9-bar example exhibiting a narrower bandwidth. Experimental demonstrations confirm the proposed structure's robustness against misalignment of each metallic layer, showcasing its potential for broadband THz absorption applications.

3.1.6 Research Paper [40] (Broadband)

Essence

This paper introduces a novel approach to achieving a switchable FSS absorber/reflector in different states by presenting a broadband and switchable absorber utilizing an absorb/reflective FSS. The top layer of the proposed structure features a periodic arrangement of square loops loaded with PIN diodes on a mechanically robust dielectric substrate. Beneath these square loops, there is a honeycomb layer of a certain thickness and a thin metal layer. The structure is thoroughly characterized through full-wave analysis, showcasing commendable absorption/reflection switching performance. The intrinsic impedance is investigated to elucidate the switching and broadband absorption mechanisms. Operating in the frequency band of 2.5 - 5.5 GHz, the switchable absorber changes states by adjusting the bias voltage. With varied bias voltages, the FSS structure seamlessly transitions between absorption and reflection states. In the ON state, it functions as a wideband absorber, with reflectivity below -10 dB in the range of 2.5 - 5.5 GHz, while in the OFF state, it exhibits fine reflective properties.

3.1.7 Research Paper [41] (Broadband)

Essence

This paper proposes the design of a wide-frequency flexible metamaterial absorber tailored for application in the C and X bands. Leveraging simulation and optimization using CST, the metamaterial absorbers demonstrate a remarkable absorption rate exceeding 90% within the 4.5-12 GHz range, with a maximum absorption rate reaching an impressive 99.999%. This achievement signifies the attainment of a perfect absorption effect for electromagnetic waves. The study extensively explores various factors influencing the absorber's performance, including the size of the metamaterial unit, incident electromagnetic wave angles, dielectric material thickness, and the electric field and surface current on the metal structure. Through a thorough investigation of the absorption principles, the analysis yields valuable insights, contributing to a comprehensive understanding of the absorber's behavior in achieving optimal absorption effects in the specified frequency range.

3.1.8 Research Paper [42] (Broadband)

Essence

This study proposes an ultrawideband metamaterial absorber (MMA) designed to operate within the 23GHz-47GHz frequency range. The ultrawideband characteristics are achieved through a staggered arrangement of metal strips combined with loaded lumped resistance. Additionally, the inner ring is symmetrically slotted at $\pm 45^\circ$ to enhance the equivalent capacitance and control the resonant frequency. The structural unit measures $5\text{mm} \times 5\text{mm} \times 1.38\text{mm}$, exhibiting symmetry for polarization insensitivity and enabling wide-angle incidence. The absorption mechanism of the MMA unit is studied using the S-parameter inversion method, confirming high absorption rates through equivalent impedance and absorption rate curves. The analysis explores the impact of lumped resistance and surface-loaded structural parameters on absorptivity to achieve impedance matching. The dielectric layer and resistance layer collaboratively absorb incident electromagnetic waves, as validated by measurement results, demonstrating the effectiveness of the proposed ultrawideband MMA in mitigating EMI in the 5G millimeter wave band. Addressing the challenge of electromagnetic interference (EMI) in the 5G millimeter wave band.

3.1.9 Research Paper [43] (Broadband)

Essence

This study presents a straightforward design model for crafting an ultrawideband ultrathin metamaterial absorber in the microwave frequency range. The proposed structure comprises two concentric circular split rings on a metal-backed dielectric substrate. Numerical simulations reveal a notable 10-dB absorption bandwidth spanning 7.85 to 12.25 GHz, covering the entire X-band, under normal incidence. The absorber's performance is explored under varying polarization angles and oblique incidence, offering versatility. Electromagnetic field distributions and surface current plots are employed to elucidate the absorption mechanism. Experimental verification at different angles of incidence and polarizations affirms the absorber's functionality. This compact and ultrathin design, with a thickness corresponding to the center frequency, provides a practical solution for constructing broadband absorbers, opening avenues for diverse applications in the microwave frequency regime.

3.1.10 Research Paper [44] (Broadband)

Essence

This paper introduces a switchable ultra-wideband metamaterial absorber designed for the THz band, featuring polarization-insensitivity and wide-incident angle capabilities. The absorber is composed of a VO₂ disk, a polyimide dielectric substrate, and a gold ground plane. The results reveal absorption rates exceeding 90% within the 3.5–8 THz range at 300 K, with the absorption band disappearing at 350 K. Notably, the proposed metamaterial absorber exhibits insensitivity to polarization states and angles, maintaining high absorption of over 80% for wide-incident angles, up to 60° for both TE and TM modes. The wideband absorption mechanism is elucidated through effective medium and surface current analysis, showcasing the versatility and switchable nature of the absorber in the THz band.

3.1.11 Research Paper [45] (Polarization insensitive)

Essence

This study introduces an innovative metamaterial absorber featuring six absorption peaks, achieved through the use of four multiple-mode Ω-shaped resonators (MMORs). The absorber is structured as a sandwich with resonators and a dielectric sheet, showcasing polarization-insensitive characteristics across a frequency range from 2 to 17 GHz. Notably, horizontal-oriented MMORs contribute to four absorption peaks, while the remaining two are generated by vertical-oriented MMORs. The combination of these discrete absorption responses forms the total absorption profile. To understand the underlying physical mechanism, the analysis includes examining surface current and power loss density distributions, along with an equivalent circuit model. The measured results align well with simulations, demonstrating an impressive average absorption rate exceeding 97.21%. This research contributes to the field of metamaterials by providing insights into the absorber's unique design and performance characteristic

3.1.12 Research Paper [46] (Polarization insensitive)

Essence

In this study, a novel ultrathin and broadband metamaterial absorber, incorporating four lumped resistors, is proposed and comprehensively analyzed. The key focus of this design is to enhance absorptivity by simultaneously reducing reflection and transmission coefficients. This is achieved by employing a continuous metallic ground, ensuring zero transmission, while impedance matching between the proposed metamaterial absorber and free space ($Z = Z_o$ or $\mu_r = \epsilon_r$) contributes to a reduction in reflection. Significantly, the absorber attains electric and magnetic resonances simultaneously, leading to perfect absorptivity. The finite element method is employed for simulation and analysis of the absorber's performance. Results indicate that the suggested design exhibits absorption rates exceeding 90% across a broad frequency range from 14.35 to 29.18 GHz, accommodating both transverse electric and transverse magnetic polarizations. Remarkably, the absorber maintains high absorption levels even with incident angle variations ranging from 0° to 50° . These findings suggest promising applications for the proposed perfect metamaterial absorber in fields such as communications, stealth technology, and imaging.

3.1.13 Research Paper [47] (Polarization insensitive)

Essence

This paper introduces analyses and fabricates a wideband and ultrathin metamaterial absorber tailored for Ku-band applications. The reported absorber demonstrates exceptional absorptivity, exceeding 90%, across the entire Ku band (12–20 GHz) under normal incidence for both transverse electric and transverse magnetic polarization. The effectiveness of this absorber is attributed to the concurrent support of electric and magnetic resonances. By carefully designing the effective permittivity and permeability, impedance matching with free space is achieved, resulting in the absorption of the entire incident energy by the metamaterial absorber. Importantly, the proposed structure exhibits robust absorption responses, exceeding 80%, even under oblique incidence ranging from 0 to 50° . These findings underscore the absorber's potential for Ku-band applications, showcasing its versatility and effectiveness in capturing incident energy across a range of angles and making it a promising candidate for practical implementation in relevant fields.

3.1.14 Research Paper [48] (Polarization insensitive)

Essence

This paper introduces an innovative approach to creating a bandwidth-enhanced and wide-angle-of-incidence metamaterial absorber through the utilization of a hybrid unit cell. The design incorporates symmetric unit cells to maintain high absorptivity for all polarization angles. Specifically, a circular-sector unit cell is employed to achieve elevated absorptivity under oblique incidence for both transverse electric (TE) and transverse magnetic (TM) modes. The proximity of these absorption frequencies results in an expanded bandwidth. The proposed concept is validated through comprehensive full-wave simulations and experimental measurements. Simulations reveal absorptivity exceeding 91% around 10.45GHz for an incidence angle of up to 70° in both TM and TE polarizations. Experimental results demonstrate a measured absorptivity close to 96.5% at 10.45GHz for all polarization angles under normal incidence. Notably, the measured absorptivity at 10.45GHz remains consistently above 90% in the TE mode and surpasses 94% in the TM mode as the angle of incidence varies from 0° to 70° . Under oblique incidence, the measured 90% absorption bandwidth spans 1.95% from 10.1–10.2GHz and 10.4–10.5GHz up to 70° in the TE mode, and 3.39% from 10.15–10.5GHz up to 70° in the TM mode, showcasing the effectiveness of the proposed metamaterial absorber design.

3.1.15 Research Paper [49] (Textile Substrate)

Essence

This study proposes an innovative approach to enhance indoor radar clarity through the development of an all-textile microwave absorber. The absorber incorporates two variations of square ring resonators with different sizes, along with a backing ground plate and a 1 mm thick felt substrate made from conductive textiles. The utilization of diverse square ring resonators is strategically employed to achieve a broad absorption band, featuring two neighbouring resonance dips. Simulated results showcase the effectiveness of the design, revealing absorptivity peaks surpassing 96.7% and a notable full width at half maximum (FWHM) of 15.7% at 9.5 GHz. Notably, the absorber maintains high absorptivity across varying polarization angles of electromagnetic waves. This novel textile-based microwave absorber presents a promising solution for absorbing indoor radar frequencies, showcasing its potential utility in advancing radar technology for practical applications.

3.1.16 Research Paper [50] (Textile Substrate)

Essence

This paper introduces a novel wearable Frequency Selective Surface (FSS) made from fabric materials with the capability to block electromagnetic radiation around the frequency of 10.64 GHz (X Microwave frequency band). Two distinct unit cell shapes, embroidered metal yarn squares, and hexagons, are tested on a cotton fabric substrate with a permittivity of 1.9 and a thickness of 0.4 mm. The proposed design is validated through a comparison of 3D electromagnetic simulations and experimental measurements. Simulations with square unit cells exhibit a maximum absorptivity of 99.23% at 10.63 GHz, while simulations with hexagons show a peak absorptivity of 99.94% at 10.68 GHz. Experimental results demonstrate maximum absorptivity of 98.39% for squares and 98.00% for hexagons, both at 10.46 GHz. These findings indicate that the textile effectively provides high-level electromagnetic shielding, enhancing safety in civil and occupational exposures to electromagnetic radiation.

3.1.17 Research Paper [51] (Textile Substrate)

Essence

This study presents a dual-band flexible metamaterial absorber (MMA) with frequency-reconfigurable features designed to address the needs of advanced wireless communication technology. The MMA consists of a square patch surrounded by a square ring on a copper-backed flexible dielectric substrate, featuring a top surface made of silver nanoparticle ink and a middle polyethylene terephthalate (PET) substrate backed by a copper groundsheets. The MMA achieves an absorption rate exceeding 99% at 24 and 35 GHz and maintains stability for oblique incident angles ranging from 10° to 50°. Frequency tunability is enabled through a varactor diode connecting the inner patch with the outer ring, allowing for capacitance stimulation. The MMA's robustness and conformability are validated through bending studies over various radii of an arbitrary cylinder. A multiple-reflection interference model is developed, showing close agreement between simulated and calculated absorption results. This dual-band flexible MMA holds promise for applications in wireless communication, particularly in dual-band sensing and filtering operations, showcasing its efficiency and adaptability.

3.1.18 Research Paper [52] (Flexible)

Essence

This paper introduces a cost-effective, flexible, and ultrathin absorber designed for wearable applications, featuring a simple square patch-shaped frequency-selective surface (FSS). The absorbing structure consists of a periodic graphite patch pattern on a thin paper substrate, backed with a copper foil-based ground plane. The unit cell's dimensions and periodicity are optimized to $0.31\lambda_o$ and $0.36\lambda_o$, respectively, with the absorber's thickness approximately $\frac{\lambda_o}{85}$, where λ_o represents the free space wavelength at 10 GHz. Utilizing a full-wave high-frequency structure simulator software (HFSS), the FSS absorber's characteristics are fine-tuned in terms of unit cell periodicity and dielectric substrate height. The proposed absorber demonstrates insensitivity to both the angle of incidence and polarization. A prototype model is fabricated, measured, and validated against simulation results, revealing a strong agreement between the two. The versatility of this absorber makes it suitable for wearable electronics, medical, and automotive applications, effectively mitigating electromagnetic interference (EMI).

3.1.19 Research Paper [53] (Flexible)

Essence

This study introduces an ultrathin and flexible dual-band absorber operating at terahertz frequencies, utilizing a metamaterial structure. The structure comprises periodical split ring resonators featuring two asymmetric gaps and a metallic ground plane, separated by a thin, flexible dielectric spacer. Notably, the dielectric spacer is a free-standing polyimide film, making the absorber highly flexible and suitable for non-planar applications like micro-bolometers and stealth aircraft. Experimental results demonstrate two resonant absorption frequencies at 0.41 THz and 0.75 THz, with absorption rates of 92.2% and 97.4%, respectively. These resonances arise from normal dipole resonance and high-order dipole resonance, which is unique to the asymmetric structure. Multiple reflection interference theory is employed to analyse the absorber's mechanism, showing agreement with simulated and experimental results. The absorber proves insensitive to polarization, maintains high absorption rates (over 90%) across wide incident angles from 0° to 45° , and retains absorption rates above 90% even when wrapped around a curved surface, showcasing its adaptability and versatility.

3.1.20 Research Paper [32] (Air Gap)

Essence

The study introduces a polarization-independent, conformal wideband metamaterial absorber, featuring a unit cell comprising a circle and a slotted sector with lumped resistors for enhanced absorption bandwidth. Both measured and simulated results reveal over 90% absorption in the frequency range of 3.90 GHz to 10.5 GHz under normal incidence, with a fractional bandwidth of 91.6%. The absorber's compact unit cell size ($0.16 \lambda_o \times 0.16 \lambda_o$) and substrate thickness ($0.098 \lambda_o$) contribute to its versatility. Wrapping the absorber on a cylindrical surface maintains its absorptivity in the target frequency band. Detailed investigations of design parameters and absorption mechanisms through impedance analysis, electric field distribution, and surface current density enhance understanding. Fabrication and measurement of the conformal absorber demonstrate excellent agreement between simulated and experimental results for both flat and curved surfaces, affirming its efficacy.

3.1.21 Research Paper [54] (Air Gap)

Essence

This paper introduces a mechanically actuated frequency reconfigurable metamaterial electromagnetic absorber. The absorber's metamaterial unit cell exploits LC resonance from inductive and capacitive coupling, with the resonant frequency determined by these components. To enable frequency tuning, a mechanical method is proposed, altering the overall thickness of the unit cell by adjusting the thickness of an air substrate. Simulation results show that varying the air substrate thickness from 17 mm to 26 mm shifts the absorber's resonant frequency from 6.96 GHz to 5.79 GHz. Experimental validation involved fabricating a metamaterial absorber array and using a linear actuator to control the air substrate thickness. Results confirm a frequency shift from 6.96 GHz to 5.78 GHz, demonstrating 0.12 (GHz/mm) sensitivity to changes in air substrate thickness.

3.1.22 Research Paper [55] (Air Gap)

Essence

The paper introduces a polarization-independent, super-thin metamaterial microwave broadband absorber designed for X-band applications. The absorber unit cell incorporates four chip resistors connected to a close ring resonator (CRR), with a circular resonator inside the CRR to enhance bandwidth. Printed on a super-thin FR4 epoxy substrate with specific dielectric properties, the absorber achieves over 90% absorption bandwidth from 6.3 GHz to 12 GHz. Its symmetrical nature ensures consistent absorption across different polarization angles up to 90°, demonstrating polarization insensitivity. The absorber maintains stable performance for oblique incident angles up to 45° for both TE and TM modes, with a reduction in absorption beyond this angle. Surface current distribution analysis elucidates the absorption mechanism. Keywords: Broadband, Polarization-independent, Super-thin, Microwave Absorber.

3.1.23 Research Paper [56] (Air Gap)

Essence

The study introduces a broadband polarization-independent circuit analog absorber utilizing multi-layer resistive frequency selective surfaces (FSS). The structure comprises square loops loaded with lumped resistors, arranged periodically on dielectric substrates with an air spacer. Simulations demonstrate reflectivity below -10 dB across the frequency range of 4.96 to 18.22 GHz (a fractional bandwidth of 114.40%) under normal incidence, spanning C, X, and Ku bands. Equivalent circuit analysis is employed to characterize the absorber, exhibiting close agreement with full-wave analysis. The impact of individual FSS layers and the air spacer is investigated, with parametric variations exploring design parameter sensitivity on absorption bandwidth. Fabrication and measurement in an anechoic chamber validate the design, showing consistent results with simulations across different angles of incidence and polarization angles.

3.1.24 Research Paper [57] (Air Gap)

Essence

This article investigates a novel polarization-independent, ultra-wideband, lightweight, and thin microwave absorber, aiming to eliminate stray and suppress unwanted radiation in high-frequency circuits. The absorber unit cell comprises two concentric circular rings loaded with lumped resistances on the top surface of a dielectric substrate. With a compact unit cell size of $0.28 \lambda_L \times 0.28 \lambda_L \times 0.067 \lambda_L$ (where λ_L is the wavelength corresponding to the lowest frequency of operation), the design achieves over 90% absorption in the frequency range of 6.7 GHz to 20.58 GHz (a fractional bandwidth of 101.7%). The novelty lies in optimizing unit cell geometry, resistance loading, and air column loading to create a wideband and ultra-thin absorber. The absorber's four-fold structural symmetry ensures polarization insensitivity. Compact, lightweight (utilizing air as a spacer), and thin (only $0.067 \lambda_L$ thick), this absorber provides an alternative for constructing wideband absorbers for electromagnetic interference reduction. Keywords: Electromagnetic interference (EMI) reduction, frequency selective surface (FSS), polarization insensitive, wideband absorber.

3.1.25 Research Paper [31] (Conformal)

Essence

The study presents a novel broadband and conformal metamaterial absorber employing two flexible substrates. Simulation results demonstrate its absorption capabilities from 6.08 to 13.04 GHz with 90% efficiency due to its planar design, offering a relative absorption bandwidth of 72.8%. Remarkably, it remains insensitive to TE and TM wave polarizations. Its ultra-thin profile, at only 0.071 thickness, facilitates versatile applications. Additionally, by adjusting resistors on the polyimide film, absorption in different frequency ranges can be tailored. When bent, the absorber's absorption bandwidth and performance are enhanced, as confirmed by both experimental and simulation data. Overall, it emerges as a promising solution for scientific and technical absorption needs, boasting broadband absorption, polarization insensitivity, and flexibility.

3.1.26 Research Paper [58] (Conformal)

Essence

This paper presents a novel broadband flexible metamaterial absorber based on a high impedance surface (HIS). The polarization-insensitive absorber effectively suppresses backward Radar Cross Section (RCS) by approximately 10 dB. Numerical simulations reveal that the HIS metamaterial absorber (HIS-MA) achieves an absorption bandwidth of 11.14 GHz, spanning from 6.86 to 18 GHz, with absorption rates exceeding 90%. Experimental results validate the simulation findings, confirming the feasibility of the HIS-MA. The absorber's flexibility and absorption performance are demonstrated through simulations and measurements when bent on cylindrical surfaces, showcasing unique properties. Bistatic RCS simulations indicate a nearly 10 dB reduction in RCS when the HIS-MA is bent on a cylindrical object compared to conventional planar HIS-MA. This flexible absorber offers advantages in conformal applications, particularly in stealth properties, compared to rigid absorbers.

3.1.27 Research Paper [59] (Conformal)

Essence

The paper presents a novel flexible absorbing material designed for practical engineering applications, addressing limitations of current absorbing materials related to thickness and flexibility. Comprising a conductive carbon paste ink resistance film layer, a flexible fabric dielectric substrate, and a metal backplane, the material offers foldability for wearable use. It achieves over 90% absorption performance at 9.5–11.5 GHz, with polarization-insensitive characteristics when the incidence angle is less than 30°. Both simulation and experimental results validate the effectiveness of the structure. This advancement lays the foundation for future commercialization of meta-devices, including wearable invisibility cloaks, sensors, optical filters/switchers, photodetectors, and energy converters.

3.1.28 Research Paper [60] (Conformal)

Essence

The paper presents a sun shape resonator-based Metamaterial Absorber (MMA) designed for efficient harnessing of solar spectrum energy and various optical applications. Comprising three layers

of materials (W-SiO₂-W), the MMA achieves broadband absorption across the visible spectrum (390-760nm). The polarization-insensitive and ultrathin unit cell exhibits an average absorption of 96.43%, with a peak absorption of 99.99% at 523.22nm. Notably, the MMA maintains satisfactory absorption under different oblique angles and demonstrates resilience to mechanical loading, retaining broadband absorbance even under bending. Numerical simulation using Finite Integration Technique (FIT) is validated with Finite Element Method (FEM). The proposed MMA holds promise for optical applications including nano solar cells, imaging, sensors, light detectors, and biochemical applications.

3.1.29 Research Paper [61] (Resistive ink)

Essence

The paper introduces a wideband Metamaterial Absorber (MA) tailored for diverse X-band applications. The MA comprises a periodic array of unit cells featuring two split square resonators printed on an FR4 substrate with a relative permittivity of 4.4. Simulation outcomes showcase a notable -10 dB absorption bandwidth spanning 5.98 GHz (from 5.94 GHz to 11.92 GHz), with a Full Width Half Maxima (FWHM) bandwidth of 7.55 GHz (ranging from 5.58 GHz to 13.13 GHz). Notably, the absorber exhibits three absorption peaks at 6.2, 8.1, and 11.1 GHz, achieving absorptivity rates of 99.59%, 99.92%, and 99.85%, respectively. With a low profile attributed to compact unit cell dimensions (9mm×9mm), the absorber's absorption mechanism is elucidated via effective electromagnetic parameters (μ_{eff} and ϵ_{eff}). Robust performance is confirmed through investigations across wide angles of oblique incidence and varying polarization angles. Experimental validation of the fabricated absorber underscores its efficacy in achieving high absorptivity across the targeted X-band spectrum.

3.1.30 Research Paper [62] (Resistive ink)

Essence

This paper introduces an ultra-wideband, angle, and polarization-insensitive laser-assisted graphene metamaterial absorber. The design features double graphene resistive layers combined with three dielectric substrates. Using laser direct writing technology, graphene-embedded nano-magnetic material Fe₃O₄ is synthesized, exhibiting high uniformity with deviations less than 6% for various sheet resistance values. Numerical simulations and analytical studies are conducted to analyze absorption

mechanisms. Experimental results confirm the absorber's operation from 1.32 to 17.9 GHz with over 90% absorptivity, achieving a remarkable 173% fractional absorption bandwidth with a thickness of $0.068 \lambda_L$.

3.1.31 Research Paper [19] (Resistive ink)

Essence

This paper introduces a broadband metamaterial absorber utilizing three-dimensional (3-D) printing technology. The design features periodic arrays of a honeycomb core as the dielectric, with resistive paint deposited for broadband absorption. Notably, the structure's perforated substrate geometry enhances mechanical strength and lightweight properties. Broadband absorption (over 90%) is achieved in the frequency range of 5.52 to 16.96 GHz under normal incidence, with a fractional bandwidth exceeding 100%. An equivalent circuit model is developed to analyze absorption mechanisms, exploring various parametric variations. Fabrication involves low-cost 3-D printing technology, with resistive ink uniformly coated using screen printing. Experimental measurements demonstrate reasonable agreement with simulated responses under normal incidence. Keywords: 3-D printing, honeycomb, metamaterial absorber, perforated geometry.

3.1.32 Research Paper [63] (Resistive ink)

Essence

The paper presents a straight forward design of a resistive ink-based microwave absorber tailored for the S and C-bands. Utilizing a double-layer structure printed on an FR-4 substrate, the absorber achieves over 99% absorption within the frequency range of 3.15 GHz to 8.4 GHz, spanning both bands. Notably, the absorber maintains stability up to 30° for oblique incidence and exhibits polarization insensitivity. The study explores the impact of paint conductivity and thickness variation on absorber performance. Additionally, an equivalent circuit model is developed to elucidate the absorber's mechanism.

Chapter 4

PROPOSED WORK

This chapter provides a comprehensive insight into the proposed absorbers, outlining the detailed design process that has been undertaken to ensure superior performance.

In this thesis, we propose two different absorber structures, each of which underwent several iterations before achieving good performance suitable for Broadband. The design flow of each absorber is elaborated below.

In [19], various substrate materials were discussed for absorber fabrication, and it was determined that a PLA material (with $\varepsilon_r = 2.1$ and loss tangent $\tan\delta = 0.07$) having a thickness of 0.5 mm was used as a substrate to achieve the desired flexibility for the absorber. Recently, a few 3-D-printed microwave absorbers structures have been developed based on the stand-up resistive film arrays, where resistive patches are coated in the sidewalls of the substrates

Simulation Testing Technique:

The proposed unit cell was investigated using the CST Microwave Studio simulator. The frequency solver was employed to determine the unit cell's characteristics. As illustrated in Figure 4.1, unit cell boundary conditions are used in the transverse x and y directions, while Floquet port boundary conditions are used in the positive z direction. The incident wave is assumed to propagate in the negative z direction.

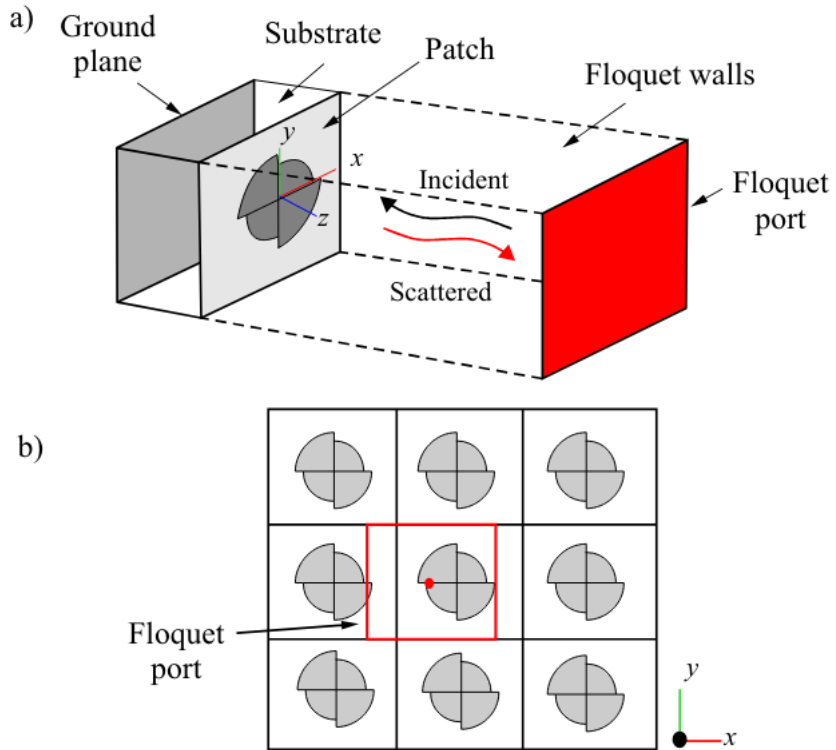


Figure 4.1: The Floquet technique: a) boundary conditions of a unit cell and b) CST MWS model of an infinite periodic array.

4.1 Absorber Design Flow

4.1.1 Absorber Design 1

We have started designing this absorber with a basic circular loop made of copper and a PLA(Polylactic Acid) substrate with a full ground plane at the back as shown in Figure 4.2a.

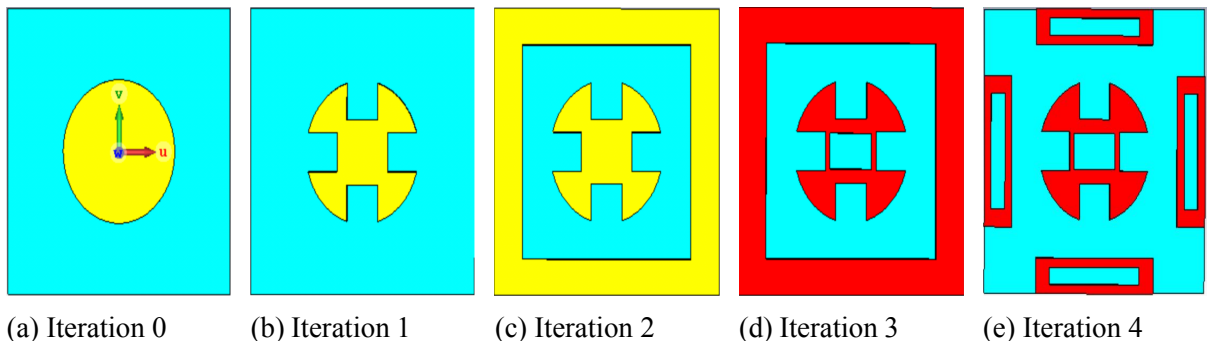


Figure 4.2: Evolution of Absorber-1 shape from iteration 0 to iteration 4

Further modifying our design in iteration 1 as shown in Figure 4.2b, we have added square-shaped slots on the left, right, top, and bottom of the circular loop. This helped us achieve absorption in three different frequency bands X-band, Ku-band, and K-band. We fine-tuned the absorption by adjusting the dimensions of these slots.

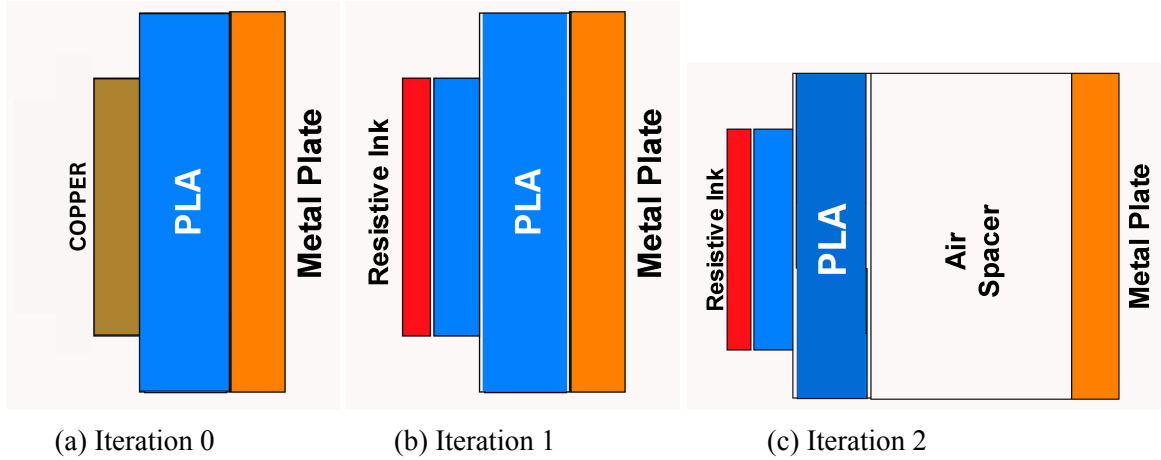


Figure 4.3: Evolution of Geometry of Absorber-1 from iteration 0 to iteration 3

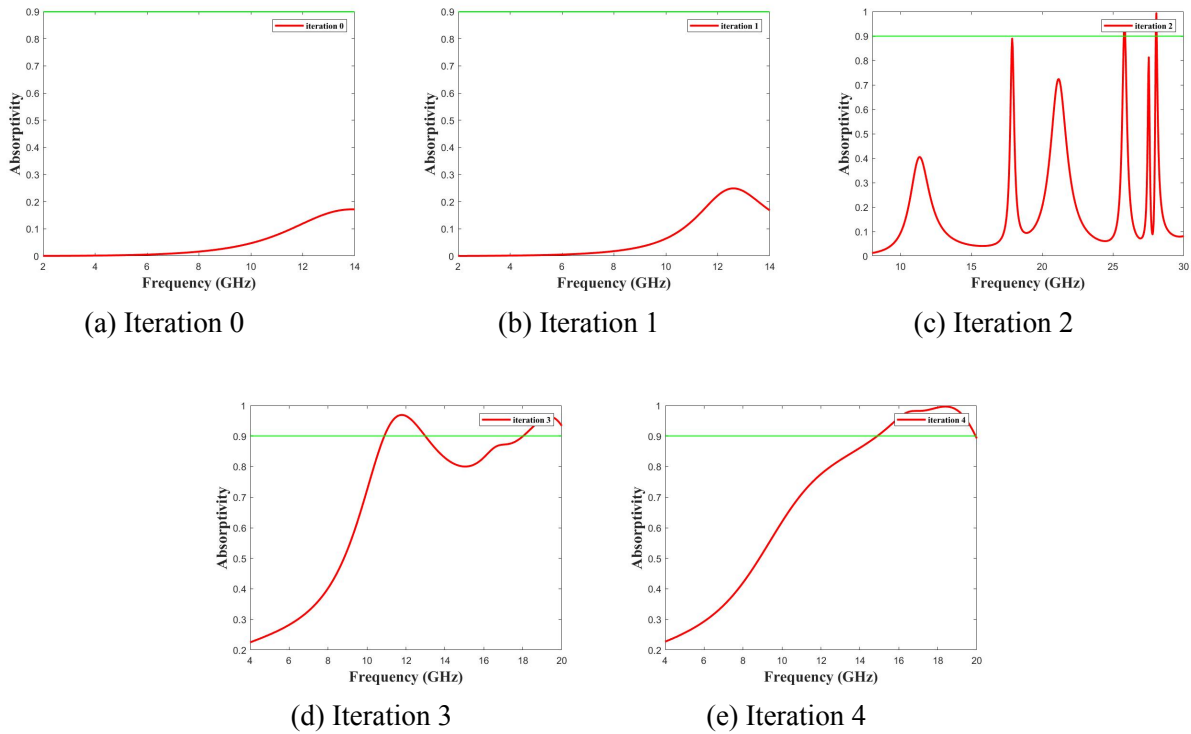


Figure 4.4: Variation of Absorptivity of Proposed Absorber-1 from iteration 0 to iteration 4

In Figure 4.2c, an outer rectangular loop was added, resulting in three narrow bands of absorption at frequencies above 18 GHz, with absorption rates exceeding 90%.

Further, the material of the loop element was changed to resistive ink in iteration 3 (Figure 4.2d). This change significantly improved absorption, providing a wideband response between 10 and 14 GHz, with absorption rates above 90%.

Finally, in iteration 4 (Figure 4.2e), a slot was added at the center of the circular loop, resulting in absorption rates above 95% from 12 GHz to 18 GHz.

Additional slots were introduced at the corners and in between the rectangular loop. This led to absorption rates above 95% in the Ku band and a wideband response from 10 GHz to 20 GHz.

Finally, circular slots were added to the circular patch, resulting in a wideband response from 10.1 GHz to 27.6 GHz, with a bandwidth of 17.5 GHz.

Table 4.1
Optimized design parameters of proposed absorber-1 in Figure 4.6a and 4.6b

Dimensions (unit: mm)				
$R_{out} = 4$	$it = 0.02$	$Gt = 0.035$	$SL = 16$	$b = 2$
$SH = 0.5$	$Mt = 1.5$	$p = 3.5$	$SW = 16$	$a = 2.2$

4.1.2 Absorber Design 2

The design process of this absorber began with the conventional Loop Resonator with a full ground in iteration 0 as shown in Figures 4.5a and 4.6a. This absorber had a resonance at around 6.5 GHz and a wideband of 8.5 GHz. To shift the resonance to the desired frequency and get more Wideband, the absorber was modified in iteration 1 as shown in Figure 4.5b, and used the same Geometry For Layers, by etching another nested Square Loop. For this iteration, I am getting the same bandwidth but an increase in absorptivity towards more than 90%. Therefore, the absorber in iteration 1 was modified in iteration 2 as shown in Figure 4.5c and Kept the Same Geometry by placing an extra Loop in the Absorber so that the effective Electrical Length Increased.

We are getting good absorptivity and a wide bandwidth bandwidth with this modification, but it only covers the X and Ku bands. To cover the K band as well, we went through another iteration where we added another shape inside and added some line shapes. In this iteration, the electric field increased at higher frequencies due to the added inner shape, and there is some additional resonance at a higher band. As a result of additional interior shape alterations, iteration 3 is producing three resonances with good absorption, as seen in Figure 4.5d.

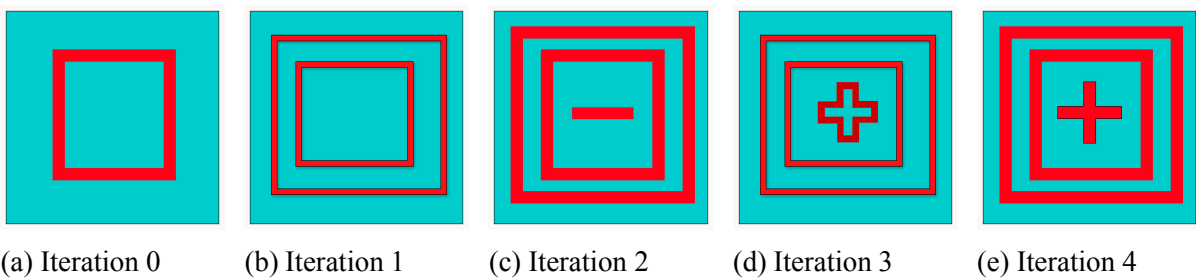


Figure 4.5: Evolution of Absorber-2 shape from iteration 0 to iteration 4

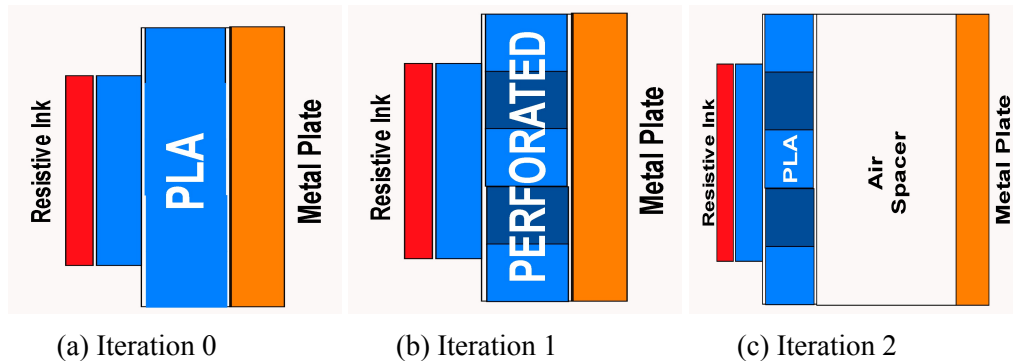
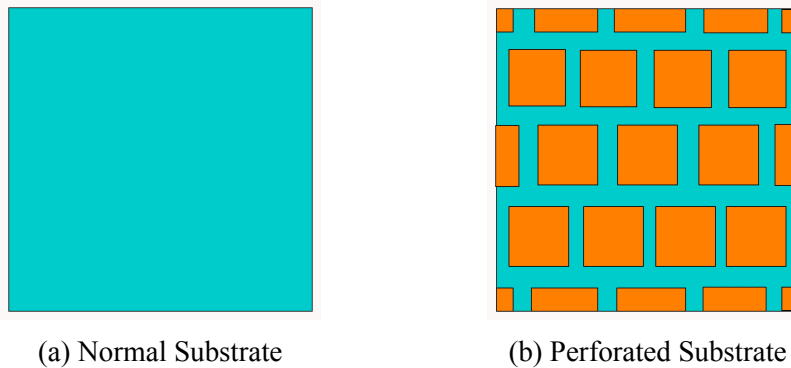


Figure 4.6: Evolution of Geometry of Absorber-2 from iteration 0 to iteration 2



(a) Normal Substrate

(b) Perforated Substrate

Figure 4.7: Modification in Substrate Shape for absorber-2

To increase the mechanical strength of the absorber and resistive ink, we attempted to modify the substrate's perforation. We began by experimenting with various shapes and ultimately settled on a rectangular perforation, as shown in Figure 4.7b, and the side view of the shape in Figure 4.6b iteration 2. As can be seen in iteration 4 in Figure 4.5e, for this we are obtaining god bandwidth with god absorptivity. For this, our bandwidth was reduced once more. To further boost our bandwidth, we opt for a modification in inner form.

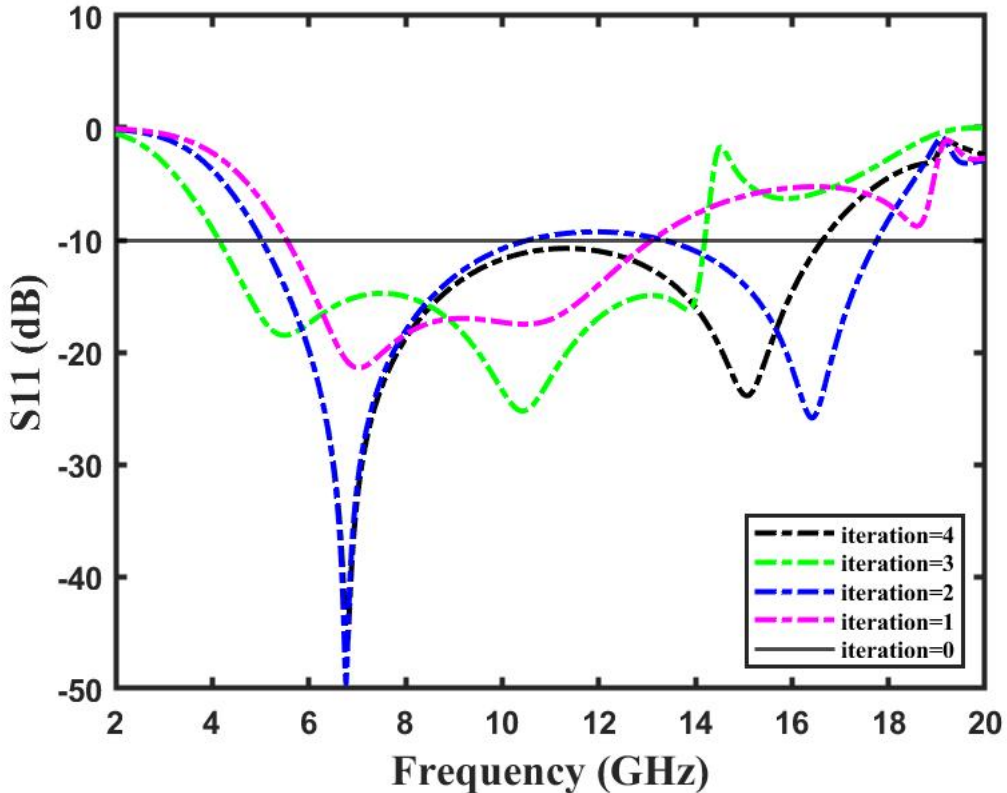


Figure 4.8: Variation of reflection coefficient (S11) of Absorber Design 2 with iterations

We changed our design layers as indicated in iteration 2 of Figure 4.6c because we wanted to create our final design in a conformal manner. By creating an air gap between the absorber and the ground plane, we would be able to provide the absorber flexibility because our substrate thickness is relatively low. In iteration 4, the absorber has ultrawideband Absorptivity with Perfect Impedance Matching with air. The absorber had a fractional bandwidth of 107.54%. The overall dimensions of the proposed antenna are 10 mm x 10 mm x 3.5 mm ($0.29\lambda_o$ mm x $0.29\lambda_o$ mm x $0.102\lambda_o$ mm). The design evolution steps of the patch and ground plane, along with their corresponding S11 of the absorber, are illustrated in Figures 4.9a, 4.9b, 4.9c, 4.9d, and 4.9e respectively. Figures 4.10a and 4.10b exhibit the superior top and bottom views of the proposed absorber, respectively. After its ultimate iteration, the optimized parameters of the absorber are enumerated in Table 4.2.

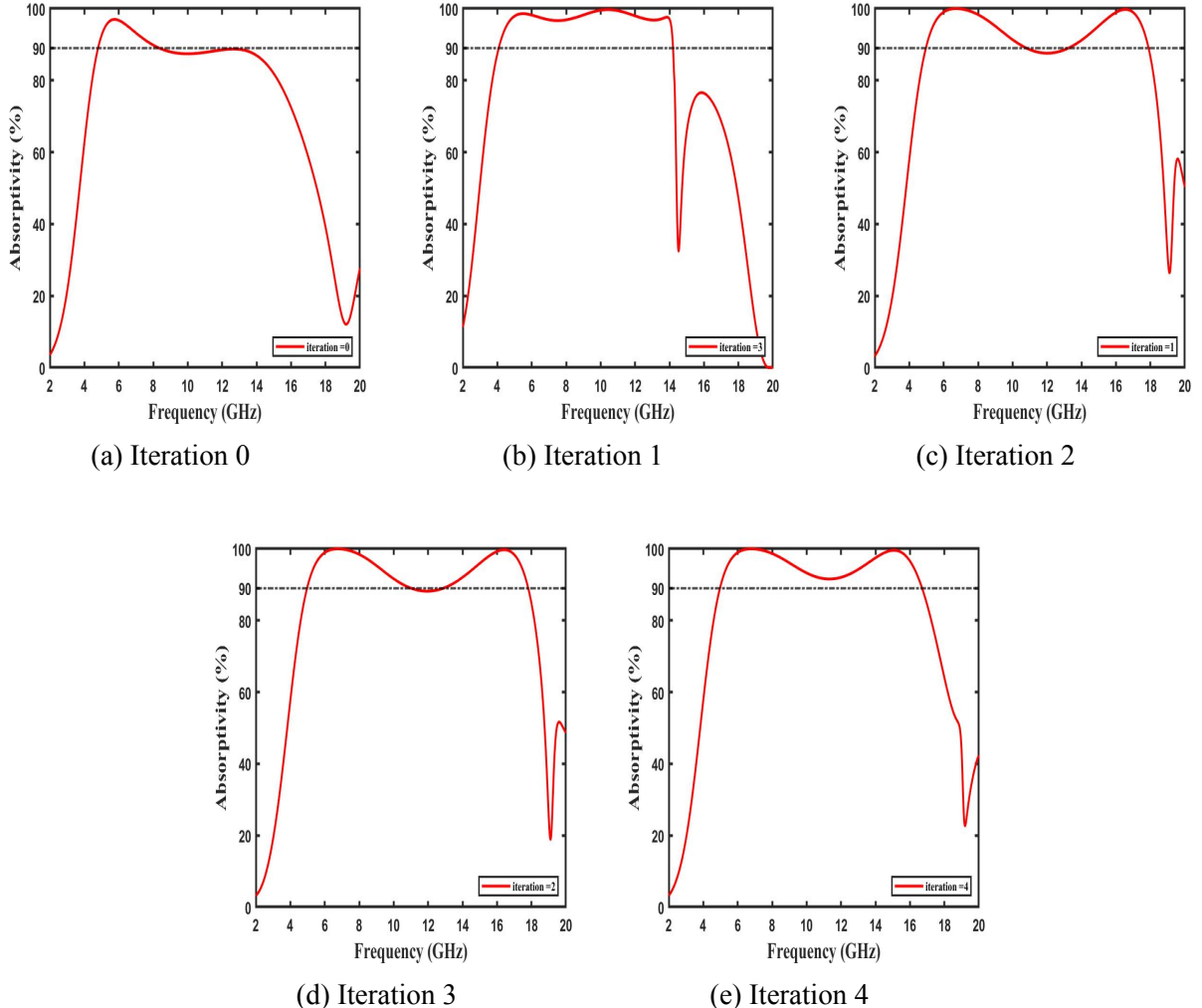


Figure 4.9: Variation of Absorptivity of Proposed Absorber-2 from iteration 0 to iteration 4

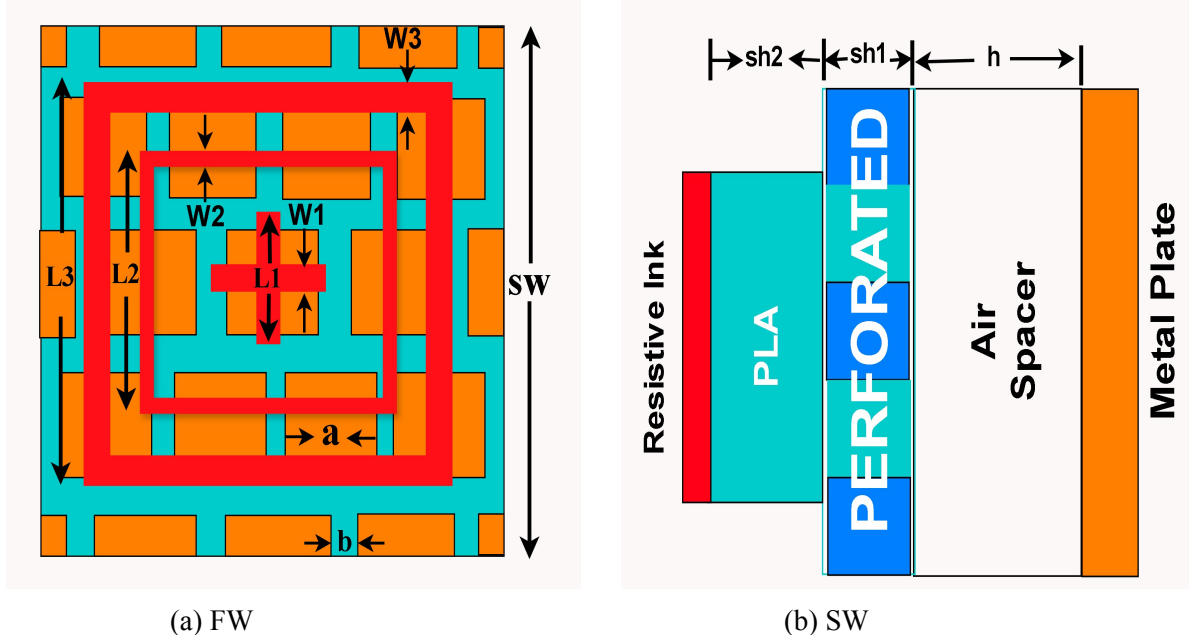


Figure 4.10: Topology of final proposed absorber-2: (a) top view, (b) side view

Table 4.2

Optimized design parameters of proposed absorber-2 in Figure 4.6a and 4.6b

Dimensions (unit: mm)					
L1 = 2.2	L2 = 4.1	L3 = 7.2	W1 = 1	W2 = 0.5	W3 = 0.8
Sh1 = 0.4	Sh2 = 0.1	h = 3	Sw = 10	a = 2	b = 0.5
mt = 0.065			abt = 0.02		

Section 6.1.2 of Chapter 6 delved into the performance of absorber design 1 and **Chapter 5** delved into the fabrication and testing technique. While the absorber does satisfy the essential performance criteria for Broadband and Conformal.

Chapter 5

FABRICATION AND TESTING

5.1 Fabrication

The fabrication Process for the proposed designs follows the following steps as shown in the figure

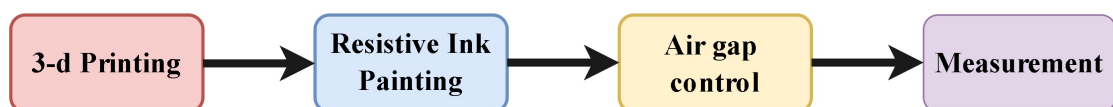


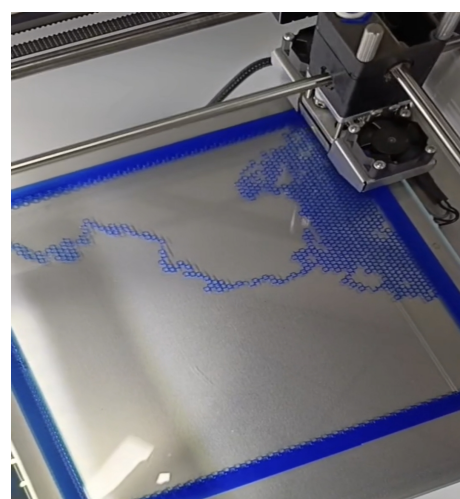
Figure 5.1: Fabrication Flow for Proposed absorbers

It involves integrating advanced 3D printing techniques with carefully selected materials to achieve a lightweight, Flexible, and cost-effective absorber.

5.1.1 3-D Printing Technology



(a)



(b)

Figure 5.2: 3D Printing (a) Printer, (b) Process

Layer-by-Layer Fabrication It is additive manufacturing, which is a process of creating three-dimensional objects by adding material layer by layer based on a digital design. It has gained significant attention and advancement in various fields due to its versatility and potential for customization. This approach enables precise control over dimensions and geometry, allowing for customized designs tailored to specific absorber shape requirements.

Optimized Printing Parameters Engineers configure 3D printing parameters such as layer height and infill density, to achieve the desired structural integrity and flexibility of the absorber. Optimized printing parameters ensure consistent quality and performance of the fabricated design.

5.1.2 Resistive Ink Painting

In this study, a systematic approach was employed to investigate resistive ink painting techniques. The research design was structured to explore the effects of different resist mediums on the outcomes of ink painting. Various resist mediums commonly used in resistive ink painting, including masking fluid, wax, and rubber cement, were selected for experimentation. Each resist medium was applied using different techniques, such as brush application, masking, and stamping, to assess their effectiveness in creating resistive effects.



Figure 5.3: Resistive Ink Material Used

Materials and tools were carefully chosen to ensure consistency and reliability throughout the experiments. High-quality ink suitable for resistive painting was sourced, and a variety of paintbrushes with different bristle types and sizes were utilized to apply the ink and resist mediums. Different types of paper substrates, including watercolor paper and specialty papers, were chosen to explore how substrate characteristics influence resistive ink painting outcomes.

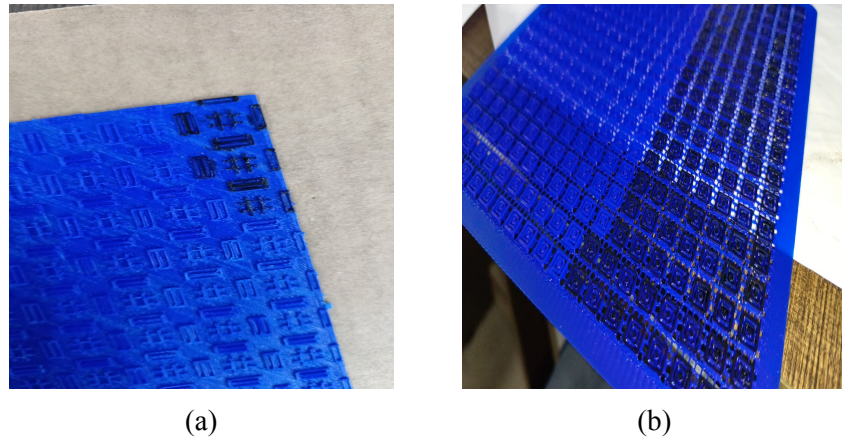


Figure 5.4: Ink painting on proposed absorber (a) Absorber-1 and (b) Absorber-2

Using a paintbrush, we apply resistive ink on 3D printed materials at a precise thickness of 2μ . We employed the material Y Shield ($\sigma = 2800 \text{ S/m}$).

5.1.3 Air Gap Control

Controlled air gaps (e.g., 2mm) between layers during printing are maintained to optimize the weight reduction and flexibility of the proposed absorbers. Precise airgap control enhances the mechanical properties and overall Performance of the fabricated absorber

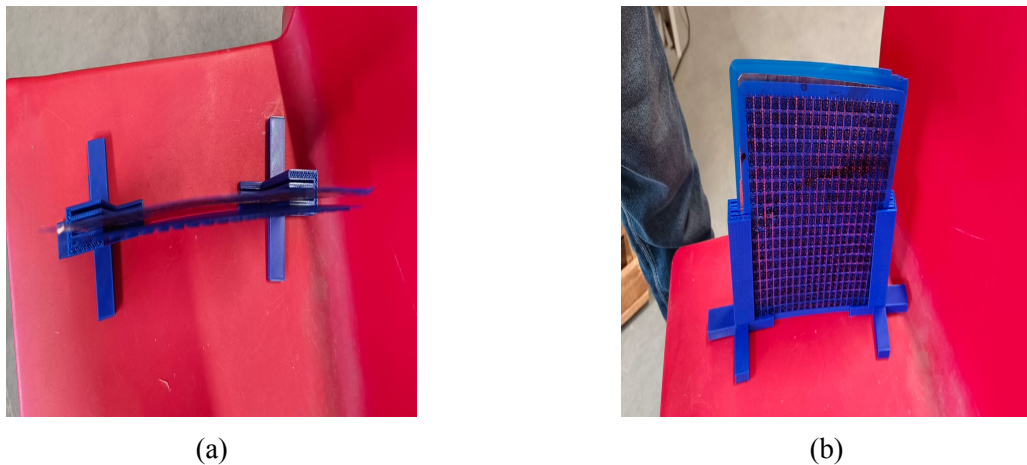


Figure 5.5: Air Gap Stand

To properly support the absorber, we created a platform with thicknesses of 2 mm and 1.5 mm, respectively. We simply used PLA material to create this stand.

5.1.4 Integration of Copper tape



Figure 5.6: Ground Plane

We used Copper tape as our material for the Ground Plane. Copper tape is strategically integrated into the Proposed absorber design to enhance conductivity and improve RF Performance. we stopped transmission via the absorber using the ground plane as a conductor, which may be accomplished with copper tape. Copper tape will enhance Conductivity.

5.1.5 Fabricated Pictures



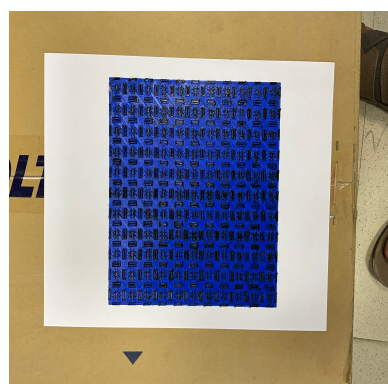
(a) Absorber 1 Unit cell



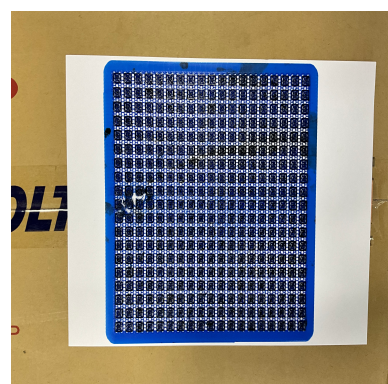
(b) Absorber 2 Unit cell



(c) Bending View



(d) Absorber 1 Ar-
ray 16x16 unit cells



(e) Absorber 1 Ar-
ray 19x19 unit cells

Figure 5.7: Fabricated Designs

5.2 Testing

5.2.1 Measurement setup

The experiment setup for evaluating the performance of the proposed absorbers involved precise measurements conducted within an anechoic chamber, utilizing specialized equipment to assess absorber characteristics and beam manipulation capabilities.

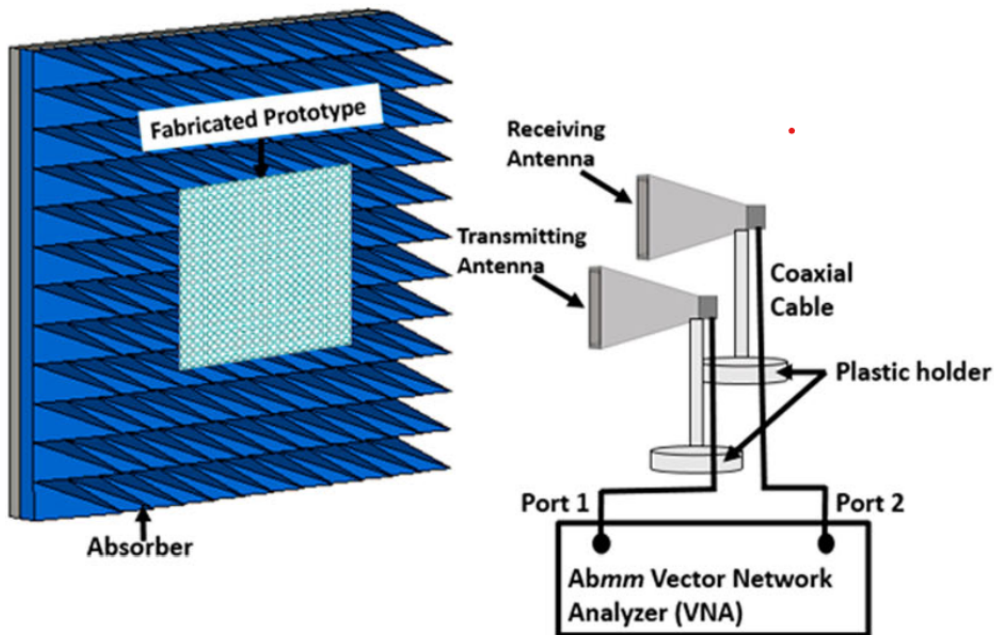


Figure 5.8: Schematic diagram of experimental setup along with ABmm Vector Network Analyzer (VNA) and two horn antenna (transmitter and receiver), and fabricated prototype.

5.2.1.1 Anechoic Chamber

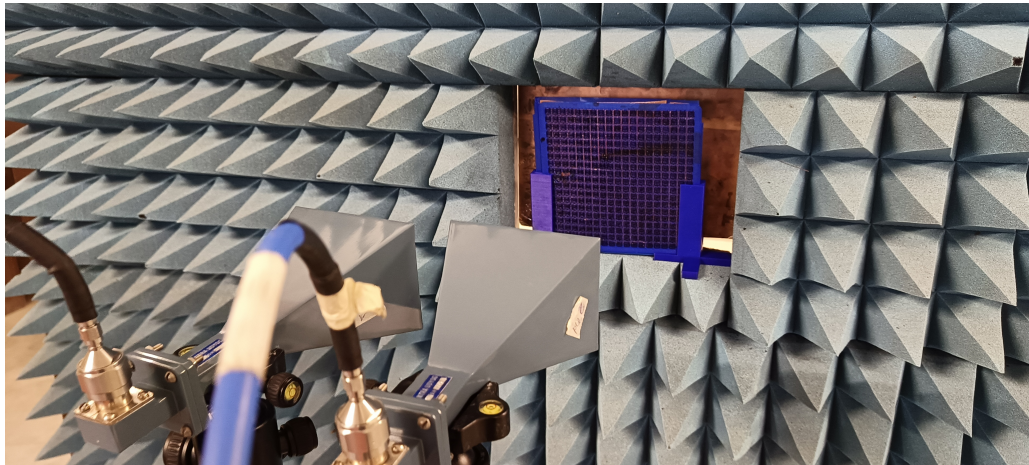
The experiment setup took place in an anechoic chamber as shown in Figure 5.8, providing an isolated and controlled environment free from external electromagnetic interference. This setting ensures accurate measurement of absorber parameters without environmental disturbances.

5.2.1.2 Antenna Configuration

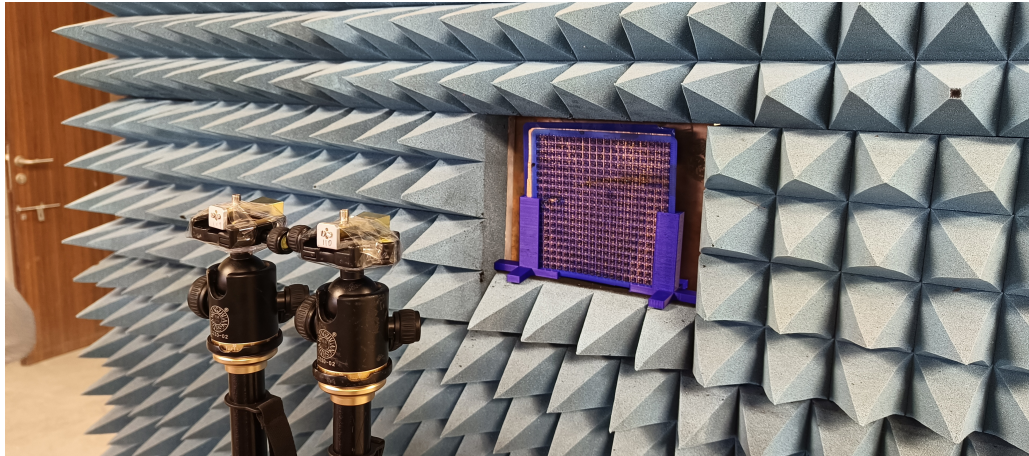
Transmitter A single transmitting antenna was positioned in the far field directly above the proposed absorber at a distance of 550mm. This setup ensures optimal interaction with the absorber for beam manipulation

Receiver The receiving antenna was strategically placed at the same angle, same distance, and same

height with respect to the transmitter antenna, facilitating optimal reception of the reflected signal



(a)



(b)

Figure 5.9: Measurment Setup (a) Horn antenna Setup-1 (4-18GHz), (b) Horn antenna Setup-2 (18-25GHz)

We have used two different antennas for testing as our absorbers are wideband we need two different horn antennas one is from 4-18Ghz and another one is from 18-45 GHz.

5.2.1.3 Measurment Equipment

Vector Network Analyzer(VNA): The experimental setup utilized a VNA equipped with high-frequency capabilities to assess absorber Performance as shown in Figure 5.10. The VNA was configured to feed central frequencies of 10GHz, and 25GHz with a frequency sweep of 0.1GHz and Intermediate Frequency (IF) bandwidth of 50Hz.

5.2.1.4 Data Acquisition and analysis

The VNA facilitated the acquisition of comprehensive data sets, capturing key absorber parameters such as reflection magnitude and beam steering characteristics across the operational frequency range (4-30 GHz). This data formed the basis for evaluating the effectiveness and performance of the proposed absorber design under various operation conditions.

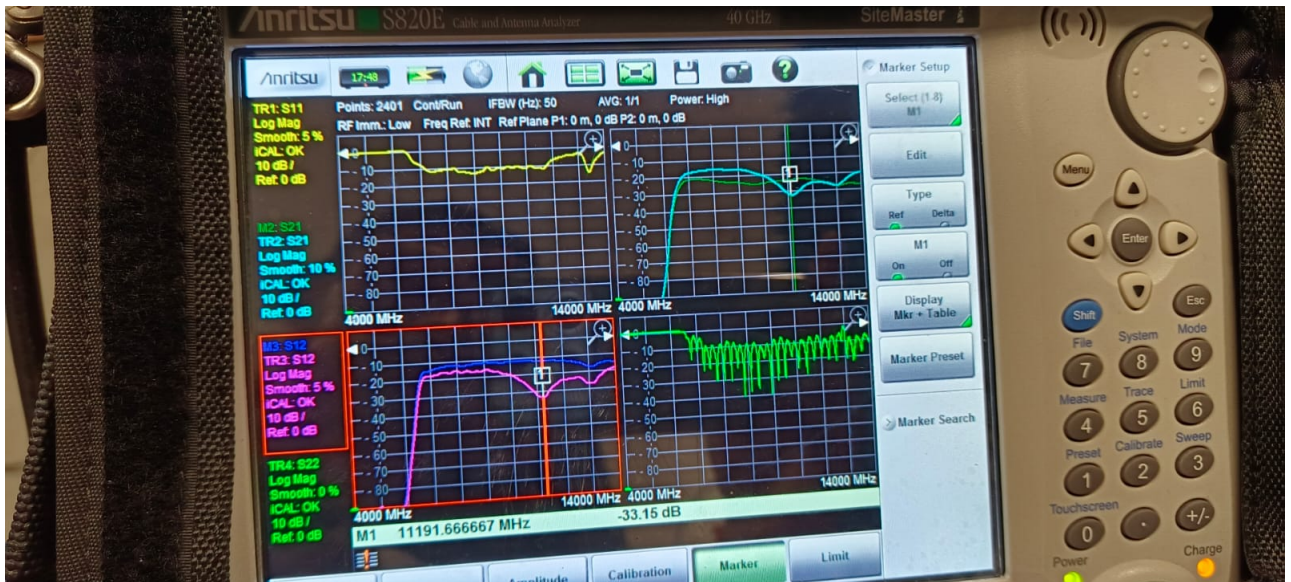


Figure 5.10: Vector Network Analyzer (VNA)

By leveraging this experimental setup within the anechoic chamber and utilizing advanced measurement equipment like that of VNA, engineers were able to conduct rigorous testing and validation of proposed absorber designs, demonstrating its capability for beam bending wide bandwidth.

Chapter 6

RESULTS AND DISCUSSION

This chapter focuses on presenting the results and evaluating the performance of the proposed absorber designs. It also conducts a comparative analysis of the proposed absorber with existing Broadband and Conformal Absorbers.

This chapter focuses on presenting the results and evaluating the performance of the proposed absorber designs. It also conducts a comparative analysis of the proposed absorber with existing Broadband and Conformal Absorbers.

6.1 Performance Analysis of Proposed Absorber Designs

6.1.1 Absorber Design 1

Figure 6.1 depicts the Final Simulated absorber design. The proposed absorber Final S11 and Absorptivity are also shown in Figures 6.2a and 6.2b.

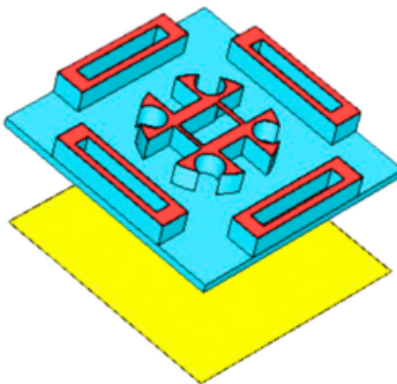


Figure 6.1: Final Simulated proposed absorber 1

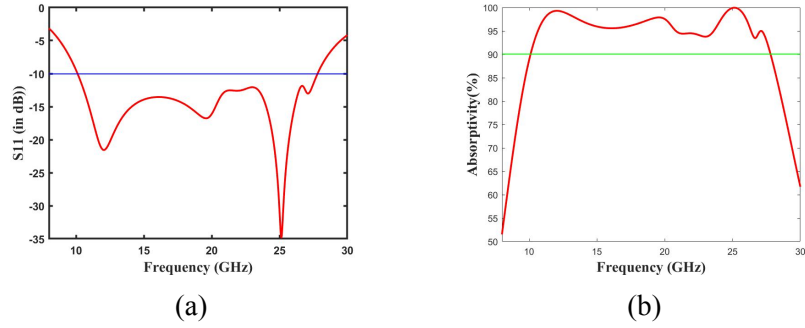


Figure 6.2: Simulated proposed absorber 1 (a) Reflection Coefficient (S_{11}) and (b) Absorptivity

6.1.1.1 S_{11} Parameter

Figure 6.3 illustrates the simulated S_{11} values of the proposed absorber. The simulated S_{11} has a bandwidth of 17.7GHz (10.1 GHz to 27.8 GHz). However, results suggest that the proposed absorber meets the requirements of the frequency band for Wideband.

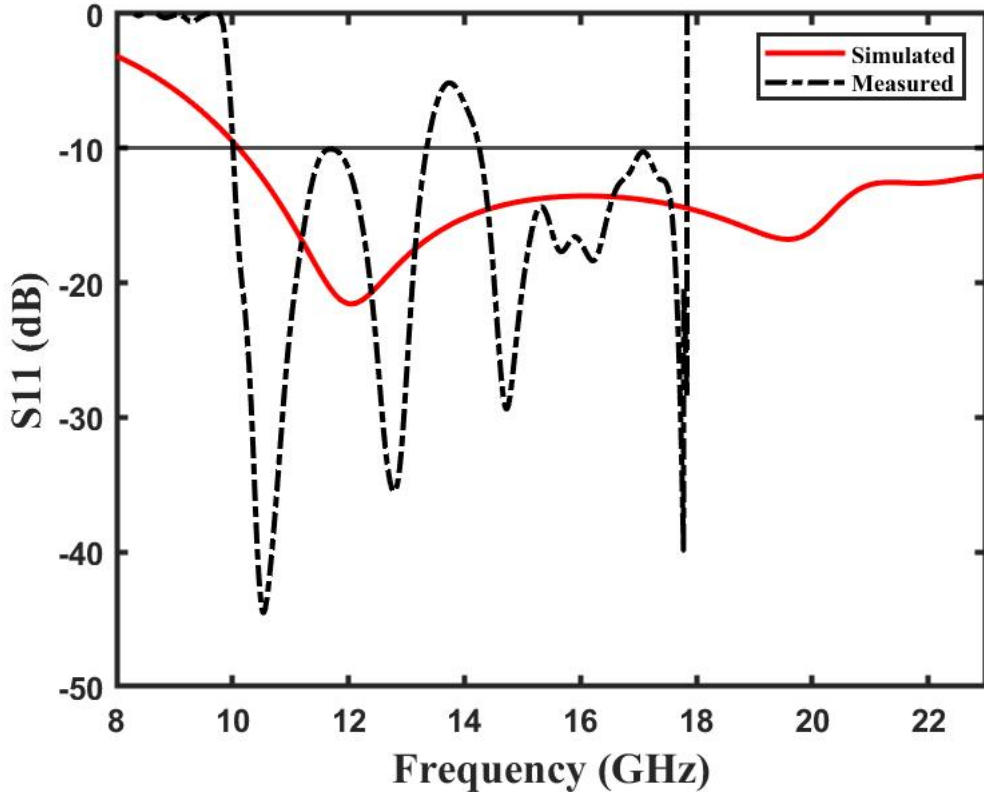


Figure 6.3: Simulated reflection coefficient (S_{11}) of proposed absorber 1

6.1.1.2 Absorptivity

Through examining the S parameters magnitudes, which include the transmission coefficient $S_{21}(w)$ and reflection coefficient $S_{11}(w)$. Using S_{11} and S_{21} , a mathematical relation (6.1) can be used to find absorption $A(w)$.

$$A(w) = 1 - |S_{11}(w)|^2 - |S_{21}(w)|^2 \quad (6.1)$$

Reflection coefficient $S_{11}(w)$ and transmission coefficient $S_{21}(w)$ should be kept as low as feasible to achieve maximal absorption. One way to accomplish zero transmission is to use a metal plate that is deep enough to prevent light waves from penetrating it. Since the other side of the substrate uses the copper ground plane, $|S_{21}(w)|=0$, (6.1) can be translated as (6.2).

$$A(w) = 1 - |S_{11}(w)|^2. \quad (6.2)$$

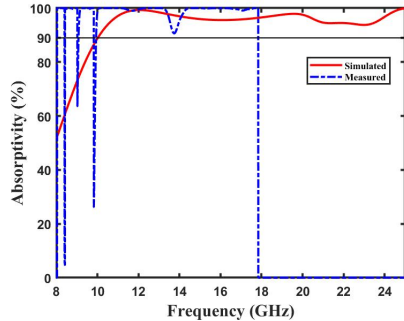


Figure 6.4: Simulated Absorptivity of Proposed Broadband Absorber 1

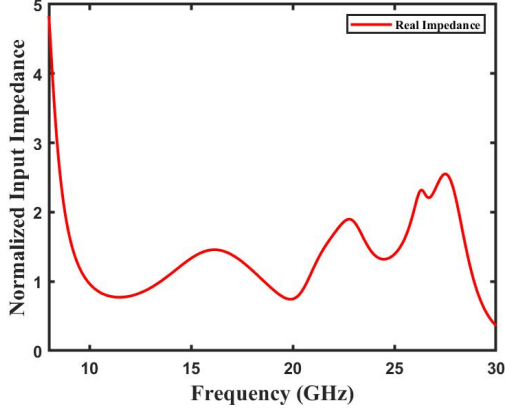
As $A(w)$ is enhanced by (6.2) to achieve greater desired absorption, it is imperative to maintain a low reflection coefficient $S_{11}(w)$.

As can be seen from Figure 6.4, this results in wideband %, which covers the entire Ku and Ka bands.

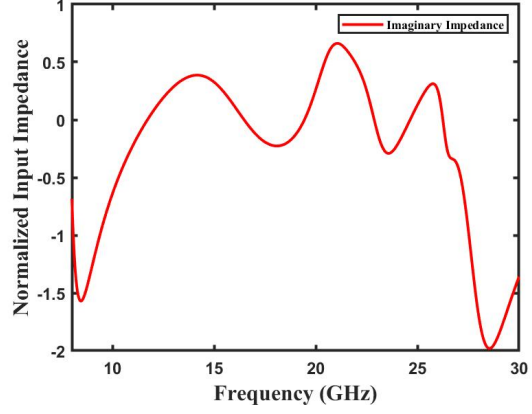
6.1.1.3 Impedance (Z_{in})

If the absorber top surface's resonator layer impedance and the free space impedance are equal, S_{11} will be minimum. Since free space impedance $Z_o = 377\Omega$ or 120π is known, the proposed absorber's input impedance $Z(w)$ must equal or substantially equal Z_o . The following formula (6.3) can be used to determine the structure's effective impedance.

$$Z_{eff}(w) = \sqrt{\frac{\mu_{eff}}{\epsilon_{eff}}} = \sqrt{\frac{(1 + S_{11}(w))^2 - (S_{21}(w))^2}{(1 - S_{11}(w))^2 - (S_{21}(w))^2}} \quad (6.3)$$



(a) Real part.



(b) Imaginary Part.

Figure 6.5: Normalized Input Impedance of Proposed Absorber 1.

where the effective permittivity and permeability are denoted by $\epsilon_{eff}(w)$ and $\mu_{eff}(w)$, respectively. The computed complex S characteristics are used to calculate the impedance's real and imaginary components. Figure 6.5a and 6.5b illustrate that the impedance's computed real and imaginary components were almost equal, with the real part approaching unity as the imaginary part neared 0 in the absorption band.

Since the absorber's input impedance is almost equal to the impedance of free space $(377 + j0)\Omega$, less power is reflected from the structure, and maximum absorptivity occurs at the desired frequency band. Consequently, impedance matching with air was accomplished, which reduced the absorber's reflection.

6.1.1.4 Polarization (Normal Incidence)

When electromagnetic waves (EM) strike an absorber surface perpendicular to its surface, it is referred to as "normal incidence". This Section discusses the design of our metamaterial absorber, which guarantees that the reflection characteristics stay the same, irrespective of the angle of polarization (ϕ) of the incident electromagnetic wave. This indicates that changes in the polarization angle of the incident wave do not affect much the absorber's reflectance.

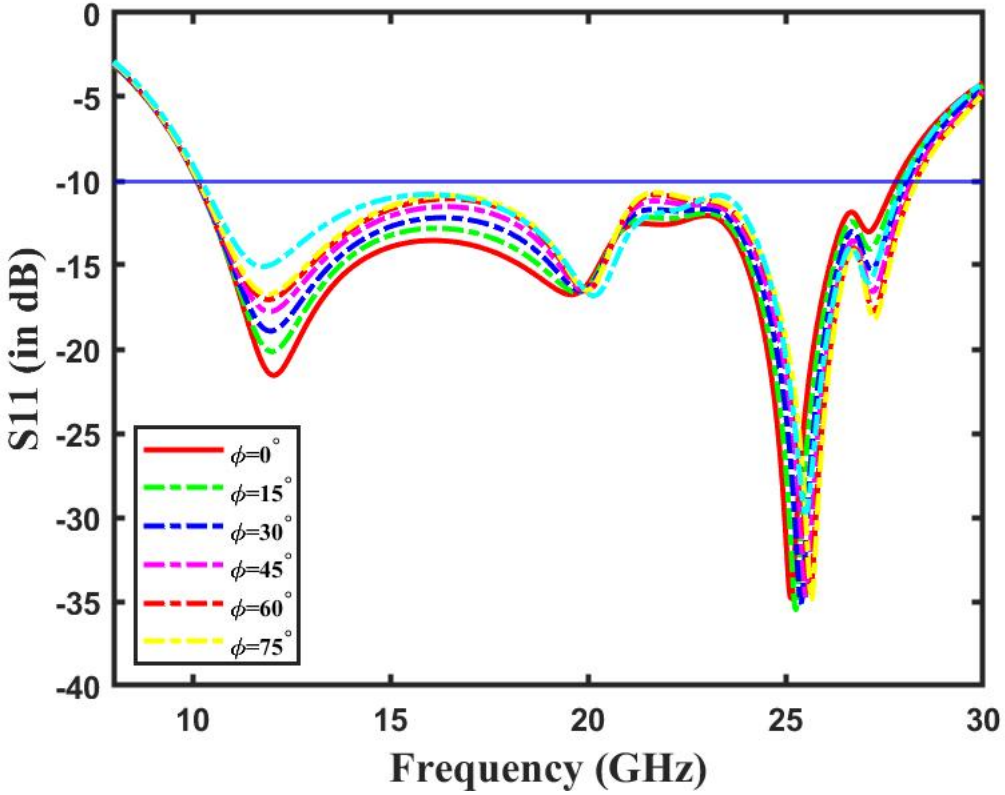


Figure 6.6: various polarization angles under normal incidence.

This leads to the same reflection properties at all angles of polarization (ϕ) of the incident electromagnetic wave, as shown in Figure 6.6. The design can be regarded as polarization-insensitive under normal incidence because of the symmetrical character of the suggested design, which maintains the reflectivity for a range of polarization angles. The synthetic sample's absorption at normal incidence was higher than within the frequency range of 10.1 – 27.7 GHz, the manufactured sample's absorption at normal incidence was greater than 90%.

6.1.1.5 Oblique Incidence

The following equations (6.4) (6.5) define the reflection coefficients under the oblique incidence angle for the TE polarization (Γ_{\perp}) and the TM polarization (Γ_{\parallel}):

$$\Gamma_{\perp} = \frac{Z(w) \cos \theta_i - Z_o \cos \theta_t}{Z(w) \cos \theta_i + Z_o \cos \theta_t}. \quad (6.4)$$

$$\Gamma_{\parallel} = \frac{Z(w) \cos \theta_t - Z_o \cos \theta_i}{Z(w) \cos \theta_t + Z_o \cos \theta_i}. \quad (6.5)$$

where the transmission angle is θ_t and the incidence angle is θ_i .

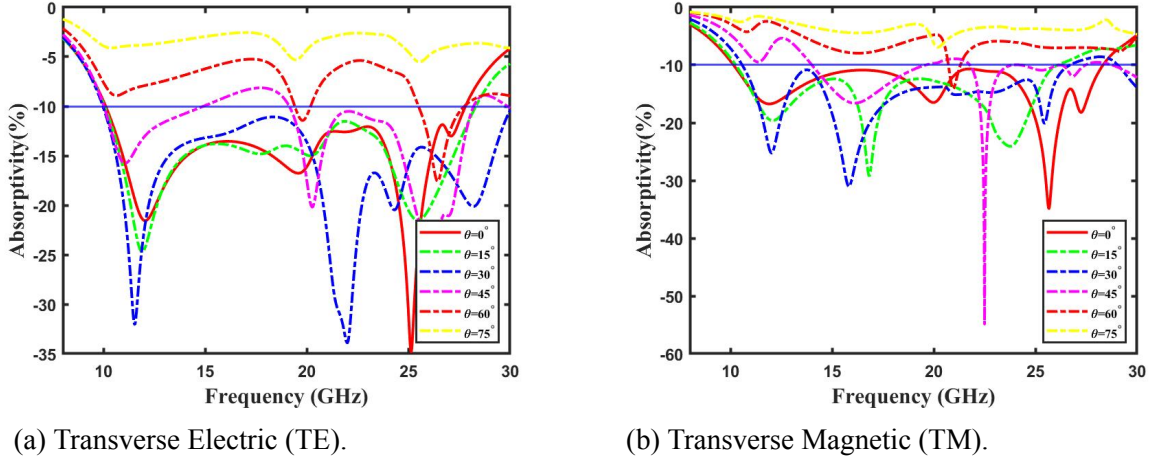


Figure 6.7: Simulated absorptivity at different incident angles.

It can be shown from Eqs. (6.4) and (6.5) that as the incident angle varies, so does the reflection coefficient. Figure 6.7a and 6.7b show the absorber structure's incidence angle (θ) fluctuations under TE and TM polarizations, respectively. As seen in Figure 6.7a, with TE polarization, the E-field direction stays constant while the electromagnetic wave's propagation direction and the magnetic field's direction rotate at different incidence angles. When there is TM polarization, the H-field direction stays constant but the electric field and electromagnetic wave propagation directions rotate at different incidence angles. The structure is therefore examined for oblique incidence. Various incidence angles were used to illustrate the reflectivity in Figure 6.7a and 6.7b. Under TE polarization, Figure 6.7a illustrates broadband absorption (reflectivity below -10 dB) up to a 45° angle of incidence; however, the response deteriorates during TM mode, as shown in Figure 6.7b for $\Phi = 0^\circ$. Transverse electric field polarization is stable up to 45° , as Figure 6.7b illustrates, and after 60° , the bandwidth narrows as the angle increases. On the other hand, absorptivity drops to 90% in the transverse magnetic field polarization, but the response is moved to a higher frequency.

6.1.1.6 Polarization Conversion Ratio (PCR)

In order to confirm the absorption behavior of the structure, the unit cell shape was examined using various polarized electromagnetic waves. Figure 6.8a displays the polarization conversion ratio (PCR) 6.8b displays the polarization conversion ratio (PCR) versus Absorptivity. Under the assumption that the incident electromagnetic wave was y-polarized, the cross-polarized component (R_{xy}) is very minor throughout the operating range, while the co-polarized reflectance (R_{yy}) is discovered matching with the real reflection coefficient (S_{11}) given above. It is further demonstrated that the PCR expression, as determined by Eq (6.6),

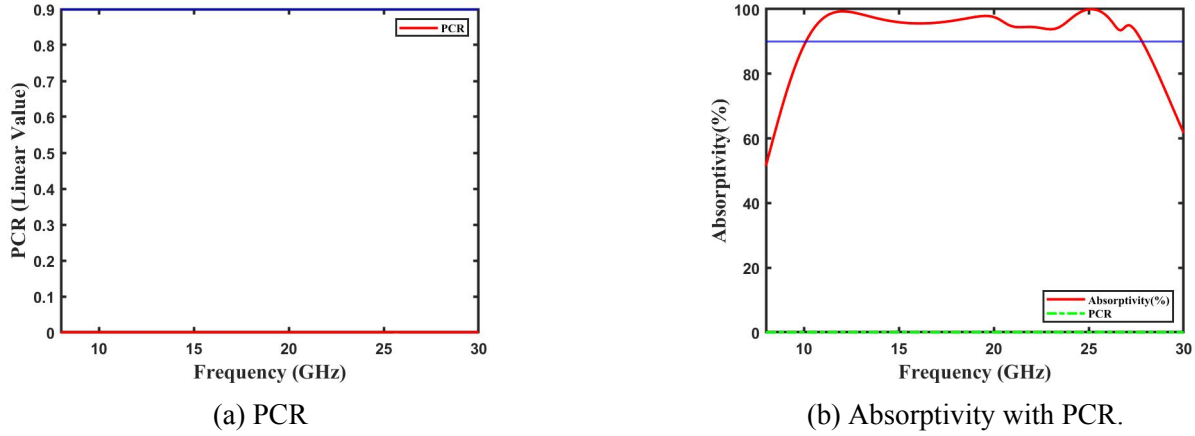


Figure 6.8: For Proposed Broadband Absorber 1.

$$R_{yy} = \frac{|E_{y_r}|}{|E_{y_i}|}, R_{xy} = \frac{|E_{x_r}|}{|E_{y_i}|}, PCR = \frac{|R_{xy}|^2}{|R_{xy}|^2 + |R_{yy}|^2}. \quad (6.6)$$

has extremely modest values (less than 0.00053) throughout the Ku-band, and Ka-band. Thus, the structure verifies that it functions as an absorber rather than a polarizer.

6.1.1.7 Parametric Analysis

We did a Parametric analysis of all the parameters that we have used for designing and for perfect results

Effect of Air gap(h):

The height of the spacer (h) has been varied from 0 mm to 4 mm with intervals of 0.5 mm in order to examine the impact of the free space between the substrate and the ground plane. As the height of the spacer grows, the corresponding capacitance also changes. This causes the $\frac{\lambda}{4}$, which is related to the dielectric thickness, to routinely increase. As a result, the absorption band shifts towards the lower frequency side. The spacer height of 1.5 mm is optimal as it covers the entire the Ku-band and Ka-band, as illustrated in Figure 6.9a. As a result, the thickness was tuned to 1.5 mm in order to attain a high bandwidth.

Effect of conductivity of INK(σ):

Figure 6.9b shows that when the conductivity is changed, the absorption performance first increases but then declines as the conductivity increases. Using the four-probe approach [19], the resistive ink's conductivity was found to be 2800 S/m through experimentation.

Effect of Substrate thickness (SH

In Figure 6.9c, the absorptivity is demonstrated by varying the substrate's thickness (SH) from 0.7 mm to 0.2 mm, with a 0.1 mm width. It is noted that the absorption bandwidth dropped slightly as SH increased. Conversely, it will not be conformal as the substrate thickness rises. and by moving toward higher frequencies while reducing bandwidth improves The flexible substrate with a thickness of 0.5 mm was selected based on availability in order to attain the highest absorption bandwidth.

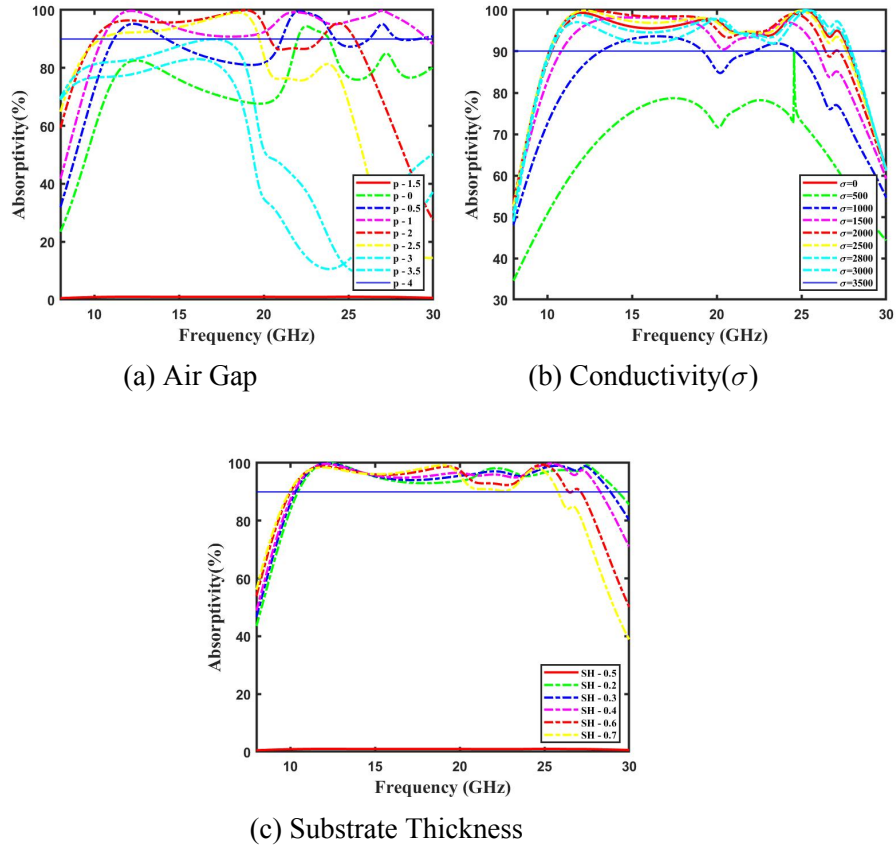


Figure 6.9: Variation of the different design parameters of the proposed broadband absorber 1.

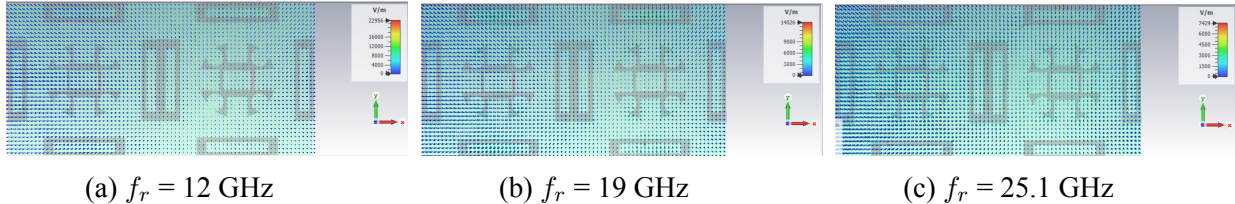
6.1.1.8 Field Distribution

In this section, we will describe the field distribution of our proposed metamaterial-based broadband and conformal absorber. As we can see from the reflection coefficient graph, there are three dips at three different frequencies: 12GHz, 19GHz, and 25.1GHz, respectively. We analyzed both fields at these three different frequencies. As shown in Figure 6.11, we plotted both electric and magnetic field distributions.

As shown in the Figure 6.11, the electric field is almost negligible in the substrate part, but there is variation between all resonant frequencies, and we have observed the electric field in both directions,

Transverse Electric (TE) and Transverse Magnetic (TM), and we have observed the difference in electric field in both cases, as we conclude that the electric field changes in the perpendicular direction in TE and TM mode respectively.

TE:



TM:

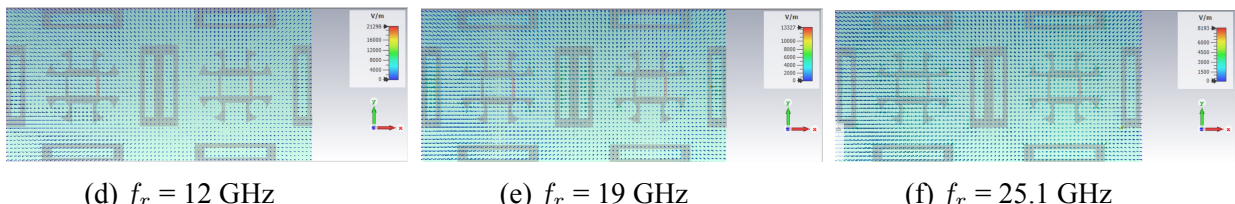
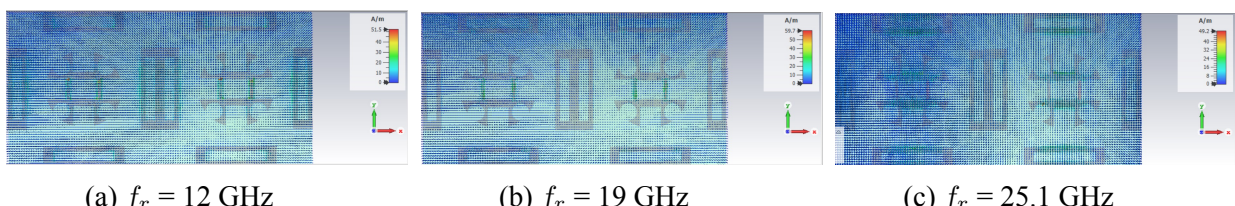


Figure 6.10: Variation of Electric Field of Proposed Absorber 1

TE:



TM:

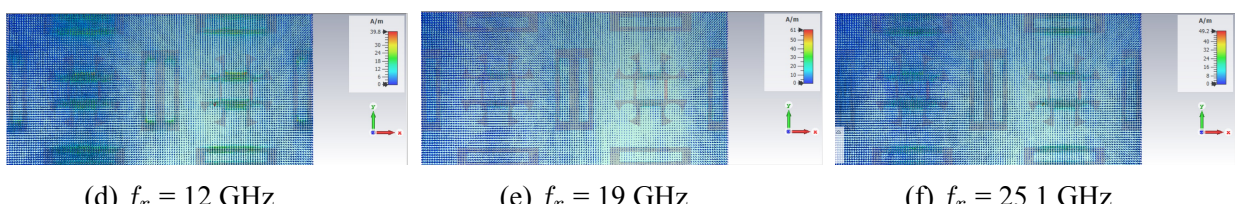
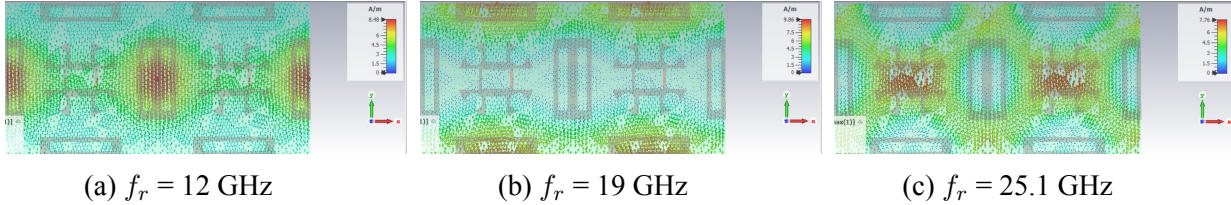


Figure 6.11: Variation of Magnetic Field of Proposed Absorber

We also saw the magnetic field distribution of our proposed absorber at 3 dips (3 resonant frequencies 12, 19, 25.1 GHz) as we can see in Figure 6.11 for the magnetic field. We also observed in TE and TM in this case and we have observed that at low frequencies outer loop contributes and for higher frequencies inner shapes contribute as we can clearly see in Figure 6.11.

6.1.1.9 Surface Current Density

TE:



TM:

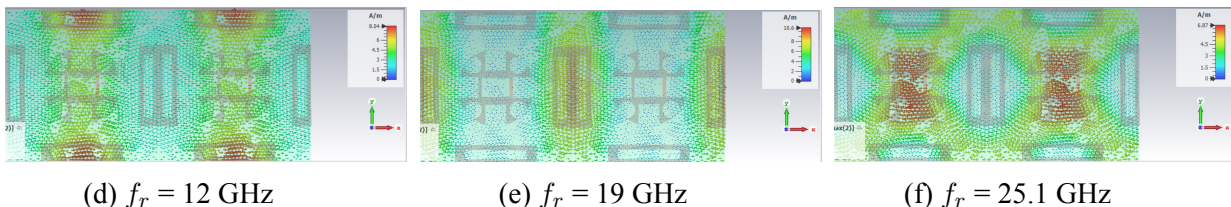
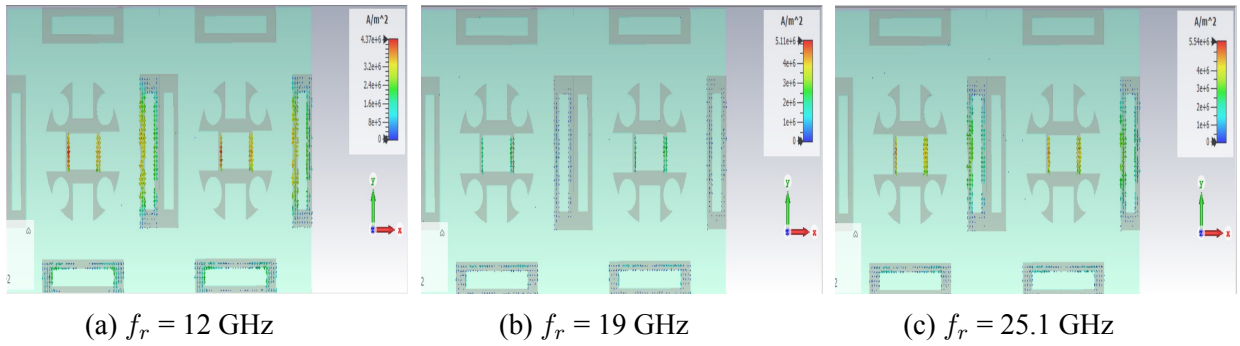


Figure 6.12: Variation of Surface Current Distribution of Proposed Absorber 1 on resistive ink

In this section, we will discuss the current distribution of the proposed absorber on the ground plane as well as resistive ink. We also observed that there is a very less electric field in resistive ink because of its high resistivity, so there will be very negligible surface current in the direction of the electric field in resistive ink. However, because our ground plane is copper, which has very low Resistivity, there will be more surface current in the ground plane while compared to resistive ink. By observing in Figure 6.12 we can observe current distribution in the loops at different frequencies and we conclude that due to the outer loop, there is more contribution of current at lower frequencies, and at 12 GHz more current is contributed in the loop as seen in Figure 6.12a as TE and 6.12d as TM and at middle frequencies like 19 GHz inner or middle loop contribute more current as we seen in Figure 6.12b as TE and 6.12e as TM as we are going to higher frequencies inner shape is started contributing current to the design for 25.1 GHz we can see in Figure 6.12c as TE and 6.12f as TM.

We also saw current distribution on the ground plane as our ground plane is very near to the substrate very small air gap of 1.5 mm only as my substrate acts as a transmission line so the electric field will transfer to the ground plane and the ground plane will act as a short circuit due to this short circuit transmission of EM wave will be very less hence this will act as perfect absorber, as we can see in Figure 6.13 there is a current in ground plane we have examined both TE and TM mode in this case

TE:



TM:

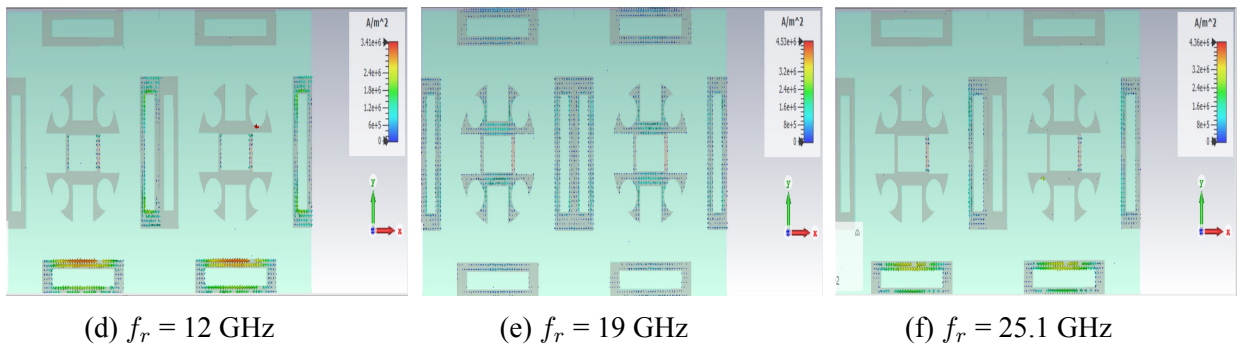


Figure 6.13: Variation of Surface Current Distribution of Proposed Absorber 1 on Resistive Ink

We evaluated these at three resonating frequencies (12, 19, 25.1 GHz), which can also be observed in Figure 6.13. In TE mode, current flows upwards, as shown in Figure 6.13a, and in TM mode, current flows left to right, as shown in Figure 6.13d, however, the density of current varies with frequency.

6.1.2 Absorber Design 2

Figure 6.14 depicts the Final Simulated absorber design. The proposed absorber Final S11 and Absorptivity are also shown in Figures 6.15a and 6.15b.

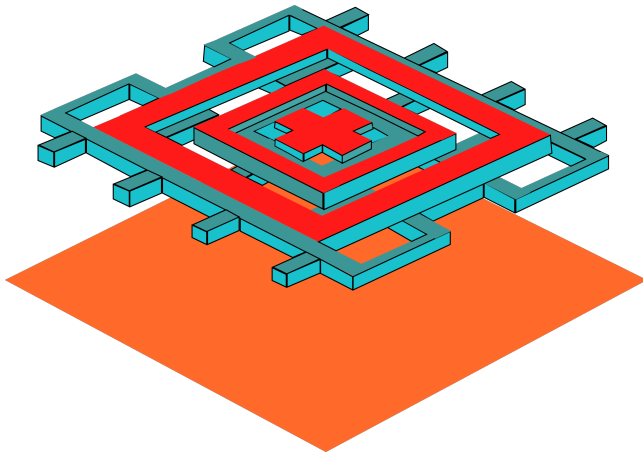


Figure 6.14: Final Simulated proposed absorber 2

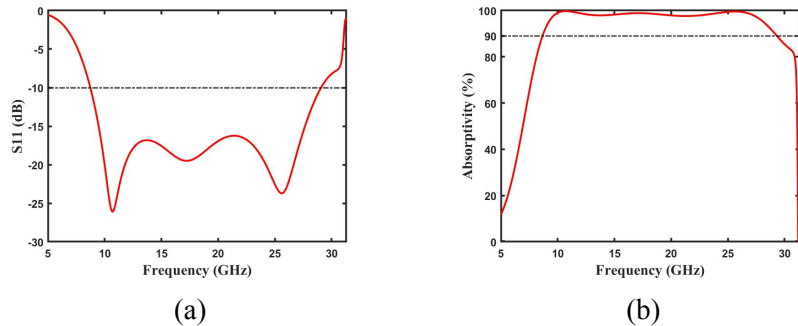


Figure 6.15: Simulated proposed absorber-2 (a) Reflection Coefficient (S11) and (b) Absorptivity

6.1.2.1 S_{11} Parameter

Figure 6.16 illustrates the simulated and measured S_{11} values of the proposed absorber. The simulated S_{11} has a bandwidth of 20.34GHz (8.73 GHz to 29.07 GHz) and a fractional bandwidth of 107.54%. The measured S_{11} , while slightly differing from the simulated values, still demonstrates a 2.4 – 2.5 GHz band, with a value of -22 dB at 2.45 GHz. The difference between these values can be attributed to fabrication and soldering errors. However, both results suggest that the proposed absorber meets the requirements of the frequency band for Wideband.

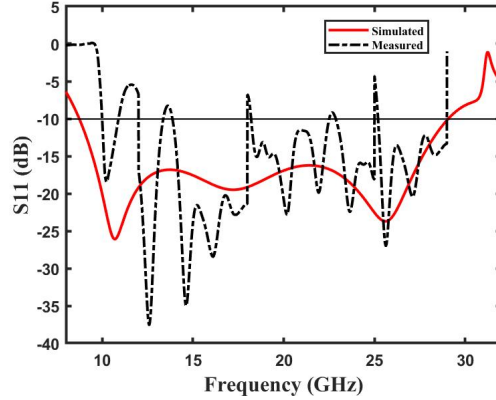


Figure 6.16: Simulated and measured reflection coefficient (S_{11}) of proposed absorber-2

6.1.2.2 Absorptivity

Through examining the S parameters magnitudes, which include the transmission coefficient $S_{21}(w)$ and reflection coefficient $S_{11}(w)$. Using S_{11} and S_{21} , a mathematical relation (6.7) can be used to find absorption $A(w)$.

$$A(w) = 1 - |S_{11}(w)|^2 - |S_{21}(w)|^2 \quad (6.7)$$

Reflection coefficient $S_{11}(w)$ and transmission coefficient $S_{21}(w)$ should be kept as low as feasible to achieve maximal absorption. One way to accomplish zero transmission is to use a metal plate that is deep enough to prevent light waves from penetrating it. Since the other side of the substrate uses the copper ground plane, $|S_{21}(w)|=0$, (6.7) can be translated as (6.8).

$$A(w) = 1 - |S_{11}(w)|^2. \quad (6.8)$$

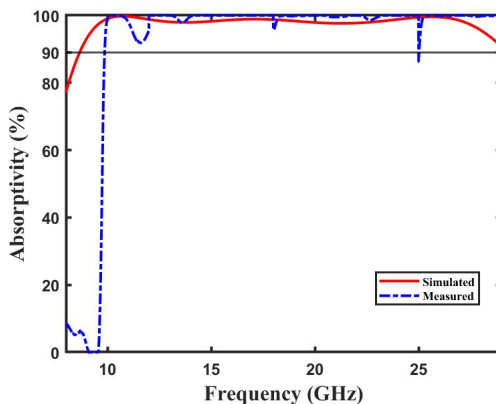


Figure 6.17: Simulated and Measured Absorptivity of Proposed Broadband Absorber-2

As $A(w)$ is enhanced by (6.2) to achieve greater desired absorption, it is imperative to maintain a low reflection coefficient $S_{11}(w)$. As can be seen from Figure 6.17, this results in a fractional bandwidth of 107.54%, which covers the X, Ku, and K bands.

6.1.2.3 Impedance (Z_{in})

If the absorber top surface's resonator layer impedance and the free space impedance are equal, S_{11} will be minimum. Since free space impedance $Z_o = 377\Omega$ or 120π is known, the proposed absorber's input impedance $Z(w)$ must equal or substantially equal Z_o . The following formula (6.9) can be used to determine the structure's effective impedance.

$$Z_{eff}(w) = \sqrt{\frac{\mu_{eff}}{\epsilon_{eff}}} = \sqrt{\frac{(1 + S_{11}(w))^2 - (S_{21}(w))^2}{(1 - S_{11}(w))^2 - (S_{21}(w))^2}} \quad (6.9)$$

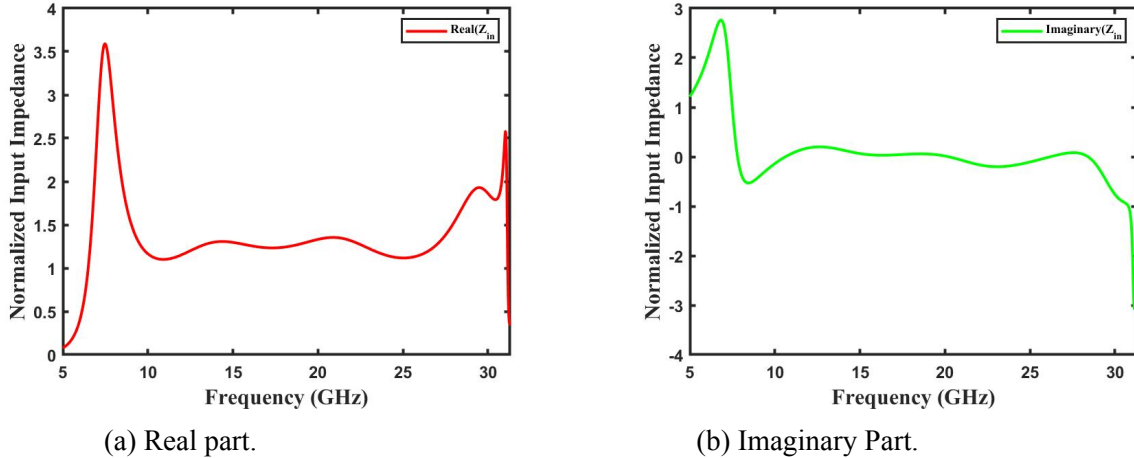


Figure 6.18: Normalized Input Impedance of Proposed Absorber-2.

where the effective permittivity and permeability are denoted by $\epsilon_{eff}(w)$ and $\mu_{eff}(w)$, respectively. The computed complex S characteristics are used to calculate the impedance's real and imaginary components. Figure 6.18a and 6.18b illustrate that the impedance's computed real and imaginary components were almost equal, with the real part approaching unity as the imaginary part neared 0 in the absorption band.

Since the absorber's input impedance is almost equal to the impedance of free space $(377 + j0)\Omega$, less power is reflected from the structure, and maximum absorptivity occurs at the desired frequency band. Consequently, impedance matching with air was accomplished, which reduced the absorber's reflection.

6.1.2.4 Polarization (Normal Incidence)

A minor anisotropy (truncation at the borders) is applied to the perforated shape core in order to ensure the unit cell structure becomes precisely square.

When electromagnetic waves (EM) strike an absorber surface perpendicular to its surface, it is referred to as "normal incidence". This Section discusses the design of our metamaterial absorber, which guarantees that the reflection characteristics stay the same, irrespective of the angle of polarization (ϕ) of the incident electromagnetic wave. This indicates that changes in the polarization angle of the incident wave do not affect the absorber's reflectance.

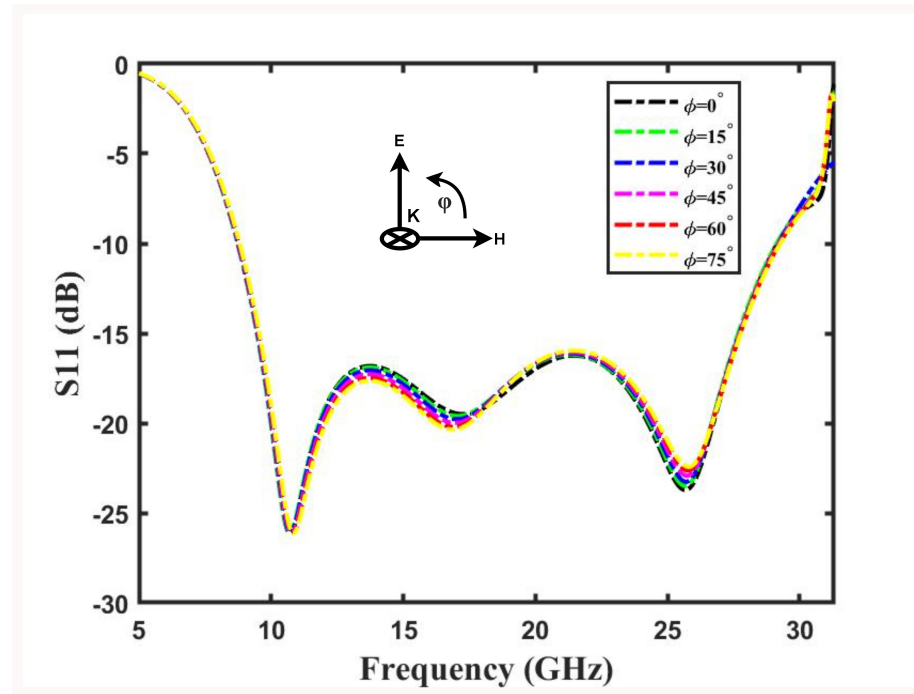


Figure 6.19: Simulated reflection coefficient of the proposed broadband absorber-2 for various polarization angles under normal incidence.

This leads to the same reflection properties at all angles of polarization (ϕ) of the incident electromagnetic wave, as shown in Figure 6.19. The design can be regarded as polarization-insensitive under normal incidence because of the symmetrical character of the suggested design, which maintains the reflectivity for a range of polarization angles. The synthetic sample's absorption at normal incidence was higher than within the frequency range of 8.74 – 29.07 GHz, the manufactured sample's absorption at normal incidence was greater than 90%.

6.1.2.5 Oblique Incidence

The following equations (6.10) (6.11) define the reflection coefficients under the oblique incidence angle for the TE polarization (Γ_{\perp}) and the TM polarization ($\Gamma_{||}$):

$$\Gamma_{\perp} = \frac{Z(w) \cos \theta_i - Z_o \cos \theta_t}{Z(w) \cos \theta_i + Z_o \cos \theta_t}. \quad (6.10)$$

$$\Gamma_{||} = \frac{Z(w) \cos \theta_t - Z_o \cos \theta_i}{Z(w) \cos \theta_t + Z_o \cos \theta_i}. \quad (6.11)$$

where the transmission angle is θ_t and the incidence angle is θ_i .

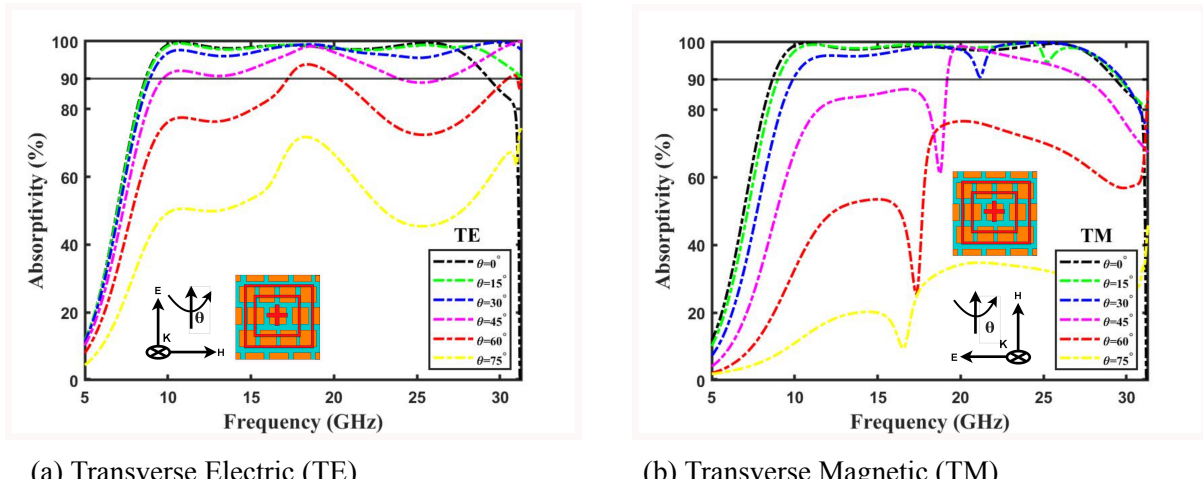


Figure 6.20: Simulated absorptivity at different incident angles.

It can be shown from Eqs. (6.10) and (6.11) that as the incident angle varies, so does the reflection coefficient. Figure 6.20a and 6.20b show the absorber structure's incidence angle (θ) fluctuations under TE and TM polarizations, respectively. As seen in Figure 6.20a, with TE polarization, the E-field direction stays constant while the electromagnetic wave's propagation direction and the magnetic field's direction rotate at different incidence angles. When there is TM polarization, the H-field direction stays constant but the electric field and electromagnetic wave propagation directions rotate at different incidence angles. The structure is therefore examined for oblique incidence. Various incidence angles were used to illustrate the reflectivity in Figure 6.20a and 6.20b. Under TE polarization, Figure 6.20a illustrates broadband absorption (reflectivity below -10 dB) up to a 45° angle of incidence; however, the response deteriorates during TM mode, as shown in Figure 6.20b for $\Phi = 0^{\circ}$. Transverse electric field polarization is stable up to 45° , as Figure 6.20b illustrates, and after 60° , the bandwidth narrows as the angle increases. On the other hand, absorptivity drops to 90% in the transverse magnetic field polarization, but the response is moved to a higher frequency.

6.1.2.6 Polarization Conversion Ratio (PCR)

In order to confirm the absorption behavior of the structure, the unit cell shape was examined using various polarized electromagnetic waves. Figure 6.21a shows the co-polarized and cross-polarized reflectance, while Figure 6.21b displays the polarization conversion ratio (PCR). Under the assumption that the incident electromagnetic wave was y-polarized, the cross-polarized component (R_{xy}) is very minor throughout the operating range, while the co-polarized reflectance (R_{yy}) is discovered matching with the real reflection coefficient (S_{11}) given above. It is further demonstrated that the PCR expression, as determined by Eq (6.12),

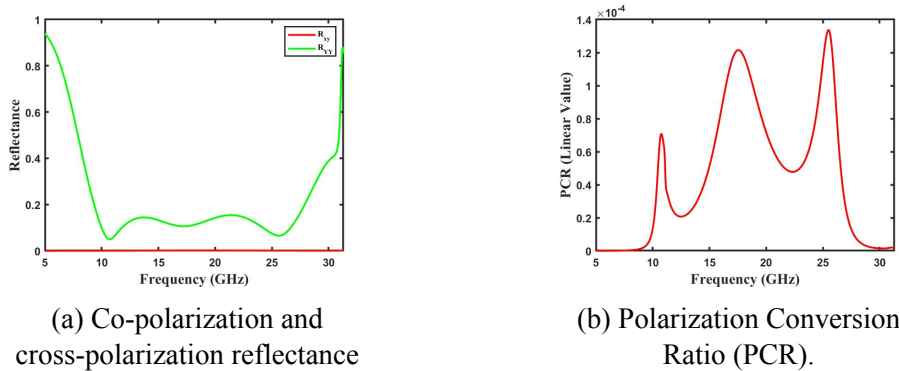


Figure 6.21: For Proposed Broadband Absorber-2.

$$R_{yy} = \frac{|E_{y_r}|}{|E_{y_i}|}, R_{xy} = \frac{|E_{x_r}|}{|E_{y_i}|}, PCR = \frac{|R_{xy}|^2}{|R_{xy}|^2 + |R_{yy}|^2}. \quad (6.12)$$

has extremely modest values (less than 0.05) throughout the X-band, Ku-band, and K-band. Thus, the structure verifies that it functions as an absorber rather than a polarizer.

6.1.2.7 Equivalent Circuit Analysis

An analogous circuit model has been created in order to analyze the suggested absorber, as shown in Figure 6.22a. Resistance, inductance, and capacitance are combined in series to replicate the geometry's square loops and plus form. R2-L2-C2, R3-L3-C3, and R1-L1-C1 correspond to the inner and outer loops and inner shape, respectively. Resistances come from the lossy characteristics of the resistive ink, while inductances are generated from the top square loop patterns. The gap between the inner loop and the inner structure results in capacitance C1, the distance between the inner and outer loop results in capacitance C2, and the gap between the outer loops across the next unit cells results

in capacitance C3.

$$Z_{in} = ZFSS1 || ZFSS2 || ZFSS3 || Z_{d1}. \quad (6.13)$$

$$ZFSS1 = R_1 + jwL_1 + \frac{1}{jwC_1}. \quad (6.14)$$

$$ZFSS2 = R_2 + jwL_2 + \frac{1}{jwC_2}. \quad (6.15)$$

$$ZFSS3 = R_3 + jwL_3 + \frac{1}{jwC_3}. \quad (6.16)$$

Each of the two dielectrics the solid with thickness sh2 and the perforated with thickness sh1 is separately modeled as individual transmission line segments. One could think of the ground plane as a short circuit segment. The analogous circuit has been designed using the Advanced Design System (ADS) software. The values of the lumped parameters are shown in Table 6.1 which have been found using the curve fitting technique. Comparing the reflection from the circuit model with the full-wave simulation, as seen in Figure 6.22b, reveals good agreement.

$$Z_{d1} = Z_d \frac{Z_{d2} + jZ_d \tan(\beta_d(sh1 + sh2))}{Z_d + jZ_{d2} \tan(\beta_d(sh1 + sh2))}. \quad (6.17)$$

$$Z_{d2} = jZ_o \tan(\beta h). \quad (6.18)$$

$$Z_o = \sqrt{\frac{\mu}{\epsilon}}. \quad (6.19)$$

$$Z_d = \frac{Z_o}{\sqrt{\epsilon}}. \quad (6.20)$$

Table 6.1
Optimized design parameters of Equivalent circuit in Figure 6.22a

Dimensions (unit: R(Ω), L(nH), C(fF), Z(Ω))		
R1 = 478	L1 = 11.38	C1 = 14.39
R2 = 1085	L2 = 43.8	C2 = 1.5
R3 = 0.065	L3 = 3.4	C3 = 16.9
Z _o = 377	Z _d = $\frac{Z_o}{\sqrt{\epsilon_r}}$ = 260.15	

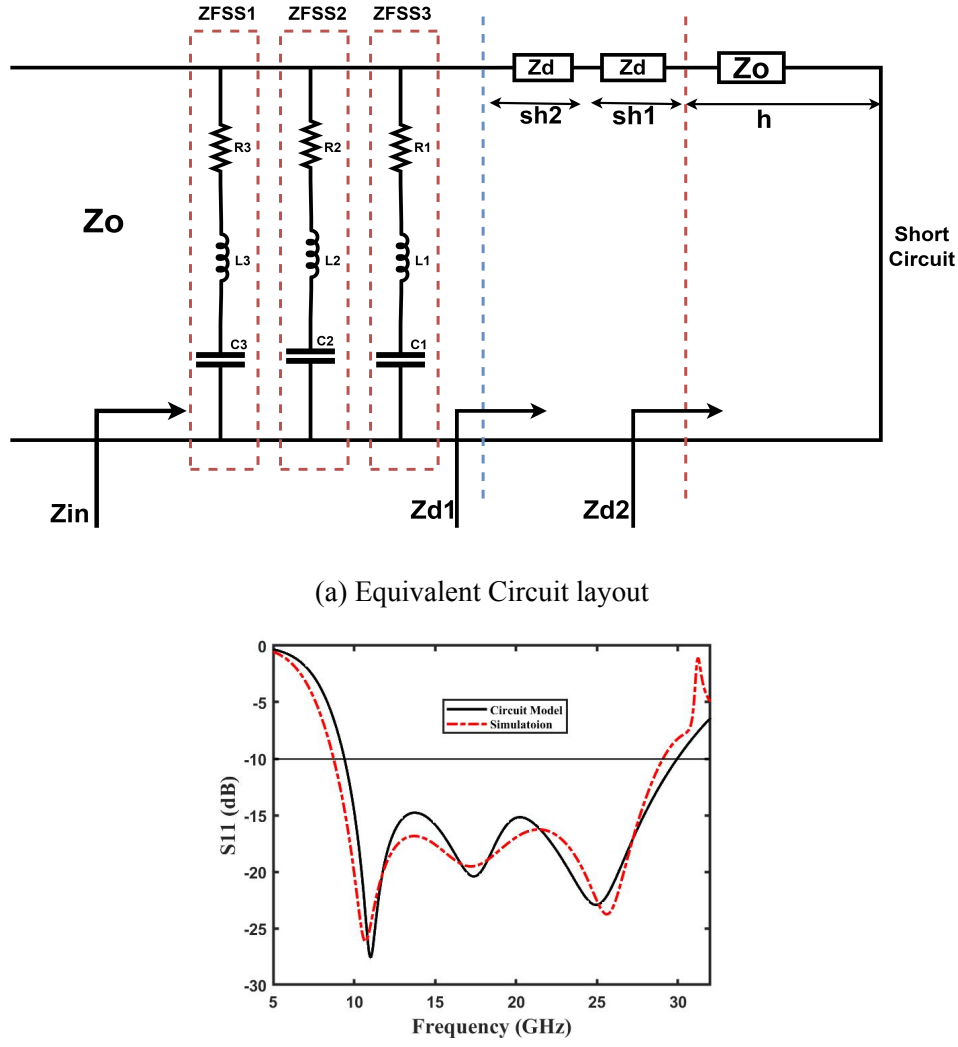


Figure 6.22: Equivalent Circuit Model.

6.1.2.8 Parametric Analysis

We did a Parametric analysis of all the parameters that we have used for designing and for perfect results

Effect of Air gap(h):

The height of the spacer (h) has been varied from 0 mm to 5 mm with intervals of 1 mm in order to examine the impact of the free space between the substrate and the ground plane. As the height of the spacer grows, the corresponding capacitance also changes. This causes the $\frac{\lambda}{4}$, which is related to the dielectric thickness, to routinely increase. As a result, the absorption band shifts towards the lower frequency side. The spacer height of 2 mm is optimal as it covers the entire X-band as well as the Ku-band and K-band, as illustrated in Figure 6.23a. As a result, the thickness was tuned to 2mm

in order to attain a high bandwidth.

Effect of conductivity of INK(σ):

Figure 6.23b shows that when the conductivity is changed, the absorption performance first increases but then declines as the conductivity increases. Using the four-probe approach [19], the resistive ink's conductivity was found to be 2800 S/m through experimentation. As a result, the thickness was tuned to 20 μm in order to attain a high bandwidth.

Effect of Perforated Substrate thickness (sh1)

In Figure 6.23c, the absorptivity is demonstrated by varying the substrate's thickness (sh1) from 0.7 mm to 0.2 mm, with a 0.1 mm width. It is noted that the absorption bandwidth dramatically dropped as sh1 increased. Conversely, it will not be conformal as the substrate thickness rises. and by moving toward higher frequencies while reducing bandwidth improves The flexible substrate with a thickness of 0.5 mm was selected based on availability in order to attain the highest absorption bandwidth. We used a perforated substrate to make the substrate more flexible.

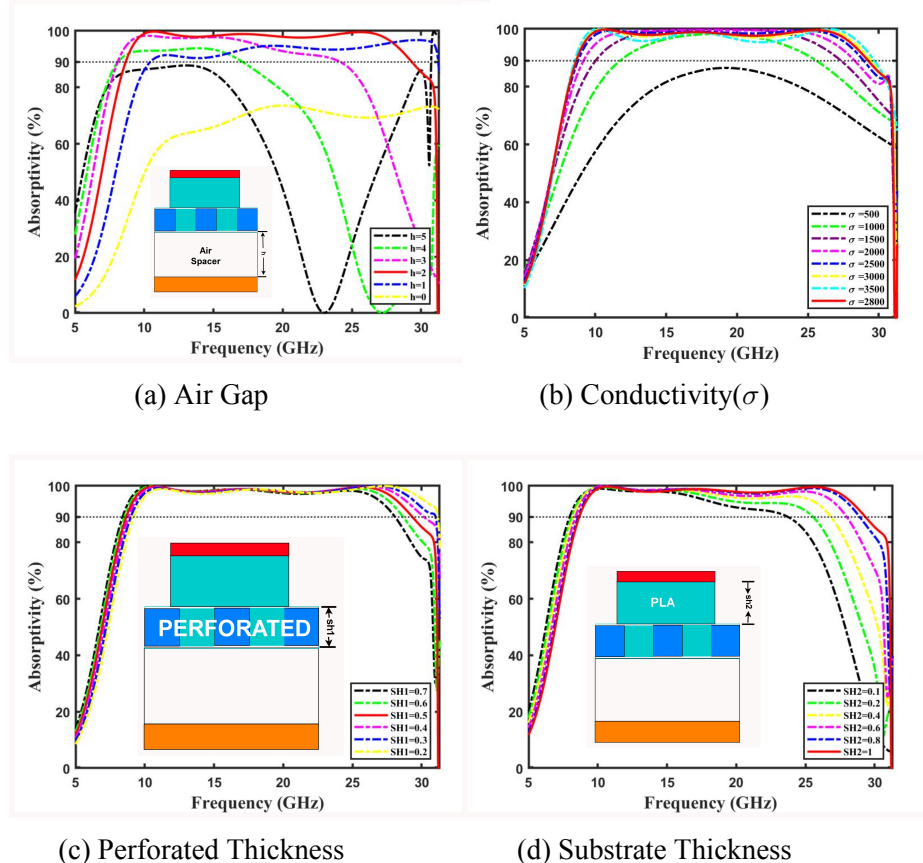


Figure 6.23: Variation of the different design parameters of the proposed broadband absorber-2.

Effect of Substrate thickness (sh2):

When the substrate (sh2) thickness was changed from 1 mm to 0.1 mm with a 0.2 mm width,

Figure 6.23d depicts the absorptivity. It is seen that the absorption bandwidth dramatically dropped as sh2 increased. and by narrowing the bandwidth, however, in this instance, there is no movement towards higher frequencies. The flexible substrate with a thickness of 1 mm was selected in order to obtain the highest absorption bandwidth while requiring less thickness and greater flexibility. Given that layer 1 is perforated, we employed this layer to provide mechanical support for resistive ink toward the substrate.

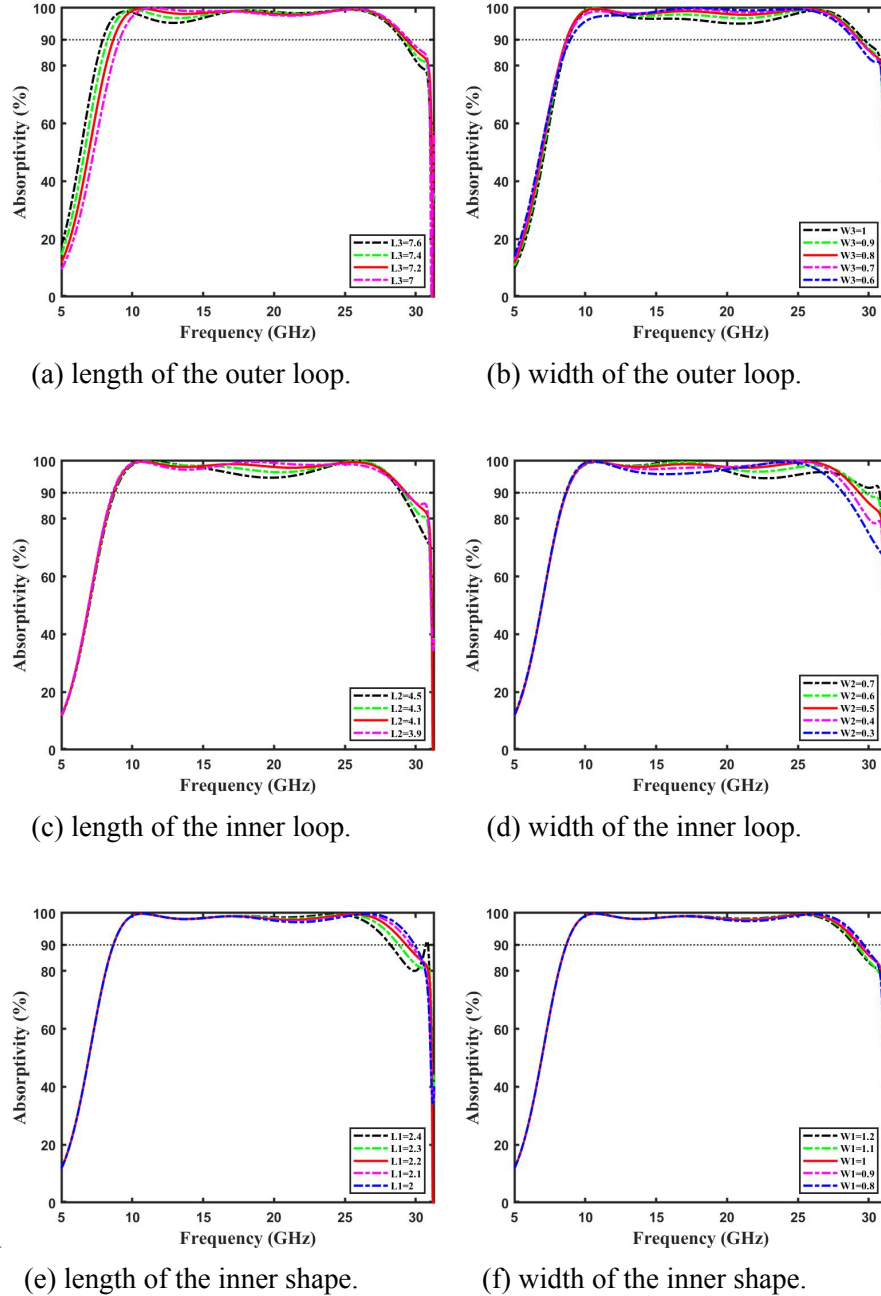


Figure 6.24: Variation of the different design parameters of the proposed broadband absorber-2.

Effect of Outer most Square Loop (L3, W3):

The absorption bandwidth at 8-10 GHz was found to decrease significantly as the length of the outermost square Loop (L3) increased, with a width of 0.2 mm, as shown in Figure 6.24a. Similarly, decreasing bandwidth increases, but absorption decreases at 8-10 GHz. Additionally, Figure 6.24b illustrates the absorbtivity by varying the outermost square Loop's (w3) width from 1 mm to 0.6 mm, with a width of 0.1 mm. It is noted that as W3 increased, the absorption significantly decreased at 8–10 GHz and that by decreasing absorption, bandwidth decreased at 8–10 GHz. The length of 7.2 mm and the width of 0.8 mm were selected to yield the highest absorption bandwidth. The primary cause of 8–12 GHz (Entire X band) absorption is this loop.

Effect of Inner Square Loop (L2, W2):

The absorptivity is shown in Figure 6.24c by varying the inner square loop (L2) length from 4.5 mm to 3.9 mm with a 0.2 mm width. It is seen that absorption dramatically dropped at 15-20 GHz as L2 grew, while absorption increased at 15-20 GHz as L2 decreased. Additionally, Figure 6.24d illustrates the absorptivity that results from varying the inner square loop's (w2) width from 0.7 mm to 0.3 mm with a 0.2 mm width. It is noted that as W2 increased, absorption significantly decreased at 15-20 GHz and that absorption increases with bandwidth decreases at 15-20 GHz and 20-27 GHz, respectively. The width of 0.5 mm and length of 4.1 mm were selected to provide the highest absorption bandwidth. The primary cause of 12–20 GHz (Entire KU-band) absorption is this loop.

Effect of Inner Shape (L1, W1):

With a width of 0.1 mm, Figure 6.24e illustrates the absorptivity by varying the inner shape's length (L1) from 2.4 mm to 2 mm. It is noted that when L1 increased, the absorption bandwidth at 23–27 GHz dramatically decreased, and that absorption bandwidth increased at 23–27 GHz. but if we cut it by another 2, manufacturing would become more difficult because the perforated substrate slot size is just 2 mm. Furthermore, as the width of the inner shape (w1) was changed from 1.2 mm to 0.8 mm with a width of 0.1 mm, Figure 6.24f depicts the absorptivity. It is noted that as W1 increased, the absorption bandwidth significantly decreased at 23–27 GHz and that absorption decreased as bandwidth increased at 20–27 GHz. The specified dimensions of 2.2 mm for length and 1 mm for width provide the maximum absorption bandwidth while maintaining high absorption. This shape is the main reason for absorption at 23–27 GHz (K-band).

6.1.2.9 Field Distribution

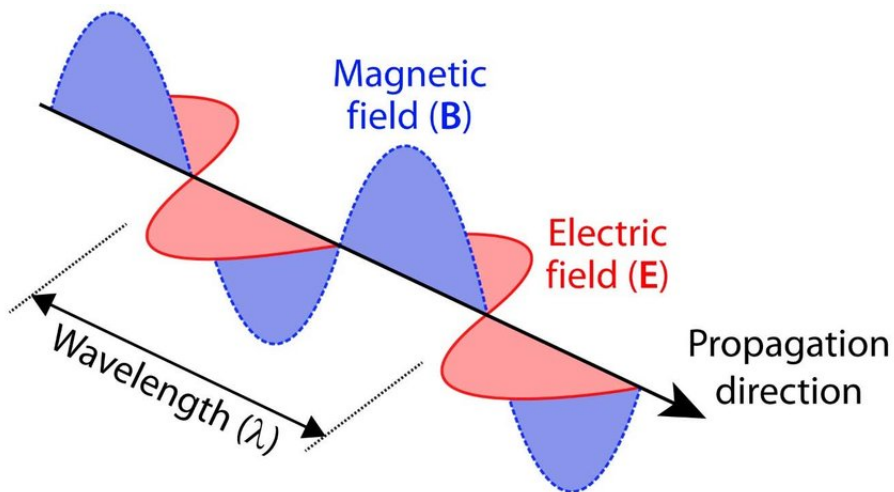
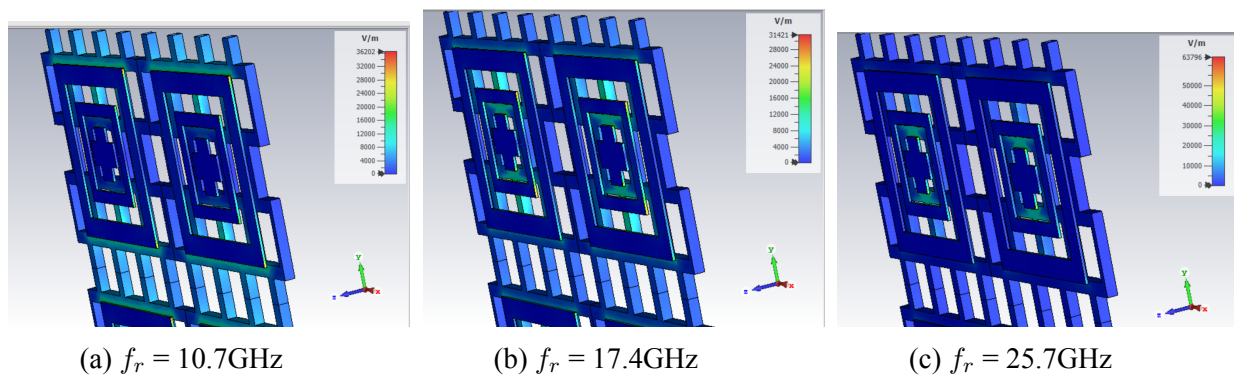


Figure 6.25: Relation of Electric and Magnetic Field

TE:



TM:

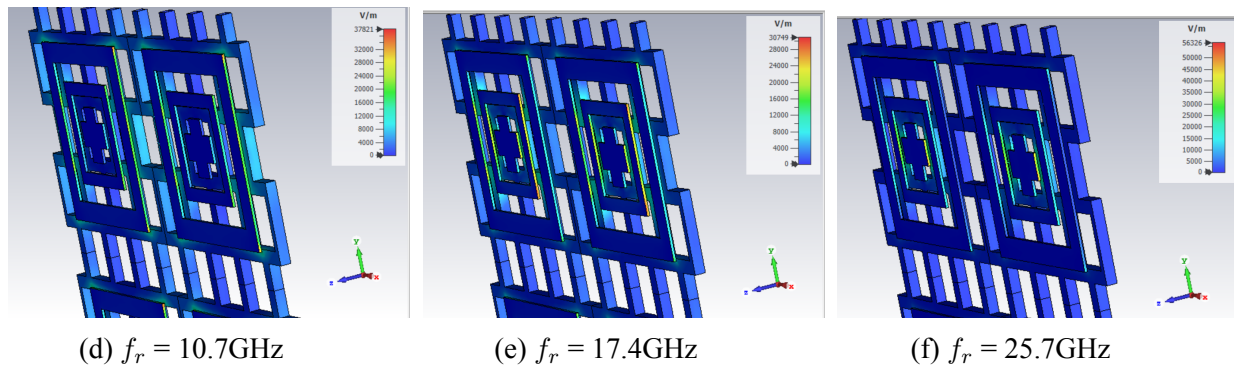


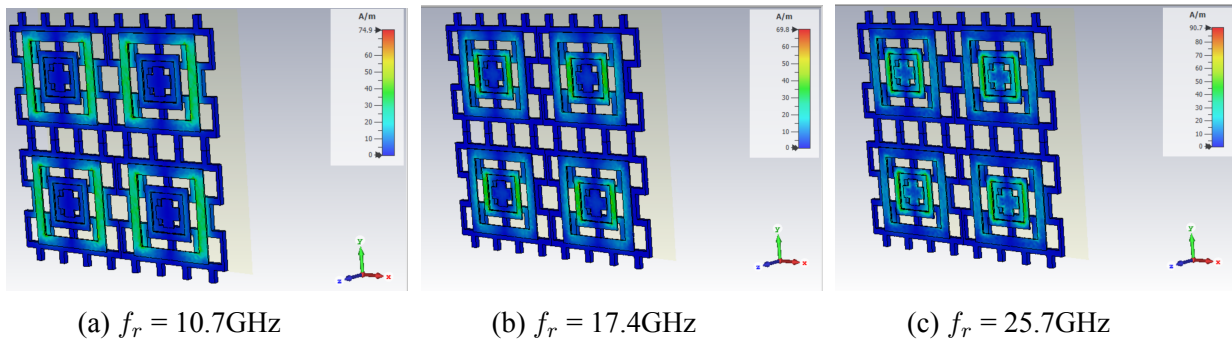
Figure 6.26: Variation of Electric Field of Proposed Absorber-2

In this section, we will describe the field distribution of our proposed metamaterial-based broadband and conformal absorber. As we can see from the reflection coefficient graph, there are three dips at three different frequencies: 10.7GHz, 17.4GHz, and 25.7GHz, respectively. We analyzed both fields at these three different frequencies. As shown in Figure ??, we plotted both electric and magnetic field distributions.

As shown in the Figure 6.26, the electric field is almost negligible in the substrate part, but there is variation between all resonant frequencies, and we have observed the electric field in both directions, Transverse Electric (TE) and Transverse Magnetic (TM), and we have observed the difference in electric field in both cases, as we conclude that the electric field changes in the perpendicular direction in TE and TM mode respectively.

We also saw the magnetic field distribution of our proposed absorber at 3 dips (3 resonant frequencies 10.7, 17.4, 25.7 GHz) as we can see in Figure 6.27 for the magnetic field. We also observed in TE and TM in this case and we have observed that at low frequencies outer loop contributes and for higher frequencies inner shapes contribute as we can clearly see in Figure 6.27.

TE:



TM:

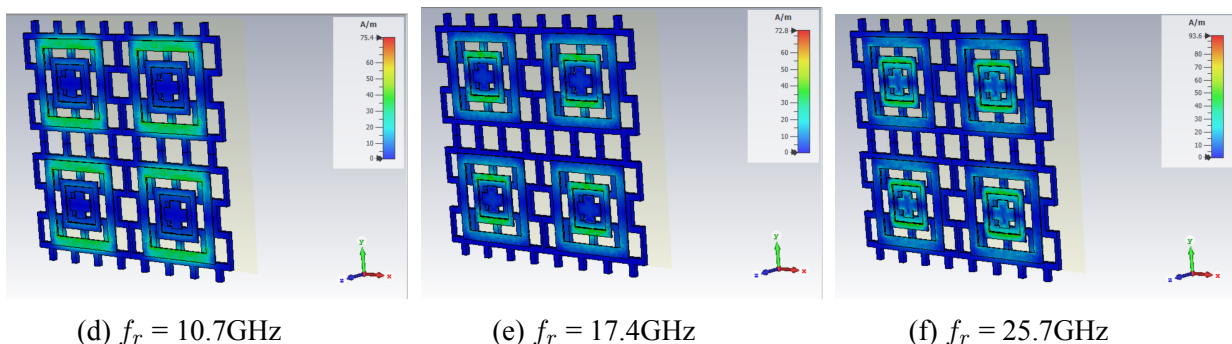


Figure 6.27: Variation of Magnetic Field of Proposed Absorber-2

6.1.2.10 Surface Current Density

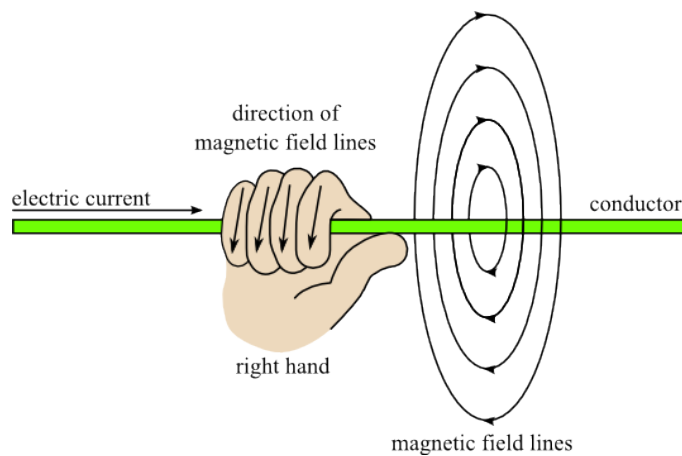
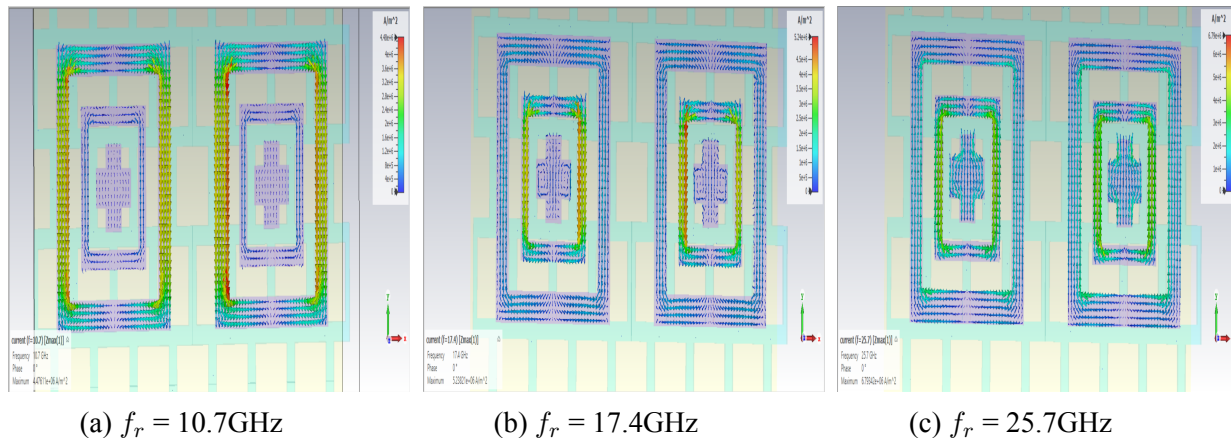


Figure 6.28: Relation of Electric and Magnetic Field

TE:



TM:

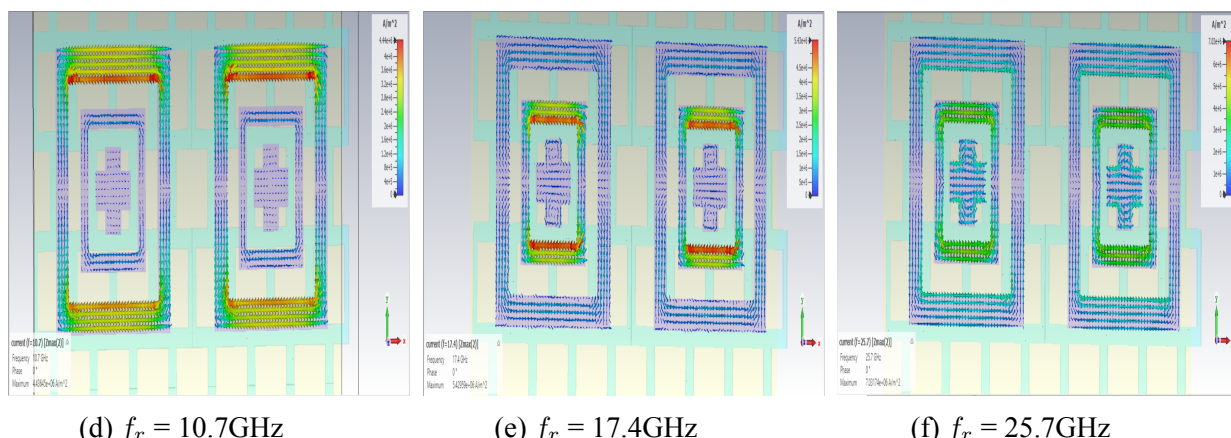


Figure 6.29: Variation of Surface Current distribution of Proposed Absorber-2 on resistive ink

In this section, we will discuss the current distribution of the proposed absorber on the ground plane as well as resistive ink. We also observed that there is a very less electric field in resistive ink because of its high resistivity, so there will be very negligible surface current in the direction of the electric field in resistive ink. However, because our ground plane is copper, which has very low Resistivity, there will be more surface current in the ground plane while compared to resistive ink.

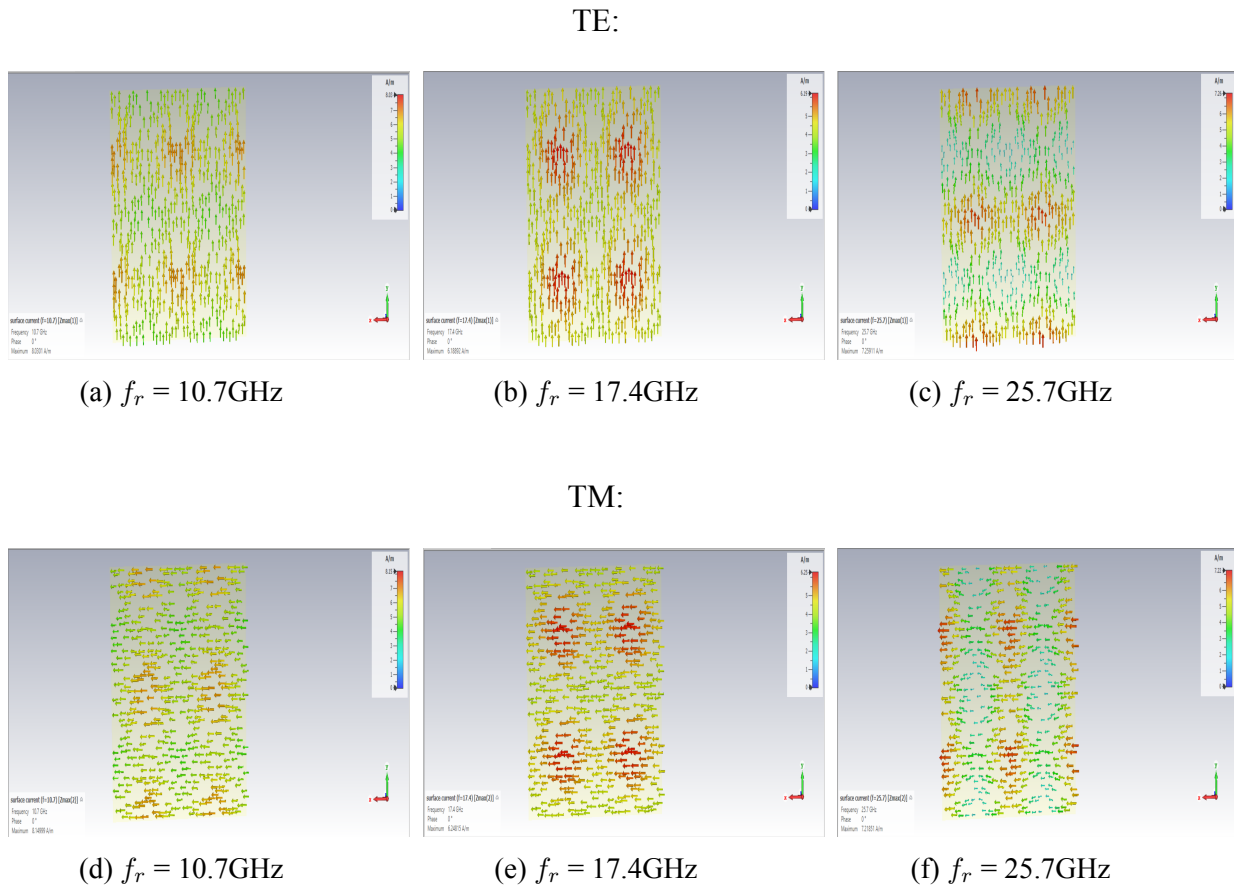


Figure 6.30: Variation of Surface Current Distribution of Proposed Absorber-2 on Ground plane

By observing in Figure 6.29 we can observe current distribution in the loops at different frequencies and we conclude that due to the outer loop, there is more contribution of current at lower frequencies, and at 10.7 GHz more current is contributed in the loop as seen in Figure 6.29a as TE and 6.29d as TM and at middle frequencies like 17.4GHz inner or middle loop contribute more current as we seen in Figure 6.29b as TE and 6.29e as TM as we are going to higher frequencies inner shape is started contributing current to the design for 25.7 GHz we can see in Figure 6.29c as TE and 6.29f as TM.

We also saw current distribution on the ground plane as our ground plane is very near to the substrate

very small air gap of 2mm only as my substrate acts as a transmission line so the electric field will transfer to the ground plane and the ground plane will act as a short circuit due to this short circuit transmission of EM wave will be very less hence this will act as a perfect absorber, as we can see in Figure 6.30 there is a current in the ground plane we have examined both TE and TM mode in this case

We evaluated these at three resonating frequencies (10.7, 17.4, 25.7 GHz), which can also be observed in Figure 6.30. In TE mode, current flows upwards, as shown in Figure 6.30a, and in TM mode, current flows left to right, as shown in Figure 6.30d, however, the density of current varies with frequency.

6.1.2.11 Bending Analysis Simulation

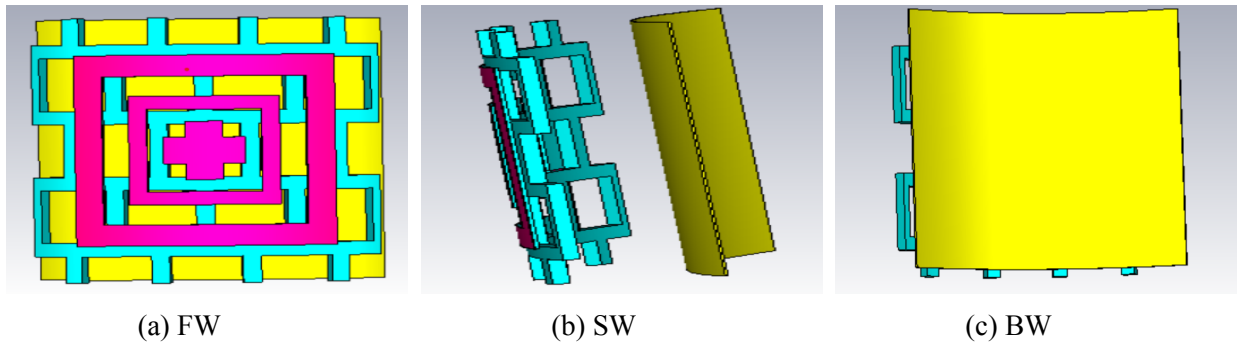


Figure 6.31: Bending analysis of a Unit cell of Proposed absorber

We bent our absorber unit cell for various radii, such as 90, 100, 135, and 180 mm, and we measured the reflection coefficient to verify that our absorber was conformal.

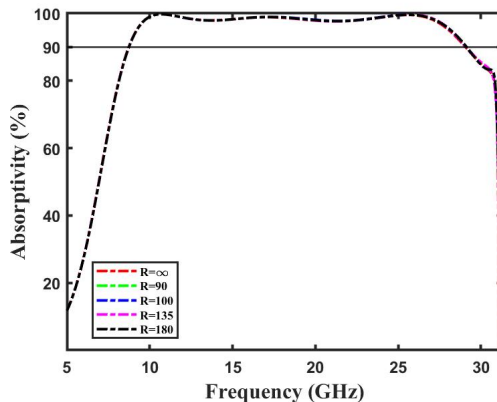


Figure 6.32: Simulated Reflectivity curve for different cylindrical radii.

The resonance frequency for all bending scenarios exhibited minimal change, indicating that the absorber's performance is not significantly affected by bending. Based on this study, the proposed antenna has the potential to be utilized in applications where bending may occur. Additionally, the study concludes that the proposed absorber is flexible.

6.1.3 Comparison with previous work

To assess the effectiveness of the proposed absorbers, a comparative analysis was carried out with existing conformal and broadband absorbers, as detailed in Table 6.2. The evaluation parameters included size, substrate material thickness, Air gap and Bandwidth. Based on the analysis, the proposed absorbers was found to be relatively broadband and conformal absorbers.

Table 6.2
Comparison Table

Ref.	Unit cell size (mm)	Dielectric Thickness (mm)	Center Freq (GHz)	Air space (mm)	Conformal	BW (GHz)	Angular Stability (>90)
[1]	16	5.5	11.24	0	NO	11.44	45 for TE
[2]	10	0.3	9.1	7	NO	5.7	30 for TE
[3]	13	1.6	11.59	3	NO	13.5	30 for TE
[4]	14.4	0.18	9.56	3.5	YES	7.04	30 for TE
[5]	15.8	0.125	12.93	2.5	YES	12.14	NA
[6]	12.5	0.07	7.2	7.5	Yes	6.6	45 for TE
work-1	16	2	12	1.5	NO	17.69	45 for TE
work-2	10	1.5	18.9	2	YES	20.34	45 for TE

Chapter 7

CONCLUSION

This chapter provides a concluding summary of the entire project.

7.1 Conclusion

In this study, we have constructed two metamaterial-based absorbers with ultra-wideband absorption and flexibility. These broadband metamaterial absorbers are based on a normal and perforated substrate as the constituent dielectric substrate. The design makes use of 3-D printing to create the perforated dielectric, which is then coated with a lossy resistive ink to achieve broadband absorption. When contrasted with its counterpart (a similar topology fabricated from solid PLA material with equivalent absorption bandwidth), it is discovered that the dielectric's total volume is significantly reduced at the expense of a somewhat increased thickness. The suggested design is based on the CA principle, in contrast to the previously documented 3-D printed absorber structures.

7.2 Future Scope

Future research on metamaterial-based absorbers with ultra-wideband absorption and flexibility can explore optimizing perforation patterns, integrating advanced materials, and enhancing mechanical properties. Efforts could also focus on developing scalable manufacturing techniques and assessing environmental durability. Tailoring designs for specific applications like EMI shielding and radar cross-section reduction, along with creating multi-functional absorbers, could significantly expand their practical use. Additionally, customizable absorbers and advanced coating materials can further enhance performance and versatility, driving innovations across various technological fields. Research into multi-functional capabilities, such as combining electromagnetic absorption with thermal management or structural reinforcement, could offer significant added value.

REFERENCES

- [1] C. Caloz, and T. Itoh, *Electromagnetic Metamaterials: Transmission Line Theory and Microwave Applications* (Wiley-IEEE Press, New York, 2005).
- [2] W. F. Bahret, *IEEE Trans. Aerosp. Electron. Syst.* 29, 1377 (1993).
- [3] 15418.courses.cs.cmu.edu. (2018). The Barnes-Hut Algorithm : 15-418 Spring 2013.
- [4] S. K. Sharma and R. K. Chaudhary, *IEEE Antennas Wirel. Propag. Lett.* 14, 1670 (2015).
- [5] R. L. Fante and M. T. McCormack, *IEEE Trans. Antennas Propag.* 36, 1443 (1988).
- [6] E. F. Knott and C. D. Lunden, *IEEE Trans. Antennas Propag.* 43, 1339 (1995).
- [7] M. J. Park, J. Choi, and S. S. Kim, *IEEE Trans. Magn.* 36, 3272 (2000).
- [8] Y. Naito and K. Suetake, *IEEE Trans. Microw. Theory Tech.* 19, 65 (1971).
- [9] L. Li, Y. Yang, and C. Liang, “A wide-angle polarization-insensitive ultra-thin meta-material absorber with three resonant modes,” *J. Appl. Phys.*, vol. 110, no. 6, p. 063702, Sept. 2011.
- [10] D. Lim, D. Lee, and S. Lim, “Angle- and polarization-insensitive metamaterial absorber using via array,” *Sci. Rep.*, vol. 6, p. 39686, Dec. 2016
- [11] B. Wang, B. Y. Gong, M. Wang, B. Weng, and X. Zhao, “Dendritic wideband metamaterial absorber based on resistance film,” *Appl. Phys. A*, vol. 118, no. 4, pp. 1559–1563, Mar. 2015.
- [12] F. Costa, A. Monorchio, and G. Manara, “Ultra-thin absorber by using high impedance surfaces with frequency selective surfaces,” *Proc. IEEE Int. Symp. on Antennas Propag.*, Honolulu, 2007, pp. 861–864.
- [13] F. Costa, A. Monorchio, and G. Manara, “Analysis and design of ultrathin electromagnetic absorbers comprising resistively loaded high impedance surface,” *IEEE Trans. Antennas Propag.*, vol. 58, no. 5, pp. 1551–1558, May 2010.
- [14] H. B. Zhang et al., “Resistance selection of high impedance surface absorbers for perfect and broadband absorption,” *IEEE Trans. Antennas Propag.*, vol. 61, no. 2, pp. 976–979, Feb. 2013.
- [15] A. Kazemzadeh and A. Karlsson, “Capacitive circuit method for fast and efficient design of wideband radar absorbers,” *IEEE Trans. Antennas Propag.*, vol. 57, no. 8, pp. 2307–2314, Aug. 2009.
- [16] M. Yoo and S. Lim, “Polarization-independent and ultrawideband metamaterial absorber using a hexagonal artificial impedance surface and a resistor-capacitor layer,” *IEEE Trans. Antennas Propag.*, vol. 62, no. 5, pp. 2652–2658, Feb. 2014.
- [17] C. Zhang, Q. Cheng, J. Yang, J. Zhao, and T. J. Cui, “Broadband metamaterial for optical transparency and microwave absorption,” *Appl. Phys. Lett.*, vol. 110, p. 143511, Apr. 2017

REFERENCES

- [18] S. N. Zabri, R. Cahill, and A. Schuchinsky, "Compact FSS absorber design using resistively loaded quadruple hexagonal loops for bandwidth enhancement," *Electron. Lett.*, vol. 51, no. 2, pp. 162-164, Jan. 2015.
- [19] Ghosh, Saptarshi, and Sungjoon Lim. "Perforated lightweight broadband metamaterial absorber based on 3-D printed honeycomb." *IEEE Antennas and Wireless Propagation Letters* 17, no. 12 (2018): 2379-2383.
- [20] G. L. Huang, S. G. Zhou, C. Y. D. Sim, T. H. Chio, and T. Yuan, "Lightweight perforated waveguide structure realized by 3-D printing for RF applications," *IEEE Trans. Antennas Propag.*, vol. 65, no. 8, pp. 3897- 3904, Aug. 2017.
- [21] M. Ahmadloo and P. Mousavi, "A novel integrated dielectric-andconductive ink 3D printing technique for fabrication of microwave devices," *IEEE MTT-S International Microwave Symposium Digest*, pp. 1-3, 2013.
- [22] Y. Yoon, D. Lim, M. M. Tentzeris, and S. Lim, "Low-cost metamaterial absorber using three-dimensional circular truncated cone," *Microw. Opt. Technol. Lett.*, vol. 60, pp. 1622-1630, May 2018.
- [23] W.-H. Choi, J.-H. Shin, T.-H. Song, W.-Y. Lee, W.-J. Lee, and C.-G. Kim, "Design of broadband microwave absorber using honeycomb structure," *Electron. Lett.*, vol. 50, no. 4, pp. 292-293, Feb. 2014.
- [24] W. Jiang et al., "Electromagnetic wave absorption and compressive behavior of a three-dimensional metamaterial absorber based on 3D printed honeycomb," *Sci. Rep.*, vol. 8, p. 4817, Mar. 2018.
- [25] Y. Shen et al., "Origami-inspired metamaterial absorbers for improving the larger-incident angle absorption," *J. Phys. D Appl. Phys.*, vol. 48, p. 445008, Oct. 2015.
- [26] P. Liu and T. Lan, *Appl. Opt.* 56, 4201 (2017).
- [27] O.T. Jang, H. Youn, Y. J. Shin, and L. J. Guo, *ACS Photonics* 1, 279 (2014)
- [28] S. Lai, Y. Wu, J. Wang, W. Wu, and W. Gu, *Opt. Mater. Express* 8, 1585 (2018).
- [29] X. Kong, J. Xu, J. J. Mo, and S. Liu, *Front. Optoelectron.* 10, 124 (2017).
- [30] R. Yahiaoui, J. P. Guillet, F. D. Miollis, and P. Mounaix, *Opt. Lett.* 38, 4988 (2013).
- [31] Kong, X., Xu, J., Mo, J.J. and Liu, S., 2017. Broadband and conformal metamaterial absorber. *Frontiers of Optoelectronics*, 10, pp.124-131.
- [32] Kalraiya, S., Chaudhary, R.K. and Abdalla, M.A., 2019. Design and analysis of polarization independent conformal wideband metamaterial absorber using resistor loaded sector shaped resonators. *Journal of Applied Physics*, 125(13).

REFERENCES

- [35]Front. Phys., 29 April 2022 Sec. Optics and Photonics Volume 10 - 2022
- [36] Sayed, S.I., Mahmoud, K.R. and Mubarak, R.I. Design and optimization of broadband metamaterial absorber based on manganese for visible applications. Sci Rep 13, 11937 (2023).
- [37] Osman Ayop, Mohamad Kamal Abd Rahim, Noor Asniza Murad, Noor Asmawati Binti Samsuri, and Raimi Dewan, "Triple Band Circular Ring-Shaped Metamaterial Absorber for X-Band Applications," Progress In Electromagnetics Research M, Vol. 39, 65-75, 2014.
- [38] S. Bhattacharyya, S. Ghosh, K. V. Srivastava, J. Appl. Phys. 2013, 114, 094514.
- [39] Liu, A broadband terahertz absorber using multi-layer stacked bars, Appl. Phys. Lett., № 106, c. 151601
- [40]S. Guo, Y. -L. Zhang, Y. He, L. Miao and J. -J. Jiang, "Design of a Broadband and Switchable Absorber Using an Absorb/Reflective FSS," 2019 Photonics and Electromagnetics Research Symposium - Fall (PIERS - Fall), Xiamen, China, 2019, pp. 2144-2148, doi: 10.1109/PIERS-Fall48861.2019.9021344.
- [41] Y. Xu, B. Zhang, J. Duan and Y. Tian, "Design of Broadband Metamaterial Absorber for C Band and X Band," 2018 IEEE International Conference on Computer and Communication Engineering Technology (CCET), Beijing, China, 2018, pp. 159-163, doi: 10.1109/CCET.2018.8542463.
- [42] X. LEI, S. HUO, M. WANG, Y. LI and E. LI, "A Compact Ultra-Wideband Polarization-Insensitive Metamaterial Absorber at 5G Millimeter Wave Band," 2020 IEEE MTT-S International Conference on Numerical Electromagnetic and Multiphysics Modeling and Optimization (NEMO), Hangzhou, China, 2020, pp. 1-4, doi: 10.1109/NEMO49486.2020.9343462.
- [43] S. Ghosh, S. Bhattacharyya, D. Chaurasiya and K. V. Srivastava, "An Ultrawideband Ultrathin Metamaterial Absorber Based on Circular Split Rings," in IEEE Antennas and Wireless Propagation Letters, vol. 14, pp. 1172-1175, 2015, doi: 10.1109/LAWP.2015.2396302.
- [44] L. Wang, D. Xia, Q. Fu, X. Ding, and Y. Wang, "A Switchable Ultra-Wideband Metamaterial Absorber with Polarization-insensitivity and Wide-incident Angle at THz Band", Frontiers in Materials, vol.8,art. no.729495,2021
- [45]Guoqing Xu, Jie Huang, Zongde Ju, Zhihua Wei, Jing Li, and Qian Zhao, "A Novel Six-Band Polarization-Insensitive Metamaterial Absorber with Four Multiple-Mode Resonators," Progress In Electromagnetics Research C, Vol. 77, 133-144, 2017.
- [46] N. K. Mishra and L. Dewangan, "Broad Band Polarization Insensitive Metamaterial Absorber for K Band Application," 2022 IEEE Microwaves, Antennas, and Propagation Conference (MAPCON), Bangalore, India, 2022, pp. 97-100, doi: 10.1109/MAPCON56011.2022.10047816.

REFERENCES

- [47] Saadeldin, A.S., Sayed, A.M., Amr, A.M. et al. Wideband ultrathin and polarization-insensitive metamaterial absorber for Ku-band applications. *J Mater Sci: Mater Electron* 34, 1797 (2023). <https://doi.org/10.1007/s10854-023-11157-4>.
- [48] Nguyen, T.T., Lim, S. Bandwidth-enhanced and Wide-angle-of-incidence Metamaterial Absorber using a Hybrid Unit Cell. *Sci Rep* 7, 14814 (2017). <https://doi.org/10.1038/s41598-017-14792>
- [49] J. Tak and J. Choi, "Design of an all-textile microwave absorber for indoor radar clear," 2016 IEEE International Conference on Network Infrastructure and Digital Content (IC-NIDC), Beijing, China, 2016, pp. 108-111, doi: 10.1109/ICNIDC.2016.7974545.
- [50] Almirall, Oriol, Raul Fernández-García, and Ignacio Gil. "Wearable Metamaterial for Electromagnetic Radiation Shielding." *The Journal of The Textile Institute* 113, no. 8 (2022): 1586–94. doi:10.1080/00405000.2021.1940662.
- [51] Alsulami QA, Wageh S, Al-Ghamdi AA, Bilal RMH, Saeed MA. A Tunable and Wearable Dual-Band Metamaterial Absorber Based on Polyethylene Terephthalate (PET) Substrate for Sensing Applications. *Polymers (Basel)*. 2022 Oct 25;14(21):4503. doi: 10.3390/polym14214503. PMID: 36365497; PMCID: PMC9657874.
- [52] Avinash, Nisha Gupta. An Ultrathin Graphite Based Absorber for Wearable Applications, 03 June 2021, PREPRINT (Version 1) available at Research Square [<https://doi.org/10.21203/rs.3.rs-480007/v1>]
- [53] Shan, Y.; Chen, L.; Shi, C.; Cheng, Z.X.; Zang, X.F.; Xu, B.Q.; Zhu, Y.M. Ultrathin Flexible Dual Band Terahertz Absorber. *Opt.Commun.* 2015, 350, 63–70
- [54] J. Kim, H. Jeong, and S. Lim, "Mechanically actuated frequency reconfigurable metamaterial absorber," *Sens.Actuators, A* 299, 111619 (2019)
- [55] G. Chaitanya and A. Chandachoriya, "Polarization Independent Super Thin Metamaterial Microwave Broadband Absorber for X-Band Application," 2020 IEEE 9th International Conference on Communication Systems and Network Technologies (CSNT), Gwalior, India, 2020, pp. 13-18, doi: 10.1109/CSNT48778.2020.9115751.
- [56] Ghosh S, Bhattacharyya S, Srivastava K V, 2016, Design, characterisation and fabrication of a broadband polarisation-insensitive multi-layer circuit analogue absorber, *IET Microw. Antennas Propag.*, 10, 8, 850 – 855
- [57] S. Sambhav, J. Ghosh and A. K. Singh, "Ultra-Wideband Polarization Insensitive Thin Absorber Based on Resistive Concentric Circular Rings," in *IEEE Transactions on Electromagnetic Compatibility*, vol. 63, no. 5, pp. 1333-1340, Oct. 2021, doi: 10.1109/TEMC.2021.3058583.

REFERENCES

- [58] Wang L-L, Liu S-B, Zhang H-F, Kong X-K, Liu L-L. High-impedance surface-based flexible broadband absorber. *J Electromagn Waves Appl* (2017) 31(13):1216–1231.
- [59] Ye Dong, Zhangyou Yang, Siqi Zhang, Rongrong Zhu, Bin Zheng, and Huan Lu, "A Flexible Foldable Broadband Metamaterial Absorber Fabricated by Intaglio Printing Technology," *Progress In Electromagnetics Research M*, Vol. 124, 29-34, 2024.
- [60] Shuvo MMK, Hossain MI, Rahman S, Mahmud S, Islam SS, Islam MT. A Wide- Angle, Enhanced Oblique Incidence, Bend-Able Metamaterial Absorber Employed in Visible Region With a Sun Shape Resonator. *IEEE Access* 2021;9:126466–80.
- [61] Ranjan, P., Choubey, A., Mahto, S. K., Sinha, R., and Barde, C. (2019). A novel ultrathin wideband metamaterial absorber for X-band applications. *Journal of Electromagnetic Waves and Applications*, 33(17), 2341–2353.
- [62] Y. Li, Y. Fang, Y. Huang, K. Pan, X. Xiao, X. Liu, L. Li, Z. Hu, Ultra-wideband, polarization-insensitive flexible metamaterial absorber base on laser printed graphene using equivalent circuit design method, *Carbon* 212 (2023) 118166
- [63] S. Malik, A. Sharma and K. V. Srivastava, "Resistive Ink Based Microwave Absorber for S and C-Band with 99% Absorption," 2021 IEEE Indian Conference on Antennas and Propagation (InCAP), Jaipur, Rajasthan, India, India, 2021, pp. 677-680.



